The Behaviour and Design of Composite Floor Systems in Fire

Neil John Kirkwood Cameron

Doctor of Philosophy

University of Edinburgh

2003

Declaration

This thesis and the research described and reported within has been completed solely by Neil John Kirkwood Cameron under the supervision of Dr A.S. Usmani and Dr B. Lane.

Where other sources are quoted full references are given.

Neil John Kirkwood Cameron

24th October 2003

Abstract

Modern composite steel framed structures possess a high degree of redundancy. This allows them to survive extreme fires without collapse as there are many alternative loadpaths which can be used to transfer load away from the fire affected part of the structure as demonstrated in the Broadgate fire. Subsequent tests carried out on the Cardington frame showed that it was not necessary to apply fire protection to all steel beams. It was possible to leave selected secondary beams without fire protection. In the event of a fire this results in large deflections due to thermal expansion and material degradation, however, in a fire where serviceability requirements do not need to be met this is acceptable so long as life safety is ensured. The weakening beams and large deflections result in a change in the load transfer mechanism with load being carried through tensile membrane action in the slab. This thesis presents a method for calculating the membrane load capacity of composite floor slabs in fire.

Extensive numerical modelling at the University of Edinburgh has shown that the temperature distribution through a structural member greatly effects the deflection and pattern of internal stresses and strains. Theoretical solutions were produced to calculate the structural response of laterally restrained beams and plates subject to thermal loads. The theoretical deflections and internal forces were shown to compare well with those from numerical models.

To determine the membrane load capacity of concrete floor slabs in fire a three-stage design method was developed. Initially the temperature distribution through the slab was calculated for the design fire. From this the deflection of the slab and resulting stress and strain distributions in the steel reinforcement due to the thermal loads were calculated using equations from the theory developed previously. Failure of the slab was defined based on a limiting value of mechanical strain in the reinforcement, this strain corresponded to a limiting deflection. The load capacity of the slab at the limiting

deflection was calculated using an energy method. When compared against results from numerical models the ultimate load capacity was shown to be accurately predicted.

None of the fire tests carried out on the Cardington structure reached failure. Although demonstrating the inherent strength of such buildings this was also a major shortcoming as it was not possible to define the point of failure. The design method developed was used to calculate the membrane load capacity of four of the six Cardington tests. All four tests were shown to have had a significant reserve capacity with none being close to failure.

Publications

The following publications have been produced as a result of this research:

Journal Papers

A.S. Usmani and N.J.K. Cameron. Limit capacity of laterally restrained reinforced concrete floor slabs in fire. Invited paper to be published in a special fire engineering issue of the *Journal of Cement and Concrete Composites*.

N.J.K. Cameron and A.S. Usmani. Ultimate capacity of composite floor slabs at the fire limit state. To be submitted to the *Journal of Fire Protection Engineering*.

A.S. Usmani, M. Gillie, S. Lamont, B. Lane, N.J.K Cameron. Since the Cardington Experiments - A Review of Structural Fire Engineering. To be submitted to the *ASCE Journal of Structural Engineering*.

Conference Papers

N.J.K. Cameron and A.S. Usmani. Analytical solutions for floor slabs in fire. In Proceedings of the Second International Structures in Fire Workshop, pp213-123, University of Canterbury, Christchurch, New Zealand.

N.J.K. Cameron and A.S. Usmani. A new method to estimate the ultimate load capacity of composite floors in fire. In Proceedings of the Third International Conference on Decision Making in Urban and Civil Engineering, London, United Kingdom.

A.S.Usmani and N.J.K.Cameron. A new method to determine the ultimate load capacity of composite floors in fire. In Proceedings of ???????

N.J.K. Cameron and A.S. Usmani. Ultimate capacity of composite floor slabs at the fire limit state. In Proceedings of Designing Structures for Fire, pp217-226, Baltimore, Maryland, USA.

Acknowledgements

Thank you to my supervisors Dr Asif Usmani and Dr Barbara Lane for their help and support during this research. I must also thank Dr Susan Lamont for her advice.
Thank you to my friends, family and flatmates
The research was funded by an EPSRC Case award through Ove Arup. This is gratfeully acknowledged.

Contents

List of Figures

List of Tables

Chapter 1

Introduction

1.1 Background to the project

Every year the economic and personal costs of fire are immense. It will never be possible to prevent fires from occurring thus the aim of the fire safety engineer is to reduce the risk presented by fire to acceptable levels. Traditionally used prescriptive methods for structural fire safety design are based on the results of fire resistance testing of single structural elements. They do not consider the complex interactions that occur between elements in a real building or alternative loadings that occur due to thermal stresses. Using these methods it is impossible to quantify the actual level of fire safety in any building.

To gain a better understanding of the real structural behaviour of modern composite steel-framed buildings in fire a series of six full-scale tests were carried out on an eight storey steel frame structure at the Cardington Large Building Test Facility (BRE). These demonstrated that such a structure was capable of withstanding extreme fires without the need to apply fire protection to all of the steel beams. Numerical modelling of the tests showed that the behaviour in fire was dominated by restraint to thermal strains and that the amount of applied load and material softening from heating did not significantly affect the response until close to failure. The large deflections generated by thermal strains produced a deflected shape in the floor slab which could efficiently transfer load away from the fire affected part of the structure through membrane action. This consisted of tensile membrane action in the centre of the slab and compressive

membrane action at the edges (often referred to as the compressive 'ring').

Theoretical methods describing tensile membrane action at ambient conditions extend the traditional yield-line approach used for concrete slab design. Where these have subsequently been extended to the fire scenario they have not altered the deflected shape or failure definition. In a fire the large deflections experienced make it unlikely that yield lines would form in a slab, failure will more likely be caused by rupture of the reinforcement over supports.

1.2 Research aims

It is generally agreed that membrane action is the final load carrying mechanism in floor slabs exposed to fire but before a structural fire engineer can utilise this strength they must be able to quantify it. The aims of this research were therefore threefold:

- To produce analytical methods describing the membrane behaviour of composite floor slabs.
- To produce a method which allowed the membrane strength of a composite floor slab to be quantified reliably.
- To analyse the Cardington tests to determine how near they were to failure.

1.3 Outline of thesis chapters

Chapter 2 Structural Fire Safety Design

Traditional methods of determining the structural fire resistance of structural elements are described and the shortcomings of prescriptive design methods in current design codes are highlighted. Principles of performance based design methods are summarised. The material properties of steel and concrete at the high temperatures experienced in a fire are described.

Chapter 3 Behaviour of Composite Steel Framed Structures in Fire

Experimental investigations of structural behaviour in fire and real building fires before the Cardington tests are detailed. The Cardington fire tests are described and the subsequent theoretical and numerical studies of structural behaviour in fire are summarised. Performance based design methods developed in the United Kingdom and New Zealand for the design of composite floor systems are described.

Chapter 4 Analytical Methods to Describe the Behaviour of Structures subject to Thermal Effects

Solutions are presented for the analysis of laterally restrained beams and plates subject to thermal loading. Equations are given which can be used to determine the deflection of the element and the resulting membrane stress and strain distributions.

Chapter 5 Proposed Method for Ultimate Limit State Design of Concrete Floor Slabs in Fire

In this chapter a new design method for calculating the ultimate membrane load capacity of a composite floor slab in fire is proposed. The method considers both the thermal and applied loads and uses an energy method to determine the load capacity based on a limiting value of mechanical strain in the steel reinforcement.

Chapter 6 Numerical Analysis of Concrete Floor Slabs in Fire

The results of a series of parametric studies that were carried out on a range of slabs are presented. These are then compared against those from theoretical analyses of the same slabs using the method presented in Chapter 5. The ultimate load capacity of the slabs and the forces in the reinforcement bars are studied.

Chapter 7 Limit State Analysis of the Cardington Fire Tests

Four of the six fire tests carried out on the Cardington building were analysed using the proposed new design method for calculating the ultimate load capacity of composite floor slabs. For the applied loads used in the tests the theoretical and experimental deflections were compared. Finally the ultimate load capacity of the test layouts were calculated to determine how near to failure they were.

Chapter 8 Conclusions and Future Work

Chapter 2

Structural Fire Safety Design

2.1 Introduction

The fire resistance of a structural element has traditionally been determined through a fire resistance test. Some modern design codes also allow fire resistance to be determined analytically using calculations based on the assumption that material degradation is the primary cause of structural failure in fire. This chapter discusses the fire resistance test, methods of calculating fire resistance in design codes and the material properties of steel and concrete at elevated temperature. The membrane behaviour of concrete slabs and performance based design are also examined.

2.2 Design of structures for fire

The fire resistance of a structural element measures its ability to resist fire. For a building to be considered safe the fire resistance of the structure must be greater than the calculated fire severity [18]:-

$$\text{fire resistance} > \text{fire severity} \tag{2.1}$$

Three variables can be used for determining whether the condition in Eqn. 2.1 is met; time, temperature or strength. Traditionally time has been used to determine whether a structural element has sufficient fire resistance. If the time to failure of a structural

element is greater than the fire duration then it is deemed to have passed. Alternatively, the temperature of a structural element can be limited to ensure that it is below that which would cause failure. Assessment of the strength of the element ensures that during the fire the load capacity of the member is greater than the applied load.

Many factors affect the fire resistance of any element, such as the material, geometry, boundary conditions and the fire design load. Traditionally the fire resistance rating has been determined through full-scale testing, however, modern design codes may allow alternative methods based on existing test results or calculation methods. There are three main categories of fire resistance rating; proprietary ratings apply to a specific product such as a type of floor, generic ratings apply to typical construction materials, or alternatively the fire resistance can be determined using an approved calculation method. The fire severity will depend among other things on the fire load, the compartment geometry and the available ventilation.

2.2.1 Fire resistance by testing

Development of the fire resistance test

Fire tests have been carried out in some form since the 1790s [19] when The Associated Architects in London carried out tests on two floor fire-proofing systems. Up to about 1900 fire tests were all ad hoc with no standard methodology or method of assessing the results. With the recognition that a standard method of testing was required the first permanent fire testing facilities were built in London in 1899 and three years later in the United States. The British tests stated two criteria that should be met for a floor to be satisfactory; collapse should not occur and flames must not show through the floor. From 1906 the deflection of the floor was also measured, however, no limit was imposed.

At this time the fire that was applied to the floor was not specified. Each testing facility had their own method of representing the temperature evolution of a fire over time. Typically this consisted of a temperature which must be applied for a certain length of time. The British Fire Prevention Committee was the first to propose a standard method that was widely accepted by the testing community [20]. Published in 1903 it

consisted of only one table specifying the test length and the minimum length of test for three classes of required fire endurance.

An American standard for floors followed four years later and specified that an average temperature of not less than 926^{o}C was to be maintained for 4 hours. Success was achieved provided no flame or smoke passed through, collapse did not occur and at the end of the test there was no permanent deflection greater than 1/96 the length of the element.

Neither of these two standards considered the heating rate during a test and this led to a revised American standard being proposed in 1917. This contained a specified temperature-time curve based on the results of tests carried out in New York in 1902. The curve did not bear any resemblance to the actual temperature-time curve in a real building fire and was constructed without any knowledge of what this might look like. This was partly as the variables that controlled the fire temperature were not known at this time.

Current fire resistance tests

Fire resistance testing in Britain is currently carried out to BS476 Part 20 [21]. Tests are carried out in a furnace, the temperature of which is controlled by the rate of fuel supply. Over the duration of the test the rate of fuel supply is altered so that the temperature-time curve follows that of the BS standard fire curve which can be described mathematically as:-

$$T = T_o + 345log(0.133t + 1) \tag{2.2}$$

where T is the temperature of the combusted gases, averaged from a number of points in the furnace, and t is the time of the fire in seconds.

The actual fire exposure of the element is a function of the properties of the walls lining the testing furnace. Radiative heat flux is the primary mode of heat transfer so furnaces with a low thermal inertia will rapidly heat the element whereas those with a high thermal inertia will take much longer. It is unlikely that two furnaces would be capable of giving the same test result [22].

Boundary conditions in a test to BS476 should be similar to those found in the construction. If they are unknown, however, then they are taken to be simply supported.

BS476 assesses the fire resistance of the structural element being tested in terms of three criteria:-

- load bearing
- insulation
- integrity

Testing the insulation ensures that the temperature rise on the unexposed surface of the element does not become too large. Similarly, it is essential that the structural integrity of the element is maintained so that the fire can not spread through cracks that may occur. There are two possible modes of load-bearing failure:-

- the maximum deflection exceeds $L/20$
- the rate of change of deflection exceeds $L^2/9000d$ (mm/min)

where L is the length of the element being tested and d is the depth.

Limitations of fire resistance testing

In its current form the standard fire resistance test is unscientific and does not represent realistically the conditions found in a fire. It was recognised in the 1920s that the temperature-time curve used was inappropriate as it is not representative of a real fire. A number of fire tests were carried out by Ingberg [23] in an attempt to measure actual fire temperatures in real office fires. From these Ingberg concluded the only variable that affected a room fire was the fuel load and so rooms with different fuel loads would require different temperature-time curves. To get around this he introduced his 'equal area severity hypothesis' which states that it was the area under the temperature-time curve that mattered rather than the curve itself. If two fires have the same area under the curve then they can be said to have been of equal 'intensity'. This was seen to

justify the use of the standard temperature curve and formed the basis of the current fire resistance test. Ingberg's hypothesis is scientifically incorrect, however, as the radiative heat flux that an element is exposed to is a function of T^4 [22].

The test only considers individual elements and is not suitable for testing structural assemblies that would allow the effect of interaction between sets of elements and their boundary conditions to be studied [24]. This is extremely limiting as it has been shown that only a small amount of restraint has a significant effect on the structural response of a single structural element to fire [15]. As it is difficult to determine the level of restraint that will occur elements are often tested with simply supported boundary conditions. Ignoring any restraint will result in the strength of the tested element to fire being underestimated.

Finally, the load-bearing failure criteria of the test are inappropriate. Defining a limiting deflection in terms of element lengths at ambient temperatures ensures safe design, however, in a fire this is not a suitable approach. Due to the large strains caused by thermal expansion, large deflections do not necessarily correspond to large and damaging mechanical strains. Using a failure deflection of $L/20$ equates to a limiting strain of only 0.6%. A beam could be at this deflection limit and yet still have a large reserve of strength as all of the strain could be due to thermal expansion.

Despite the many flaws of the fire resistance test in its current format it is still widely accepted. This is primarily because no building is known to have failed that has shown the method to be unsafe prior to the recent failures at the World Trade Centre complex, particularly WTC 7 where the failure was solely due to the fire.

2.2.2 Fire resistance by calculation

British Standards

BS5950-Part 8 [25] provides recommendations for determining the fire resistance of steel structures. It considers the fire limit state to be an accidental limit state which allows non-permanent imposed loads to be reduced using appropriate safety factors as shown in Table 2.1. The code specifies two performance criteria which should be met:-

1. Members should maintain their load capacity for the required period of fire resistance.

2. Integrity and insulation requirements should be maintained.

If the steel member has been hot-rolled then, as an alternative to testing, the fire resistance can be determined by calculation. Two methods are described either of which may be used, these are the limiting temperature method and the moment capacity method. Both make use of the load ratio concept:

$$\text{Load ratio R} = \frac{\text{Load at fire limit state}}{\text{Load at ambient conditions}} \tag{2.3}$$

Columns, tension members and beams with low shear load may be designed using the limiting temperature method. The limiting temperature is defined as the temperature of the element at failure in a fire. If this is not less than the design temperature (the temperature of the element at the end of the required fire resistance period in a fire test to BS476) for a given load ratio then the element can be left unprotected, otherwise protection is required. For common lengths of fire resistance period tables within the code specify the design temperature for elements of different section size. The limiting temperature is a function of the load ratio, the temperature gradient, the stress profile and the dimensions of the section.

An alternative method of design is the moment capacity method and this can be applied to beams with either plastic or compact webs. The moment capacity of the section can be calculated if the temperature profile through the section is known. If this is greater than the applied moment at the fire limit state then the member can be left unprotected.

BS5950-Part 8 was the first design code to allow the fire resistance of a member to be determined by calculation, however, it has a number of limitations:

1. it only allows use of the standard fire

2. it does not consider structural continuity or interaction with the surrounding structure

3. it can only be used for hot-rolled sections

Load	γ_f
Dead load	1.00
Imposed loads:	
a) permanent	1.00
b) non-permanent	
1) in escape stair and lobbies	1.00
2) all other areas	0.80
Wind loads	0.33

Table 2.1: BS5950-8 load factors for fire limit state

BS5950-Part 4 [26] covers the design of composite floor and roof slabs. It allows their fire resistance period to be taken as 30 minutes if simply-supported and with no protection. Where there is continuity over supports then this can be taken advantage of to give a higher capacity provided that the reinforcing steel has sufficient ductility. Calculation of the load capacity is carried out assuming a flexural failure with unlimited redistribution of moments allowed. A minimum slab thickness based on the geometry of the slab ensures that the topside of slab does not get sufficiently hot that fire will spread to the compartment above. To ensure that the fire cannot spread by flames travelling through cracks the profiled steel sheeting must form a continuous membrane.

BS8110 provides rules for the design of concrete structures [27]. The methods provided for design for fire in BS8110-Part 2 [6] are very similar to those for steel. Three methods are allowed; use of tabulated data, fire testing or the use of fire engineering calculations. The code recognises that the fire resistance of a complete structure will not be the same as that of the individual members and that continuity of reinforcement, composite construction and redundancy will lead to improved fire performance.

The most straightforward method is the use of tables and these contain minimum dimensions of the element and minimum cover to the main reinforcement for common periods of fire resistance. Account is taken of the type of concrete (dense or lightweight), whether it is reinforced or pre-stressed and the end support conditions. The values are based on data from testing and aims to limit the temperature in the main reinforcing bars such that it does not exceed 550^{o}C at which point it will have lost 50% of its ambient temperature strength. Abridged versions of these tables are included in

Load	γ_f
Dead load	1.05
Imposed loads	1.00

Table 2.2: BS8110-2 load factors for fire limit state

BS8110-Part 1 [27] which is the general section of the code.

The use of fire resistance calculations are only allowed for members carrying load through flexure. It is stated that the behaviour of such elements in fire is governed by the compressive strength of the concrete and the tensile strength of the reinforcement at elevated temperature. No consideration is given to forces or deflections induced by the change in temperature. When carrying out such a design the safety factors as shown in Table 2.2 are different from those contained in BS5950-Part 8 for steel buildings. Unlike the steel code no distinction is made between permanent and non-permanent imposed loads and a safety factor of 1 is used for both. The dead load is increased by 5% from ambient.

Eurocodes

The Eurocodes define two performance requirements for fire resistance; mechanical resistance and compartmentation. Depending on its role a member will be designed to meet either one or both of these criteria. Where mechanical resistance is required it is stated that 'the member will be designed and constructed in such a way that they maintain their load-bearing function during the relevant fire exposure'. There are four allowable methods which can be used to determine the fire resistance of a structure or part thereof:

1. Global structural analysis
2. Analysis of parts of the structure
3. Member analysis
4. Testing

The design methods presented in the Eurocodes are more general than in the British Standards. Simplified methods similar to those in the British Standards allow a quick

analysis to be carried out using either tables or simple calculations but they also provide scope for more complicated methods to be used as long as they analyse the structural behaviour using fundamental principles of structural mechanics. Compatibility between all parts of the structure must be ensured and the analysis should include geometrical non-linearity and thermally induced strains and stresses due to temperature rises and thermal gradients. This gives the engineer the opportunity to use advanced numerical models or alternative design methods as they are developed.

Eurocode 2 Part 1.2 [28] covers design of concrete elements against fire. The tabulated data is presented in a similar fashion to BS8110 with minimum concrete thicknesses and reinforcement covers being specified. Consideration is given to the boundary conditions of the slab (1-way or 2-way spanning) and if 2-way spanning then the required cover is dependent on the aspect ratio. Slabs with an aspect ratio between 1.5 and 2.0 are required to have more cover than those with an aspect ratio between 1.0 and 1.5.

Determining the fire resistance using the simplified calculation method is different to that in the British Standard. The hottest part of the concrete cross-section is ignored with the amount of concrete that is ignored depending on the temperature distribution through the member and the number of surfaces exposed to the fire. Reduced material properties should then be used to determine the load bearing capacity.

Simple calculations for the analysis of structural steelwork for fire can be carried out in two ways according to Eurocode 3 [29]. The strength of the member can be determined by calculating the design resistance using reduced material properties. Alternatively, the critical temperature of the element can be determined based on the utilisation factor of the element in ambient conditions. The higher the utilisation factor the lower the critical temperature.

Advanced analysis techniques meeting the same requirements as for analysis of concrete structures can also be used for the design of individual members, sub-assemblies or entire steel structures.

2.2.3 Passive protection methods

A fire engineer has a number of passive methods available to limit the temperature rise in a steel element exposed to fire. The choice of system will depend on the required

fire resistance, weight, aesthetics, durability and cost effectiveness.

Concrete encasement is a traditional method of fire protection and was the most common up to the late 1970s. [30]. The approach is expensive, takes a lot of time to apply and the finish is very bulky with a resulting increase in the weight of the building. Prescriptive codes generally provide tables stating the required thickness of concrete for a given fire resistance rating. An advantage of encasement is that in corrosive environments the fire protection is still maintained.

Rigid boarding, spray-on materials and intumescent paints now account for 85% of the fire protection market [31]. Use of spray-on cement based materials [32] provides the cheapest form of protection for steel members. Fibres added to the mix ensure that it holds together. It is easy to apply the protection especially to complicated details at connections, however, it is a wet-process which is messy and the finish cannot be decorated making it unsuitable for exposed members. An alternative is the use of boarding which is usually manufactured from either gypsum plaster or calcium silicate. The boards are fitted by attaching them to a frame, usually made of metal or wood, that sits on the steel member being protected. Although slower to install and more expensive than spray-on systems they are easy to construct and the installation is a dry process. Use of boarding allows the protected surfaces to be decorated so it is often used for columns which are usually exposed. If hollow steel sections are used then they can be filled with concrete. The concrete draws heat away from the steel exterior and as the steel weakens can start to carry the load. This method results in there being no external protection and is particularly suitable for use in seismic regions.

In comparison to cement based protection, organic coating methods require a thinner protective layer and are more resistant to mechanical damage [33]. For office buildings the most popular organic method of providing protection is the use of intumescent paints which provide many advantages over the methods previously discussed, particularly from an aesthetic perspective. It is commonly used on exposed steel frames as it has the same appearance as a normal decorative paint. When heated the intumescent, which is normally an epoxy-based material, expands at a temperature of approximately 200^oC to form a protective foam barrier [34]. The expanded foam has a low thermal conductivity which limits the temperature rise of the steel underneath.

Paints, although relatively expensive, have a number of advantages over other

protection systems; they can be quickly applied and do not take up much space. As they can be applied off-site the construction period can be reduced [31] (fire protection application is usually on the critical path of a project) and quality control improved. It may be necessary to apply several coats, however, to obtain the necessary fire resistance rating.

For a concrete structure or a concrete slab in a steel-framed structure the required fire resistance is usually achieved by limiting the temperature rise in the reinforcement bars. Normally the concrete cover provides sufficient insulation but if not it is possible to apply external protection such as boarding or plaster. This may be necessary if it is required to limit the weight of the structure. When external protection is used it is possible to calculate an 'equivalent concrete layer' which would provide the same degree of protection to the reinforcing bars [35].

2.3 Design of concrete slabs incorporating membrane behaviour

Concrete slabs are designed to carry load through bending using small-deflection theory [27]. A number of different methods exist for determining the load capacity of a slab. The yield line method developed by Johansen [36] is one such method and is typical in that it considers moments and shears and assumes that there are no membrane forces in the slab. In fact membrane forces will always exist and, in general, they increase the amount of load that a slab can carry. Membrane enhancement in slabs takes two forms; compressive membrane action and tensile membrane action. Their development is dependent on the degree of restraint along the slab boundaries. The load-deflection behaviour of both a simply-supported and a laterally-restrained slab are shown in Fig. 2.1.

Put in fig. 5.41 from Wang book.....

Where a slab has lateral restraint to movement then compressive membrane forces will rapidly develop if the slab deflection is less than its depth. As the slab deflects its edges try to move out and as it is prevented from doing so compressive forces are generated creating an arching action between opposite supports. This allows the slab

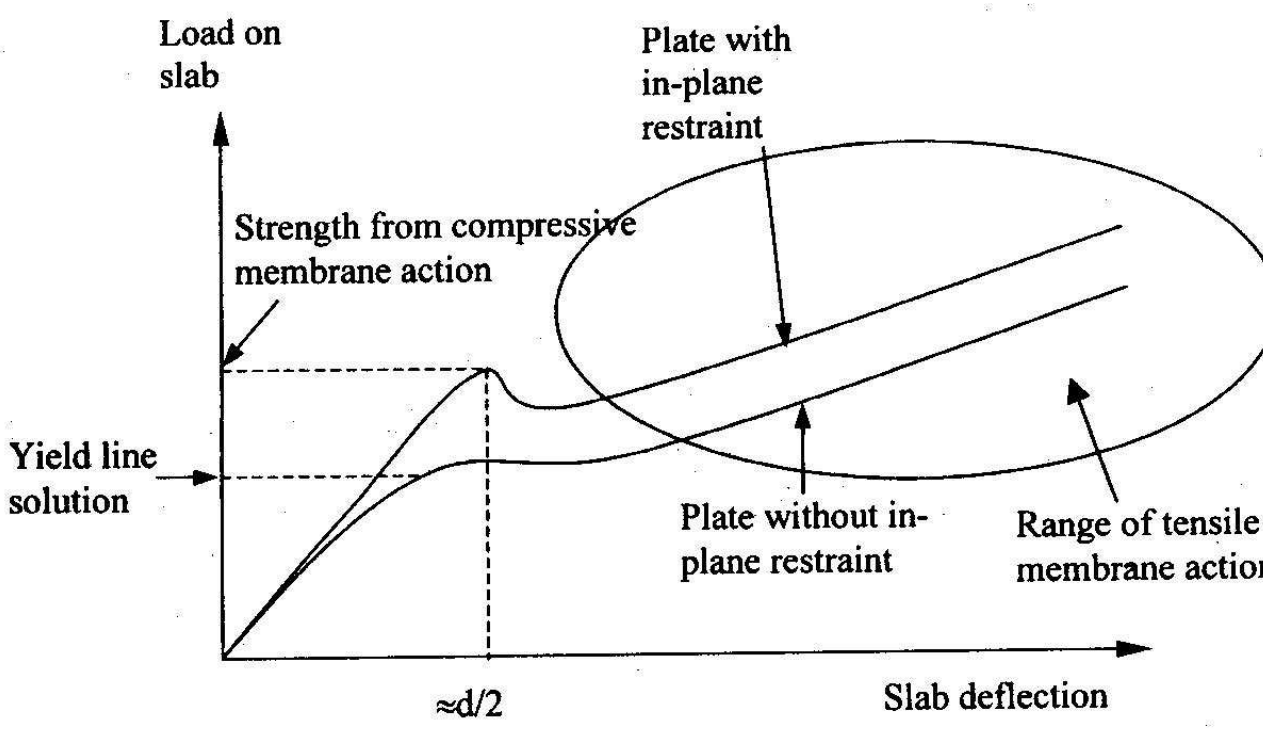

Figure 2.1: Load-deflection behaviour of concrete slab [1]

to carry a load considerably greater than that predicted by yield-line theory as shown in Fig. 2.1. Beyond the point of peak load under compressive membrane action the capacity temporarily decreases as the compressive forces reduce. This could lead to a sudden large increase in deflection as the slab 'snaps through'. Although compressive membrane action increases the load capacity it is an unstable mechanism and so engineers are not likely to make use of it for standard design. Simply supported slabs cannot develop compressive membrane action because they have no lateral restraint.

Tensile membrane action is a far more stable load carrying mechanism. At sufficiently large deflection full depth cracks will have developed through the slab. As this results in there being negligible bending resistance across any yield lines the load must be carried through tensile forces in the reinforcing bars. If the slab is laterally restrained the force is transmitted to the boundary as shown in Fig. 2.2. Failure of the slab occurs when the reinforcement ruptures due to large mechanical strains. Tensile membrane action will only occur in strips in the centre of the slab where the deflections are highest. Along the edges of the slab where deflections are low there are strips where compressive membrane action is occurring.

Although not able to develop compressive membrane action simply supported slabs can carry load through tensile membrane action. The restraint to the tensile forces in the reinforcement comes through the formation of a 'compressive ring' as the edges of the slab try to pull in. Figure 2.3 shows the position of the ring around the boundary of the slab, however, the degree of restraint provided by the compressive ring has never been quantified. The tensile membrane load capacity of the laterally restrained slab is larger than that of the simply supported slab as shown in Fig. 2.1. This is due to the difference in lateral restraint.

Put in fig 2.19 from Susan's thesis.....

Put in fig 2.20 from Susan's thesis.....

Many researchers have studied the membrane behaviour of slabs and proposed methods for determining their load capacity. Park [37] produced a method for determining the tensile membrane behaviour of slabs with fully restrained edges that produced conservative results in comparison with with those from experiments. Recently Eyre proposed a solution to determine the compressive membrane strength of one-way

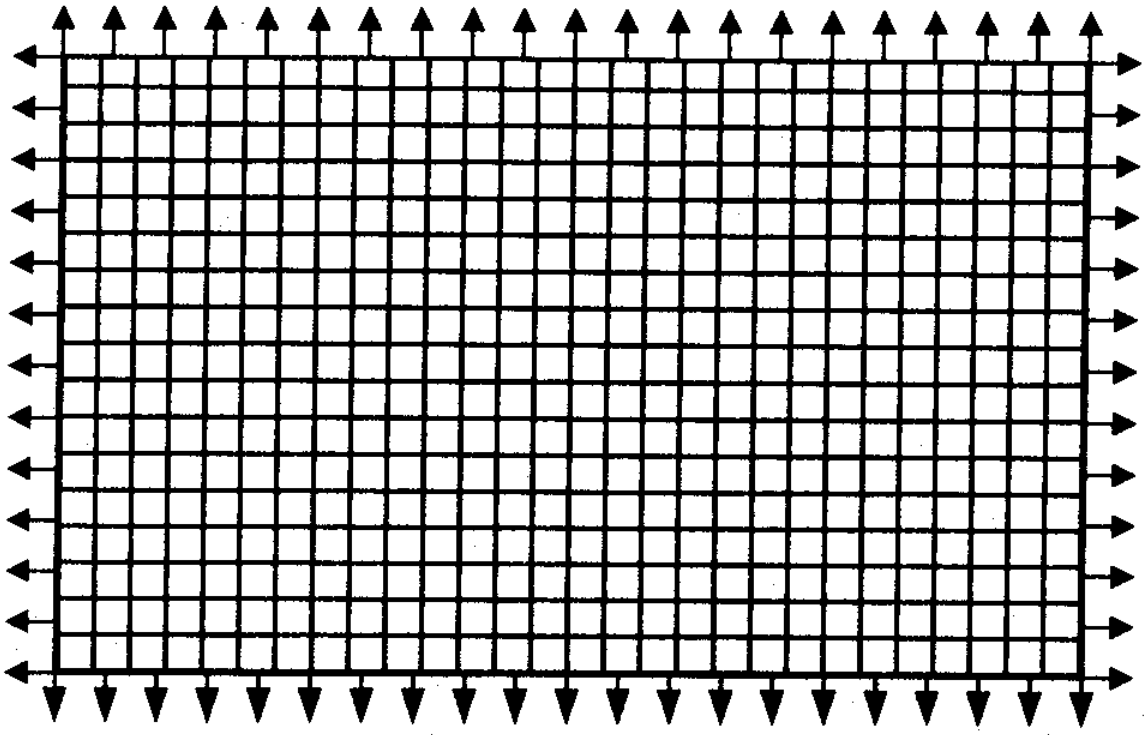

Figure 2.2: Tensile membrane forces in a laterally restrained concrete slab []

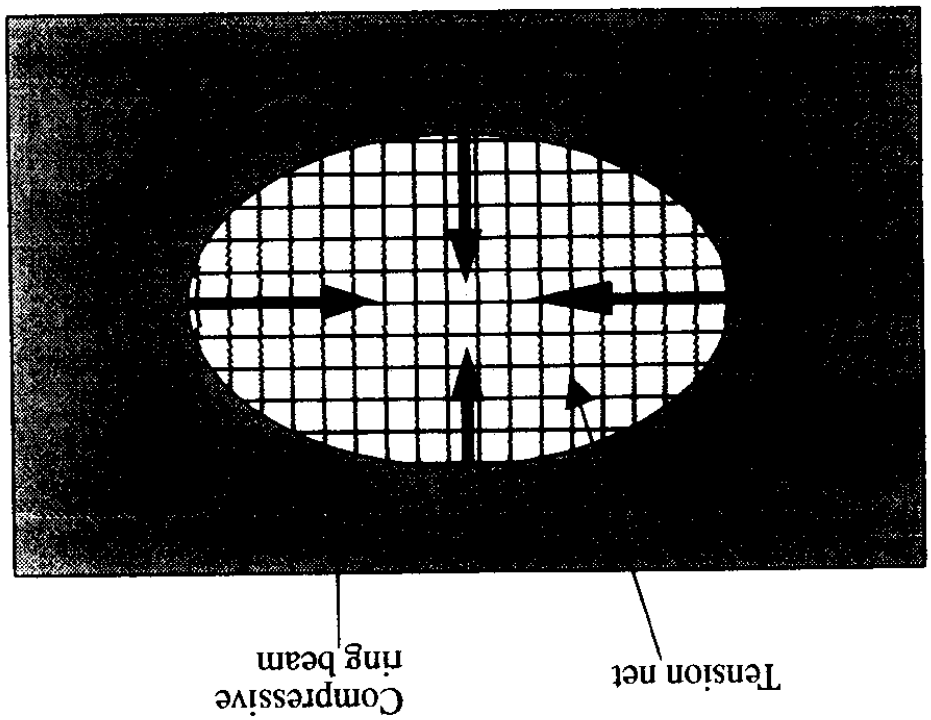

Figure 2.3: Tensile membrane forces in a simply supported concrete slab []

spanning and isotropic square slabs [38]. These methods, however, are not suitable for designing slabs for ambient conditions. The deflection necessary for a slab to develop tensile membrane action would not allow serviceability requirements to be satisfied. Although compressive membrane action does not require such large deflections it is not suitable due to its unstable nature.

When designing for fire the large deflections necessary to develop tensile membrane action are not such an issue. As fire is an accidental state serviceability requirements do not need to be met. This has led a number of researchers to develop design methods for slabs in fire which incorporate tensile membrane action [39, 40].

2.4 Performance based design

Countries that follow prescriptive design codes do not allow designers any freedom to obtain solutions to engineering problems. Instead the design solution must conform to rules which, although easy to use, are very limiting and do not allow innovation. In the case of designing for fire protection these would specify sprinkler spacing or, for an allowable material, the thickness of protection that should be applied. Materials that were not listed could not be used even if they provided better fire resistance than those which were.

More and more countries are moving to performance based design methods. Whereas prescriptive codes specify a solution, performance based codes specify performance objectives. It is the role of the designer to decide how best to achieve these objectives. This allows the engineer to produce a solution that is specific to the problem and so can consider the loss potential or unusual structural layouts. Although the initial costs to the client of a performance based design solution are higher than for a prescriptive design the potential savings could be many times this initial outlay.

The philosophy of a performance based code can be described as [41]:

1. State objectives clearly.
2. Specify performance requirements clearly.

3. Allow any solution which meets these requirements. Also allow the use of new knowledge as it becomes available.

These allow the designer to be much more flexible in obtaining a solution. In the case of unusual structures the fire engineering approach used will not be one developed to meet the requirements of more typical buildings. Comparing prescriptive and performance based codes Hadjisophocleuos et al [42] found that there were three main advantages of performance based codes:

1. they facilitated the use of new knowledge and technology
2. they were flexible enough to be used in one-off and unusual structures
3. they led to cheaper designs

A further advantage of a performance based solution is that the design is integrated rather than consisting of a series of systems all designed individually [43]. This will lead to a more cost-effective solution and improved knowledge of the loss potential. In producing a prescriptive design the loss potential is unknown.

One of the difficulties of performance based designs is the difficulty in proving that a design meets the prescribed requirements [**?**, 44]. This is particularly true in an area such as fire safety engineering where the technology is developing extremely rapidly and often the only method of doing this is using complex computer models which have been validated against large scale fire tests. Approving authorities may be reluctant to accept a design if they do not have a full understanding of the methods used.

Many modern design codes use a multi-level approach to fire engineering [18]. Objectives are specified and various methods are allowed to achieve these. Generally these consist of a prescriptive method, an approved calculation method and a performance based alternative. The Eurocodes [28, 29] have used this approach which allows the use of new performance based design methods such as that produced by the SCI for the design of steel framed buildings [45].

BS7974 [46] was released in the UK in 2001. The code describes the fire safety engineering philosophy to be adopted for the design of buildings and outlines the

principles to be used in obtaining a solution. A series of Published Documents accompanies the standard and these provide practical guidance on its application. It is intended that the standard, which does not contain methods of calculation but rather the intended objectives, will not be required to be updated very often whereas the published documents can be updated regularly as new methods of analysis appear [47]. Published Document 3 [48] deals with structural design for fire. Unlike BS5950 and BS8110 it recognises that the fire itself can create loads such as those due to thermal expansion that need to be considered, however, it allows users to design elements to these codes. Use of new performance-based methods such as those produced by the Steel Construction Institute are also allowed [45].

2.5 Material behaviour at elevated temperature

At high temperatures the material properties of steel and concrete are considerably different to those at ambient. With increasing temperature the strength and stiffness of both materials decrease whilst their ductility increases. At a time t in a fire the total strain ϵ consists of four different components:

$$\epsilon = \epsilon_\sigma (\sigma, T) + \epsilon_{th} (T) + \epsilon_{cr} (\sigma, T\ , t) + \epsilon_{tr} (\sigma, T) \tag{2.4}$$

The mechanical strain ϵ_σ is the strain induced by mechanical stresses in a member and is determined by the stress-strain-temperature relationship for a particular material. Thermal strains ϵ_{th} are caused by the increase in temperature. Depending on the amount of restraint and the temperature distribution within a member these can induce large deformations or stresses. Creep strain ϵ_{cr} is caused by the long-term deformation of a material acted upon by a constant load. It becomes more significant at higher temperatures as materials start to lose their strength. The final strain component is transient strain, ϵ_{tr}, and this only occurs in concrete. It is due to the expansion of the cement paste the first time the material is heated.

The increasing use of analytical techniques for the design of structures against fire requires validated models describing the material behaviour at elevated temperature [49]. It is important that when testing a material the test should be carried out in a

way that is consistent with the anticipated temperature exposure that will be found during a fire [18].

2.5.1 Material properties of steel under elevated temperature

Stress-strain-temperature behaviour

For normal structural design the load capacity of a structural steel element is calculated based on its yield stress. Determination of the yield stress is straightforward at ambient temperatures as it is clearly defined allowing the stress-strain behaviour of steel to be adequately represented by a simple bi-linear relationship. Up to the yield stress linear-elasticity is assumed beyond which the steel deforms at constant stress. With increasing temperature the stress-strain relationship of steel becomes increasingly non-linear as can be seen in Fig. 2.4 and both the strength and stiffness decrease. Above approximately 200^oC the yield point where the the material moves from the elastic regime to the plastic regime becomes less well defined. This requires use of the proof stress concept to define a yield stress [50]. The yield stress is defined as that measured at a predefined strain, typically between 0.2 and 1%.

Put in fig 8.24 from Buchanan book.....

Stress-strain curves used for design are based on the results from tensile testing. To determine the relationship at an elevated temperature there are two possible methods [51, 52]; isothermal testing or anisothermal testing. In an isothermal test the specimen is heated to a constant temperature. Strain is then applied at a constant rate and the stress measured. For anisothermal testing a load is applied and the sample is then heated at a constant rate. It is necessary to carry out a test with zero load applied so that the thermal strain-temperature relationship is known. For a given temperature the thermal strain is then subtracted from the total strain obtained from the test to give the stress-strain curve. Neither method gives a realistic representation of the conditions found in a fire as it is likely that a combination of the two testing methods will be found.

Eurocode 3 [3] provides a set of equations describing the stress-strain curves for use in design. These include strain hardening at temperatures below 400^oC. The effects of

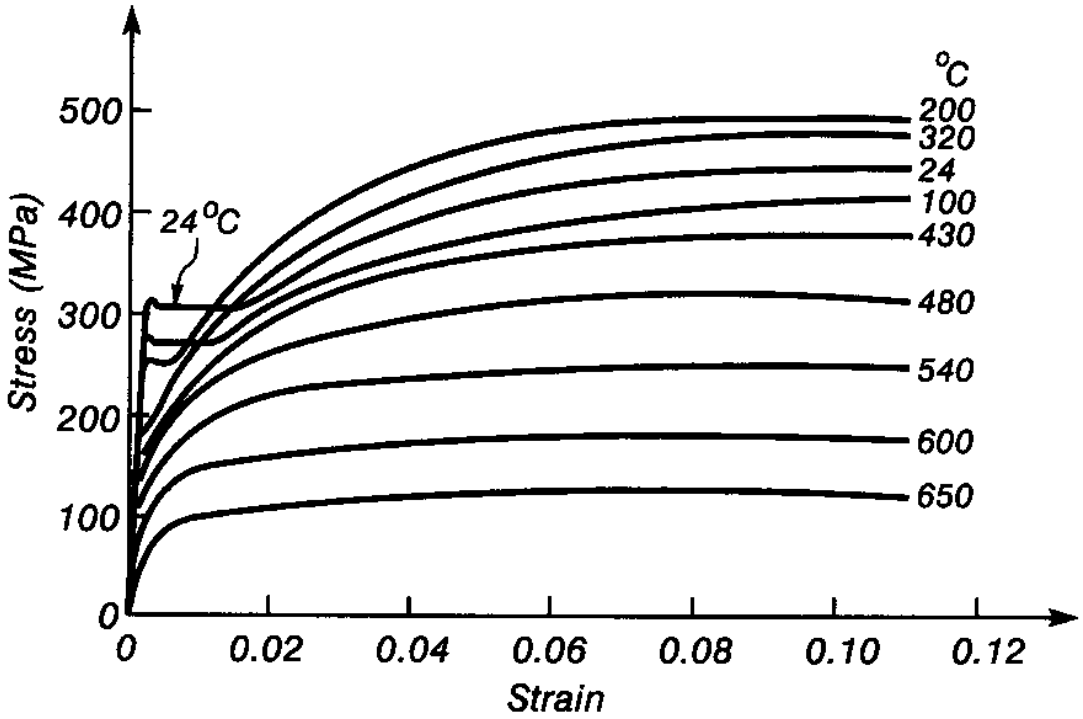

Figure 2.4: Stress-strain-temperature relationship for steel [2]

increasing temperatures are accounted for by using a set of reduction factors as shown in Fig. 2.5.

Put in fig 8.30 from Buchanan book.....

Thermal expansion

The expansion or shrinkage of a material caused by temperature change is measured by its coefficient of thermal expansion. It is defined as the expansion of a unit length of material when its temperature is increased by 1^oC:

$$\alpha = \frac{\epsilon_{th}}{\Delta T} \tag{2.5}$$

where ϵ_{th} is the thermal strain and ΔT is the change in temperature of the specimen.

Up to a temperature of 700^oC the thermal expansion of steel is approximately linear as shown in Fig. 2.6. Between 700 and 800^oC a phase change occurs in the steel as it changes from pearlite to austenite which causes a shrinkage in the steel of approximately

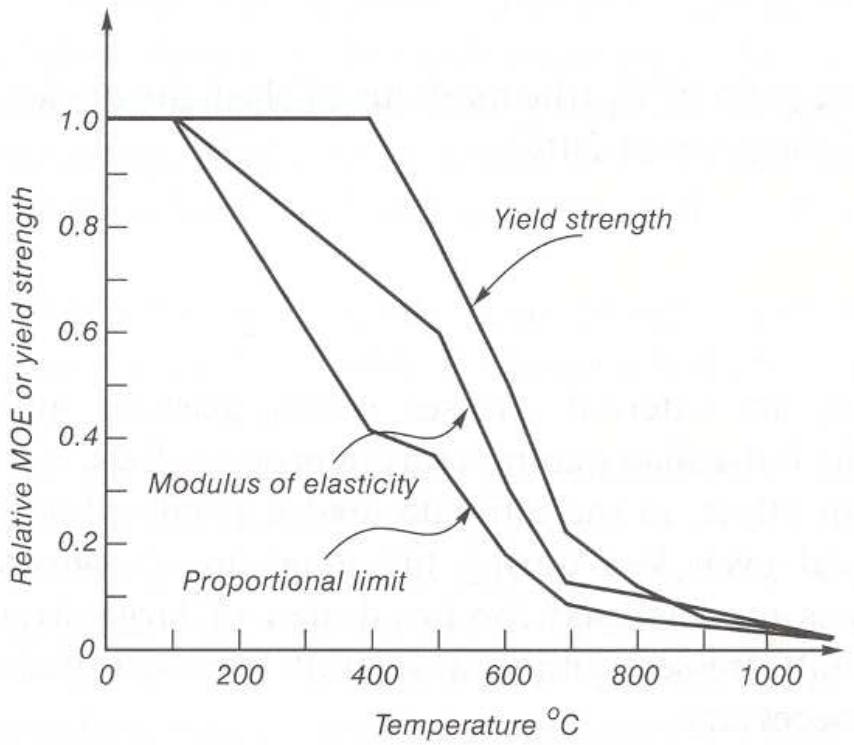

Figure 2.5: Eurocode 3 reduction factors for yield stress and Young's modulus of steel [3]

15%. Although the type of steel does not greatly affect the thermal expansion coefficient [52] the shape of the thermal expansion-temperature curve in the region of the phase change depends on the carbon content [50].

When used for design it is normal to assume an average value for the coefficient of thermal expansion. BS5950-Part 8 assumes a value of $14\text{x}10^{-6}$ [25]. A more thorough approach is adopted in Eurocode 3 [3] where a set of three equations is used to describe the thermal expansion strain that occurs in steel up to a temperature of 1200^{o}C. Three regions are used which allows the effect of the phase change to be incorporated.

Put in fig. 7.25 from Lie p.142.....

Poisson's ratio

The Poisson's ratio of a material is the ratio of its lateral strain to longitudinal strain. Reported values of Poisson's ratio do not appear to vary significantly with temperature. Clark [53] reports a value of 0.27 at 20^{o}C increasing to 0.31 at 650^{o}C. These results are consistent with other tests showing a value of 0.34 at 1000^{o}C [50].

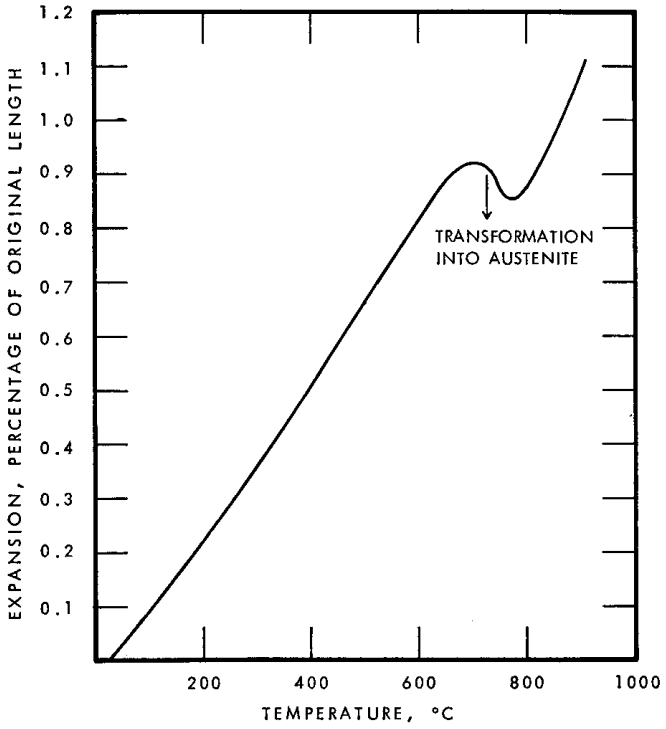

Figure 2.6: Thermal expansion coefficient of steel [4]

Creep behaviour

Creep strains occur when, under constant loading, the deformation of a material increases over time. Although not significant at normal temperature and stress levels, above 400 or 500^{o}C the effect of creep can be significant. Creep is both temperature- and stress-dependent and the rate of creep strain increases as temperature and stress increase. EC3 [3] includes creep strain implicitly in its stress-strain curves.

2.5.2 Material properties of concrete under elevated temperature

Stress-strain-temperature behaviour

Due to the composite nature of concrete its stress-strain relationship is highly complex as it behaves very differently depending on whether it is in compression or tension. Failure occurs by crushing in compression but cracking in tension which leads to a discontinuous stress-strain curve very different from the ductile curve of steel. Its strength in tension is typically taken as being 10% of the compressive strength [7]. A

number of factors affect the strength of concrete such as the amount of cement paste, the type and size of aggregate, the water/cement ratio and the age of the concrete. This also leads to the behaviour being less predictable than that of steel.

Figure 2.7 shows the compressive stress-strain relationship of a typical concrete at different temperatures. As the concrete is heated the ultimate compressive strength and Young's modulus decrease, however, the ductility increases [54].

Put in fig. 9.13 from Buchanan p.241.....

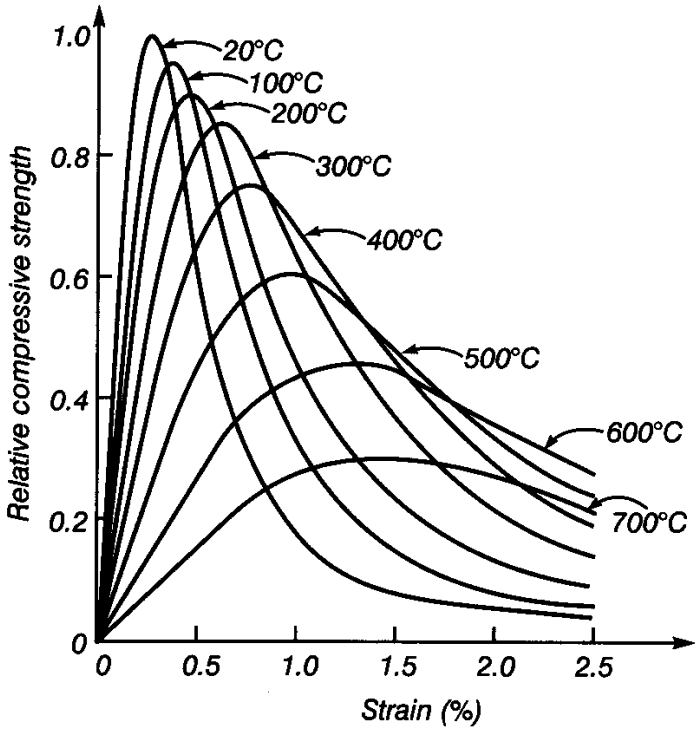

Figure 2.7: Stress-strain-temperature for concrete in compression [5]

The simplest concrete models use a bi-linear curve to represent the compressive region and assume zero strength in tension. Eurocode 2 [5] uses a cubic equation to describe the stress-strain behaviour and the formulation implicitly includes the effects of creep. Eurocode 2 allows the designer to assume the tensile strength is negligible. Figures 2.8 and 2.9 show the design values used in BS8110 for the reduction of the concrete crushing strength and Young's modulus with temperature. The dotted line in Fig. 2.9 was a later revision added so that the temperature at which the crushing strength and Young's modulus reach zero are the same.

Put in fig. 9.15 from Buchanan p.243.....

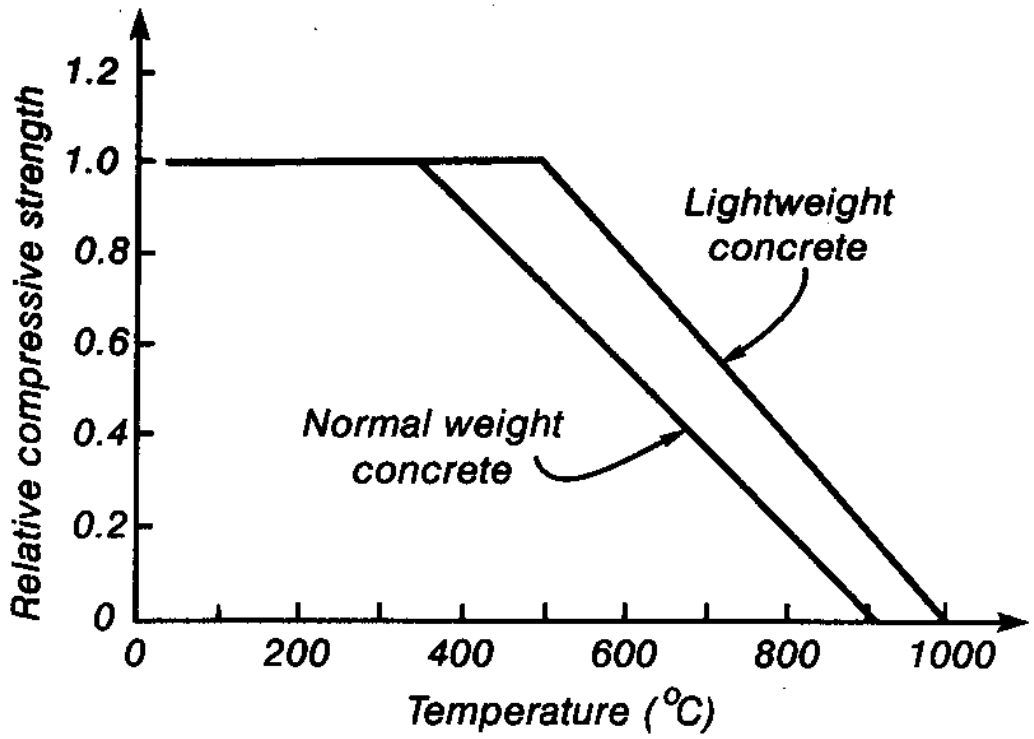

Figure 2.8: BS8110 reduction factors for crushing strength of concrete [6]

Put in fig. 9.16 from Buchanan p.243.....

Thermal expansion

The thermal strain of concrete as it heated depends on the type of aggregate, the quantity of aggregate, the rate of heating and the stress level [55]. Cement paste expands up to a temperature of 100^{o}C and then starts to shrink due to water evaporating and chemical changes in the material. This is illustrated in Fig. 2.10 which shows the thermal strains of different concrete mixes under heating.

Put in fig. 15 from Schneider FSJ paper.....

The main factor affecting the thermal expansion coefficient is the type of material used for the principal aggregate [7] and it is common for the thermal expansion-temperature curve of the concrete to follow that of the aggregate [2]. In the case of weak principal aggregates such as pearlite and vermiculite, however, they are not strong enough to

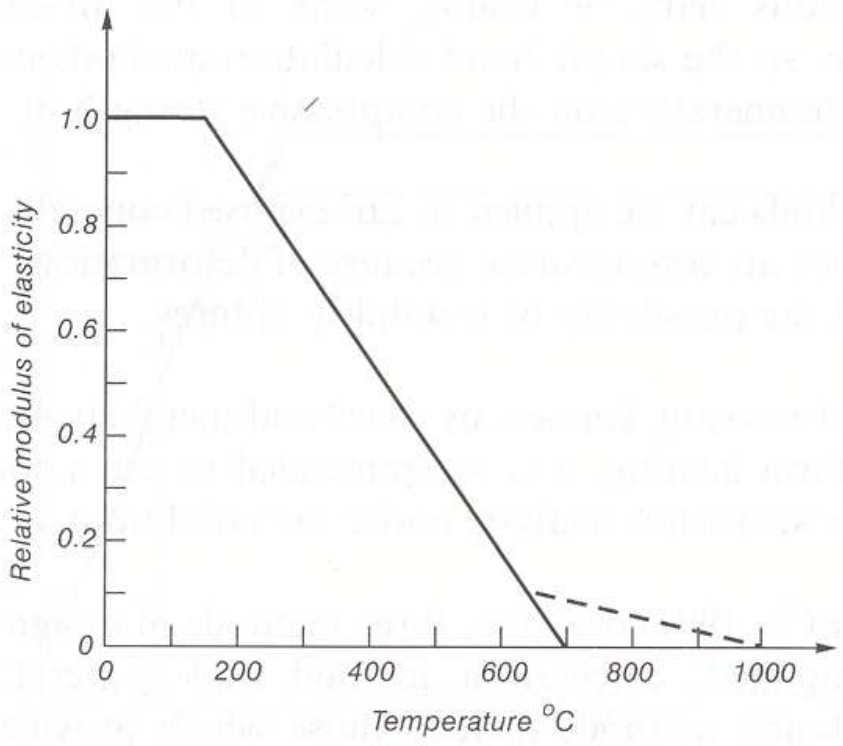

Figure 2.9: BS8110 reduction factors for Young's modulus of concrete [6]

resist the shrinking of the cement paste and therefore the thermal strain curve follows that of the paste.

In Eurocode 2 [5] a constant value of 8 x 10^{-6} is assumed for the thermal expansion coefficient up to a temperature of 1000^{o}C.

Poisson's ratio

Limited data is available on the effect of temperature on the Poisson's ratio of concrete. In 1985 Ehm [56] carried out a study and found that under ambient temperature conditions the value of Poisson's ratio is constant up to a load level of approximately 70% of the ultimate load. As temperature increases the load level at which the value of Poisson's ratio starts to increase rapidly decreases as can be seen in Fig. 2.11.

Put in fig.11 from Schneider FSJ paper.....

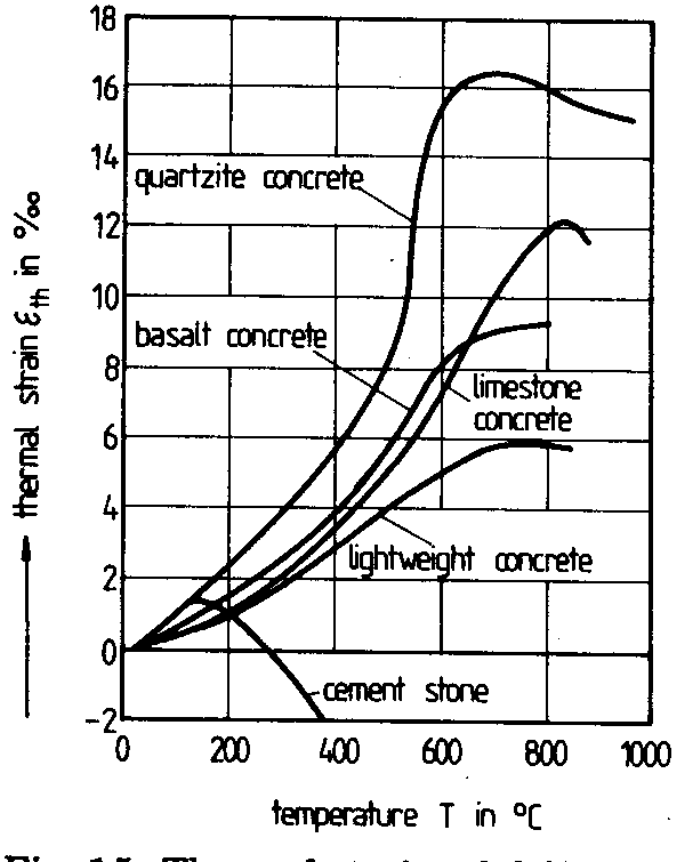

Figure 2.10: Thermal expansion strain of different concretes [7]

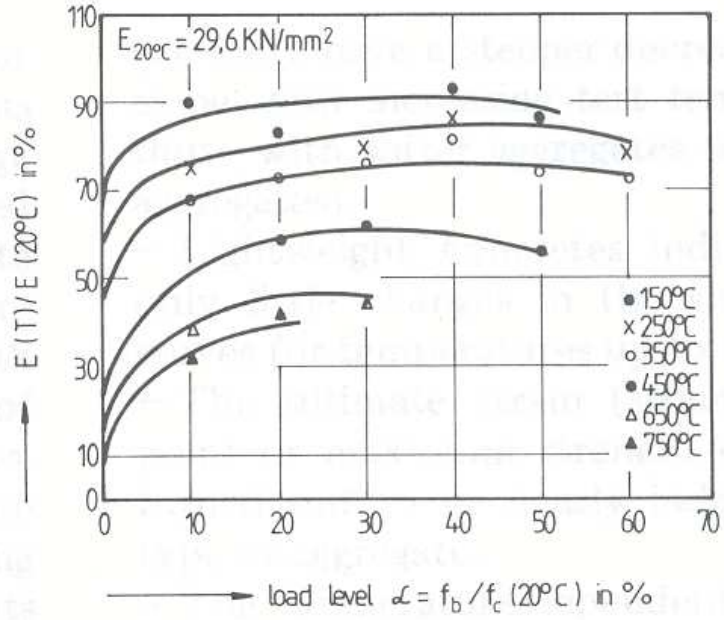

Figure 2.11: Effect of temperature on Poisson's ratio of uniaxially loaded concrete at high temperature

Creep behaviour

The creep of concrete consists of two components; that of the cement paste and that of the aggregate. It is the ability of the cement paste to creep that ensures the concrete does not fall apart due to the thermal incompatibility between the paste and aggregate. Based on an elastic analysis Lea and Stradling [57] predicted that concrete would otherwise break down at approximately 100^{o}C.

Spalling

Concrete is very susceptible to spalling at the high temperatures experienced in a fire. It is generally thought that spalling is caused by the water vapour released from the cement paste during heating [41] leading to high pore pressures creating tensile stresses greater than those which the concrete can tolerate. In this instance spalling is most likely to occur in concrete with a high moisture content and low permeability, however, other factors such as local stresses and differential thermal expansion between the cement paste and aggregate and concrete and reinforcement also contribute [2]. It is more likely, however, that spalling is due to restrained thermal expansion [58]. This creates compressive stresses parallel to the exposed surface which are released by brittle fracture of the concrete.

2.6 Conclusion

Current methods of determining the fire resistance of steel and concrete structures have been described. Shortcomings of the fire resistance test and simplified calculation methods have been discussed. The material behaviour of steel and concrete at elevated temperatures has been described.

Chapter 3

Behaviour of Composite Steel Framed Structures in Fire

3.1 Introduction

Before the Cardington frame tests of 1995/96 a number of other full-scale fire tests had been carried out to study structural response to fire. In Australia BHP undertook tests for a specific building in Melbourne whilst in Germany, the University of Stuttgart-Vaihingen examined the benefits of various construction techniques [59]. Although they showed the inherent fire resistance of modern buildings the tests were not thorough enough to allow broad conclusions to be made about structural response to fire.

The Broadgate fire of June 1990 demonstrated that a modern composite steel-framed building without fire protection can withstand a severe fire. This led to six full-scale tests being carried out on the Cardington building. From the tests and subsequent numerical and theoretical studies the structural behaviour of modern composite steel-framed buildings was much better understood. This has allowed the development of performance-based design guidelines for use in the UK [45] and New Zealand [60].

3.2 Real Building Fires

3.2.1 Broadgate Phase 8

The Broadgate development in London was a typical modern office structure consisting of a steel frame with composite concrete floor slabs. During construction a fire broke out in a site hut on the first level of the building [61]. A fire resistance period of 90 minutes was required for the building but as construction was not complete the passive fire protection had not been finished whilst the sprinkler system and active fire protection were not yet operational. The fire lasted for four and a half hours and for two of these hours the temperatures reached over 1,000^{o}C. Although the structural elements in an area 20m x 40m needed to be replaced the structural repair costs were small and made up only GBP2million out of the total repair bill of GBP25million. The remainder of the costs were due to smoke damage.

Tests carried out after the fire revealed that there was no significant loss of strength in any of the structural elements as the structural steelwork had not exceeded a temperature of 600^{o}C and the bolts 540^{o}C [62]. There were large deflections, however, with columns shortening by up to 100mm and some floor areas being left with permanent deflections of 600mm. It was observed that some of the reinforcing bars had failed and in certain areas the steel deck had de-bonded from the concrete floor slab. Despite all of this there was no structural failure and floor slab integrity was maintained.

3.2.2 Churchill Plaza

In 1991 a fire started on the eighth floor of the Mercantile Credit Insurance Building in Churchill Plaza, Basingstoke [59]. Built in 1988 the building was a twelve-storey structure with a fire resistance period of 90 minutes. The columns had passive fire protection in the form of boarding and the composite floor beams had spray applied protection. No protection had been applied to the bottom of the composite floor system.

As the glazing in the building failed the fire spread to the tenth storey. After the fire there was no permanent deformation of the steel frame. As in the Broadgate fire the steel decking had de-bonded from the concrete in the composite floor. The worst

affected area of floor was load tested and shown to have sufficient strength that no repairs would be needed. The majority of the GBP5 million repair costs were due to smoke damage and, although visually undamaged, the fire protection was replaced.

3.3 Fire Tests

3.3.1 BHP Fire Tests - William Street

BHP is the largest manufacturer of steel in Australia. In 1990 they carried out a series of fire tests to assess the response to fire of the 41-storey building at William Street in Melbourne [59]. External steel columns and steelwork around the inner core were all protected by concrete. The beams and composite deck floor were protected by an asbestos based material and during a refurbishment in 1990 it was decided to remove this. Australian regulations at that time for the required fire resistance period of 120 minutes would have needed alternative fire protection to be applied to the beams and floor and for the sprinkler system to be upgraded. During 1990 the fire resistance of buildings in Australia was under scrutiny and this provided the opportunity to determine whether the fire protection and sprinkler upgrade was necessary for this building.

A total of four fire tests were carried out at BHP's Research Melbourne Laboratories on a specially constructed test building. This consisted of a typical 12m x 12m corner bay with an adjacent 4m x 4m small office. Both were furnished with standard office contents and furniture.

The first two tests were intended to examine the existing sprinkler system. both showed that there was no need to upgrade this as it performed satisfactorily. Test three looked at the behaviour of the unprotected composite slab while the supporting beams had partial protection. A maximum atmospheric temperature of 1254^{o}C was reached and after it had peaked the fire was extinguished. During the test a maximum temperature of 72^{o}C was reached on the top surface of the slab which had no problems supporting the imposed load.

The final test looked at the behaviour of the composite floor system with the beams left unprotected. A peak temperature of 1228^{o}C was reached and the fire was extinguished

after this had peaked, the steel reached a temperature of 632^{o}C. The central beam deflected by 120mm but most of this was recovered during the cooling process.

It was concluded that with no protection applied to the composite floor or supporting beams that the building would behave satisfactorily as long as the steel temperatures were not greater than those achieved during the tests. The steel temperatures were limited, however, as were shielded by a suspended ceiling which remained intact during all of the tests.

3.3.2 Stuttgart-Vaihingen University Fire Tests

In 1985 the University of Stuttgart-Vaihingen carried out fire tests on a four-storey building [59]. A number of different construction methods were used in the building such as partially encased columns, concrete filled columns, water filled columns, composite beams and various different composite floor types. After the fire tests the building was used as office and laboratory space.

For the main fire test wooden cribs were used as the fire fire load. The maximum atmospheric temperature was greater than 1,000^{o}C and the maximum beam temperature was 650^{o}C. All of the columns performed well and were left with no permanent deformation. During the fire there was spalling of the concrete infilled webs in the beams which exposed some reinforcement, however, there was no permanent deformation. The maximum deflection of the floor slab was 60mm.

After the fire the building was refurbished. The external wall panels were completely replaced due to fire damage, however, there was little actual structural repair needed. Any damaged areas of the floor slab decking and concrete infill to the beams were replaced. In addition, the floor was strengthened by placing rebar at the soffit and spraying on concrete. The cost of this refurbishment was low.

3.3.3 Cardington Fire Tests

The design of the Cardington tests was based on previous tests or real fires that had occurred. Most influential was the Broadgate fire where no protection had been applied to the steelwork a tht time the fire occurred.

Test	Description	Floor area (m^2)
BS Test 1	Restrained beam	24
BS Test 2	Plane frame	53
BS Test 3	Corner test	76
BS Test 4	Demonstration test	136
BRE Test 1	Corner compartment	54
BRE Test 2	Large compartment	340

Table 3.1: Summary of the Cardington fire test programme

The building itself was intended to be typical of that found in a modern European city centre office development [59]. It was a braced frame with a plan area of 21m x 45m and a height of 33m. Across the width there were three bays of 6m, 9m and 6m and across the length there were five equally spaced bays. At either end of the building were 4m x 4.5m stairwells and in the centre a 9m x 3.5m lift core.

All beams were designed as simply supported and acting compositely with the floor. The floor system was of grade 35 lightweight concrete sitting on a 0.9mm steel deck continuous over a minimum of two spans. An A142 anti-cracking mesh was used and the minimum slab depth was 130mm. Static loading was applied to the floors using sand bags to provide a total load of $5.48 kN/m^2$.

The tests had three objectives:

1. To provide data to verify computer models of steel frame behaviour in fire
2. To demonstrate the behaviour of large scale structures in fire
3. To provide the basis for the preparation of a more rational design methodology for steel framed buildings under fire conditions

To meet these objectives six tests were carried out between January 1995 and July 1996. The tests were designed to be complementary and to have increasing levels of complexity. Table 3.1 shows details of the tests and their position within the Cardington building is illustrated in Figs. 7.1 and 7.2.

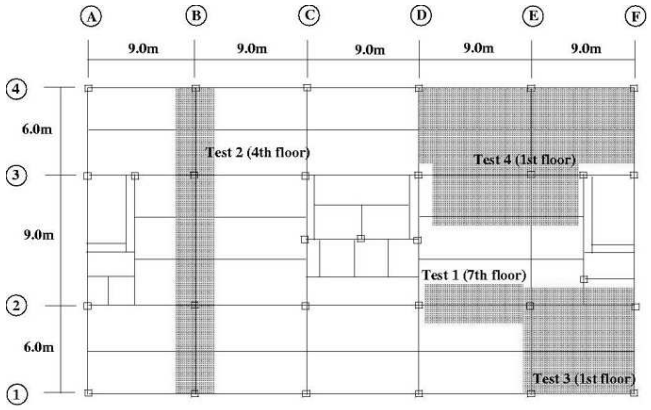

Figure 3.1: Plan of Cardington test building showing location of the British Steel fire tests [8]

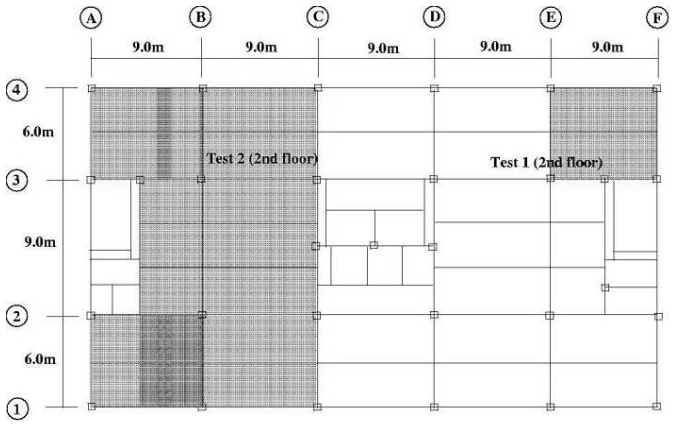

Figure 3.2: Plan of Cardington test building showing location of the BRE fire tests [8]

British Steel Test 1 - Restrained Beam

This was the simplest test carried out and was intended to study the behaviour of a single member that was restrained by the surrounding structure. The element being tested was a 9m long 305x165x40UB acting compositely with the slab. At either end it was connected to protected columns. A specially constructed gas-fired furnace covering an area of 8m x 3m was used to apply the fire load. Heat was applied to the beam over the middle 8m of its length which left a small length at either end of the beam and the beam-column connections unheated.

Heating took place at a rate of 3-10^{o}C per minute with a maximum beam temperature of 887^{O}C being recorded. The rate of heat increase was deliberately slow for an unprotected member and was similar to that of a protected member. This was so that the concrete would reach a higher temperature and the composite action of the beam and slab would be more evident. At the point of maximum temperature in the beam the maximum deflection was 232mm. The test was stopped when some of the control instrumentation failed. A permanent deflection of 120mm was measured after cooling.

After the test was finished it was observed that the beam had buckled just inside each end of the furnace. There was also evidence of buckling of the beam web and the lower flange in the unheated areas of the beam between the furnace and the connections. This was because of restraint provided by the cooler concrete slab. During cooling fracture of the partial depth endplates occurred at both connections.

British Steel Test 2 - Plane Frame

The second British Steel test investigated the behaviour of a plane frame through a slice of the building along gridline B. One of the aims of the test was to look at the behaviour of both the structure close to connections and the connections themselves so that the need for protection in that area could be determined. A gas fired furnace was again used to provide the fire load and it measured 21m long x 2.5m wide x 4m high. Within the furnace there were three primary beams consisting of two 6m long 356x171x51UBs and one 9m long 610x228x101UB. The four supporting columns all had protection applied to within 200mm of the beam-column connections.

A maximum steel temperature of 830^{o}C was recorded and a maximum beam deflection of 285mm. However, this does not include 180mm of extra deflection due to squashing of the columns giving a total deflection of 465mm. All of the floors above the squashed columns deflected by 180mm (see Fig. 3.3) which, in a real building, would have resulted in them being unusable until the damaged columns were replaced. It was therefore concluded that columns should be protected over their full height to ensure that any damage due to a fire was localised.

Figure 3.3: Shortening of columns in British Steel Test 2: Plane Frame Test

A similar response was observed to that of the earlier test. There was evidence of local buckling occurring at either end of the primary beams and during cooling the partial depth endplates had fractured. The bolts on the tab plate connections between the primary beams and secondary beams had also failed in shear during cooling.

British Steel Test 3 - Corner Test

Test 3 covered a much larger area than the previous two tests and was intended to look at the behaviour of an actual fire compartment and the membrane action of the floor in redistributing load to the surrounding structure. The test was carried out on a corner compartment and covered an area of 7.6m x 10m. Within the compartment there were two primary beams of which one was external and one internal and three secondary beams of which two were internal and one was external. Protection was applied to

the external beams while the internal beams were left unprotected. All of the columns had protection fully applied including the connections. The fire load was supplied from timber cribs representing 45kg/m^2. This represented a very severe office fire load.

During the test a maximum steel temperature of 1,020^{o}C was recorded and the maximum floor deflection was 428mm. Local buckling occurred at the end of the secondary beam where it connected to the primary beam as shown in Fig. 3.4. No local buckling occurred at the end connected to the edge beam as there was insufficient axial restraint. During cooling the partial depth endplates fractured. Between the unheated structure and the test compartment cracking occurred in hogging regions of the concrete slab.

Figure 3.4: Local buckling at connections in British Steel Test 3: Corner Test

British Steel Test 4 - Demonstration Test

The final British Steel test was intended to show that when subjected to a more realistic fire scenario the structural behaviour observed in the earlier tests would still occur. A much larger compartment was used with a floor area of 135m^2. It was intended that it represent an open plan office and was furnished with computer workstations, modern furnishings and paperwork. The furniture used as the fire load corresponded to an equivalent fire load of 45kg/m^2 if using wooden cribs. Fire protection was applied to all columns to the height of the slab whilst all other steel work including the external beams was left unprotected.

A maximum unprotected steel temperature of 1,150^{o}C was recorded. The maximum displacement was measured as 640mm. Although there was a large amount of cracking around the internal column it is thought that this occurred during cooling. There were no signs that the structure was near failure. Figure 3.5 shows the permanent deformations that remained after the structure had cooled.

Figure 3.5: Permanent deformations after British Steel Test 4: Demonstration Test

BRE Test 1 - Corner Compartment

The first test carried out by BRE was on a 6m x 9m corner compartment. All columns were protected up to the height of the slab but all beams, including edge beams, were left unprotected. Wooden cribs were used with a fire load of 40kg/m^2. A maximum steel temperature of 903^{o}C was recorded and a maximum displacement of 269mm. After cooling the residual deflection was 160mm. Unlike all of the other fire tests carried out on the Cardington structure no local buckling occurred during heating and no fracture occurred in any of the connections on cooling.

BRE Test 2 - Large Compartment

BRE's second fire test was the largest of all the tests with a total floor area of 340m^2. Similar to previous tests the columns were protected to the underside of the slab with all other steelwork left exposed. Wooden cribs supplied a fire load of 40kg/m^2.

The windows to the compartment broke early in the test which resulted in a relatively low maximum fire temperature of 746^oC but this was sustained for a long period of time. A maximum steel temperature of 691^oC was recorded. During the test the maximum vertical displacement was 557mm which recovered to 481mm after cooling. Most internal beams suffered from local buckling of the bottom flange and part of the web near to the connections. During cooling the partial depth endplates fractured and in one case the web had fractured. In the beam-to-beam connections shearing of the bolts occurred during cooling.

3.4 The PIT Project

In 1996 a multi-centre research team was awarded funding by the then Department of the Environment, Transport and Regions under the Partners in Technology scheme to investigate the behaviour of composite steel-framed structures in fire [10]. Under the title 'The behaviour of steel framed structures under fire conditions', the stated aim of the project was 'To understand and exploit the results of the large scale fire tests at Cardington so that rational design can be developed for composite steel frameworks at the fire limit state'. This was the most comprehensive study of structural behaviour in fire undertaken and utilised the experience and knowledge of may different bodies. The main partners were Edinburgh University, British Steel (now CORUS) and Imperial College and their primary task was developing numerical models of the tests. Theoretical models were developed based on fundamental principles of structural behaviour to confirm the results of the numerical models. BRE and the SCI were also involved with the SCI having the task of producing design guidance based on the numerical output.

3.4.1 Numerical modelling

At the time of the project proposal it was decided that Edinburgh University and British Steel would use the commercial finite element code ABAQUS for the modelling of the tests. The reasoning behind this was that a commercial code would have been thoroughly verified thus allowing the user to concentrate solely on interpreting the behaviour of the model. Imperial College provided independent verification of

the ABAQUS output using ADAPTIC [63], a non-linear structural mechanics code developed inhouse over the previous ten years.

At the University of Edinburgh most of the detailed modelling work was undertaken on Tests 1 and 3 carried out by British Steel [64–67]. These covered the most important cases for compartment fires. Of the other two tests the plane frame test, Test 2, was unlikely to happen in real life whilst the demonstration test, Test 4, did not have sufficient instrumentation to allow a detailed comparison to be made between the numerical and experimental results. Initially the concrete slab was represented by shell elements and the ABAQUS concrete material model, however, this caused convergence problems due to the discontinuous stress-strain curve of the concrete. Use of a stress-resultant approach reduces any problems with convergence that may be encountered in a highly non-linear material model due to locally high stresses. This led Gillie to develop the FEAST suite of programs which define the behaviour of shell elements using a stress-resultant approach [68]. The programs were incorporated into ABAQUS as user defined subroutines. FEAST accounted for non-linear thermal gradients, non-linear material behaviour and coupling between membrane and bending forces. As it could not deal with elastic unloading it was not suitable for studying structural behaviour in the decay period of a fire. The second stress-resultant approach to be used was a grillage model. This represented the slab as two orthogonal load-carrying mechanisms using beam elements [69].

In applying the temperature loading to the structural models it was found that it was necessary to make some assumptions regarding the temperature rise in each element. Models were analysed up to the peak temperature with the non-linear temperature distribution represented as an equivalent thermal gradient and mean temperature increase as in Fig. 3.6. These were calculated based on a method developed from the calculation of thermal loads for bridge decks [70].

British Steel produced ABAQUS models of all four of their fire tests [71–79]. Four different modelling approaches of varying complexity were used from a simple grillage model to one which represented the beams using shell elements and so could account for local buckling. This showed that the global behaviour of the model was unaffected by such a level of detail thus allowing beams in future models to be represented using simpler elements.

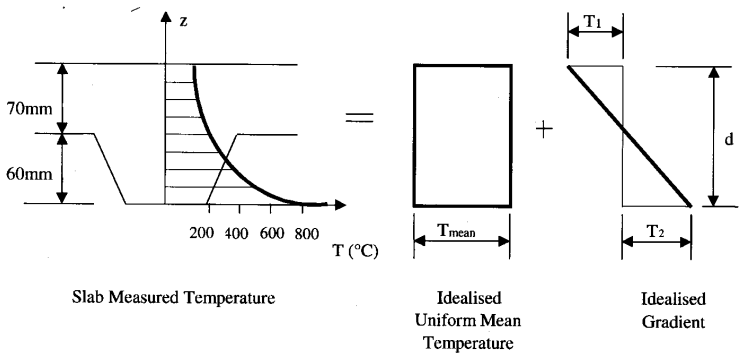

Figure 3.6: Equivalent temperature distribution used in modelling of Cardington tests [9]

Imperial College modelled all four British Steel tests using ADAPTIC [80]. The results produced agreed with both the experimental results and those from ABAQUS models.

The Edinburgh University models were validated by comparing them with:-

- measurements taken during the actual tests of vertical deflections, lateral deflections and strains
- solutions obtained from theoretical studies
- numerical results from models produced at Imperial College using ADAPTIC

These all confirmed that the numerical models captured the behaviour of the tests both quantitatively and qualitatively.

The general trends of the structural behaviour of all the ABAQUS models of Test 1 were similar. Any difference between the results were due to the modelling assumptions used. These results matched those from Imperial College very closely. Test 3 results all agreed well and showed the importance of restraint where even at the edge of the building, although there was little rotational restraint, there was still sufficient lateral restraint for membrane action to develop in the floor slab.

3.4.2 Structural response of composite floor systems to fire

The structural behaviour of a composite floor system in fire was found to be a complex interaction of membrane and bending forces. Many reports were published detailing

the full findings of the PIT project [9, 10, 13, 81]. A brief summary of the behaviour of such systems is provided in this section.

At ambient conditions a composite floor slab is designed to carry load through bending only. In reality, restraint at the slab edges will lead to considerable compressive forces developing which help to carry the load through compressive membrane action. At the start of a fire these compressive forces will increase, particularly in the supporting steel beams which heat up much more rapidly than the concrete slab. Eventually the compressive forces in the beam increase sufficiently that buckling of the lower flange will occur at the supports [10]. The compression comes from three sources; hogging moments from the normal design load, restrained thermal expansion and the thermal gradient between the slab and beam creating a hogging moment due to rotational restraint. A temperature increase of only 100-200^{o}C is normally enough for local buckling to occur [81].

After buckling of the secondary beams has occurred deflections increase rapidly as thermal expansion strains manifest themselves as deflections rather than stresses leading to large P-Δ moments. The rotational restraint at the ends of the beam is soon lost as the hogging moments there continue to rise. At approximately 500^{o}C the steel beam reaches its axial capacity. Beyond this temperature the axial force and P-Δ moments decrease due to material degradation. From this point the load-carrying mechanism of the beam changes [82]. Rather than the load being carried through flexure it is carried through membrane action in the slab. Where the deflections are largest at the centre of the slab tensile membrane action occurs, at the edge of the panel where the deflections are small then compressive membrane action occurs. Figure 3.7 shows the section forces in the ribs at different positions in the first British Steel test. Beyond approximately 800^{o}C the steel beam is so weak that, even in catenary action, its load capacity is so small that the slab must carry the load.

Put in figure 3.45 from main PIT report.....

3.4.3 Parametric Studies

After the models constructed of the tests had been verified a series of parametric studies were carried out. These aimed to examine the sensitivity of the models to their input

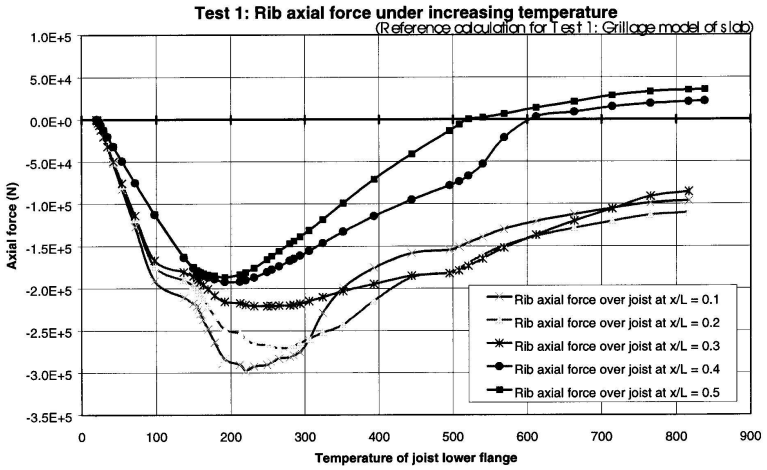

Figure 3.7: Forces developed in the ribs during British Steel Test 1 [10]

parameters, to identify which factors were the most important when carrying out fire resistance design and how they affected the structural response described in Section 3.4.2. Four aspects were investigated:-

- loading
- section size variation
- temperature distribution
- tensile membrane action

The grillage model of Test 1 was used for the comparisons.

Effect of loading

Loading was found to have little effect on the response of the structure until near the point of failure [83]. Researchers at Imperial College analysed Test 1 with no load, the actual test load, double the test load and triple the test load [80]. The effect on the total displacement was small as shown in Fig. 3.8. Doubling the test load or removing it only produced a variation in the maximum deflection of +/- 15%. This showed that restraint to thermal expansion was the dominant factor in producing deflection.

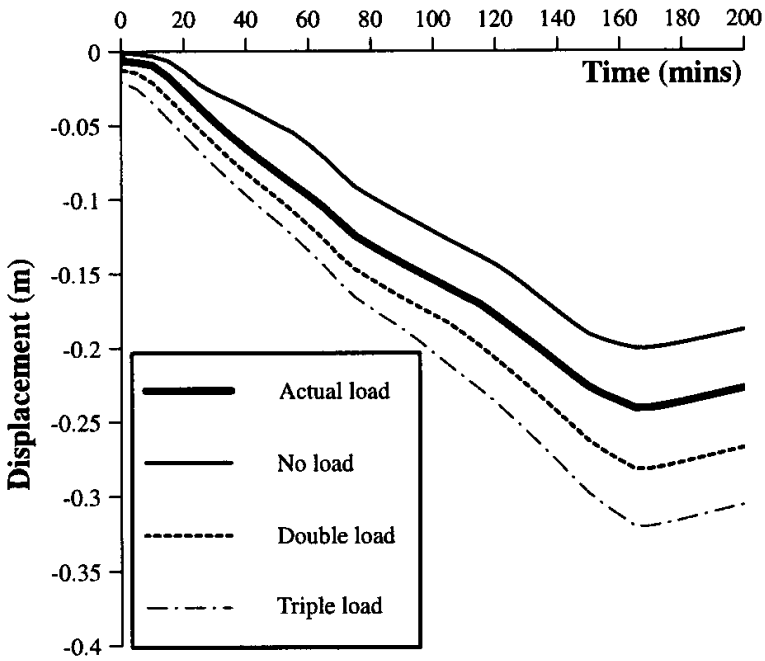

Figure 3.8: Effect of load level on deflection response of British Steel Test 1 [11]

Effect of section size variation

Changing the size of the secondary beam was also found to have little effect on the deflection response of the slab [12]. Figure 3.9 shows the experimental results in comparison with those from models with the actual section size and those with a second moment of area of -50% and +50%. As would be expected a change in the steel area is reflected in the internal forces produced. A larger steel section will produce larger compressions due to restrained thermal expansion and the effect of the P-Δ moment increases. The opposite is true for the beam of reduced section. The size of the secondary beam does not have a significant influence on the development of tensile membrane action in the slab as by that stage of the fire the section is very weak due to the high temperatures.

Effect of temperature distribution

The most extensive parametric study looked at the effect of the temperature distribution within the slab on its structural behaviour [84]. Figure 3.10 shows the compartment, the secondary beam and the location of the ribs in Test 1. Due to

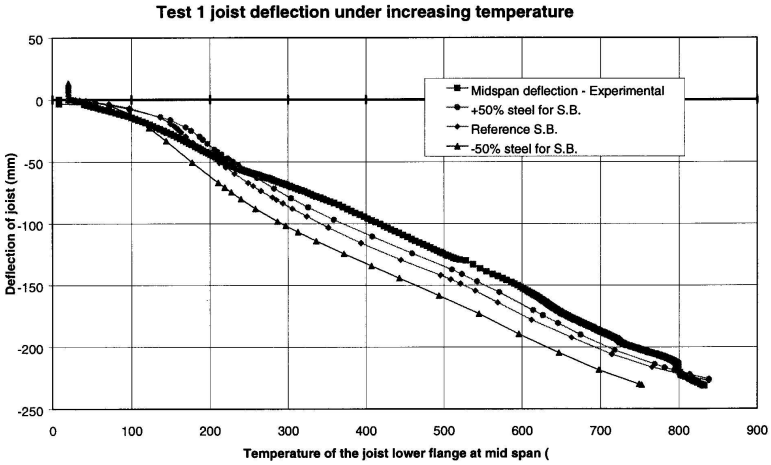

Figure 3.9: Effect of steel section size on deflection response of British Steel Test 1 [12]

the geometrical anisotropy of the slab the temperature distribution within it will be extremely complex. In the direction of the ribs the temperature distribution in the ribs and the troughs will be different, this will in turn affect the distribution in the direction perpendicular to the ribs.

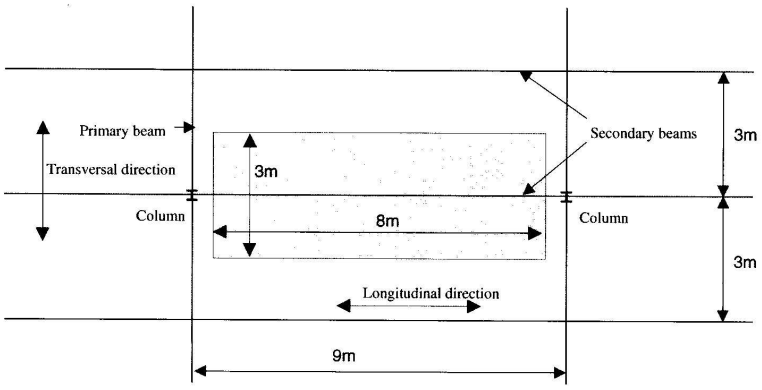

Figure 3.10: Layout of British Steel Test 1 [?]

For the computer models developed the non-linear temperature distribution through the depth of the slab was idealised as an equivalent mean temperature increase and thermal gradient as shown in Fig. 3.6. The effect of changing each variable both parallel and perpendicular to the ribs was studied to determine how sensitive the models would be to variations in the temperature input data. Table 3.2 shows the reference values used.

Structural member	Reference final temperature (^{o}C)	Reference final gradient (^{o}C/mm)
Secondary beam	800	0.26
Composite slab	265	4
Ribs	360	5

Table 3.2: Reference thermal load temperatures for Test 1 [9]

The initial study looked at the effect of changing the temperature gradient in the slab in the direction of the composite beam [9]. Varying thermal gradients of 50-200% of the reference value were applied but this had little effect on the deflections and internal forces. This was because, in the composite beam, most of the thermally induced moment was due to the coupling action between the slab and beam rather than the internal thermal moment in the slab. Later in the fire, as the strength of the steel beam reduces the moment from the coupling effect, the difference in the deflections is still small as by this time compatibility with the transverse direction is governing the deflection. In the direction of the ribs there is little difference in the internal forces generated as they are governed by compatibility of deflection with the longitudinal direction.

Changing the gradient in the direction of the ribs has more effect. Rotational restraint provided by the slab results in the thermal gradient creating a hogging moment which resists the deflection of the composite beam. The larger the thermal gradient the larger the resistance leading to lower deflections and larger compressions.

The value chosen for the mean thermal expansion was shown to have a more significant effect on the response of the slab than the choice of thermal gradient [13]. In the direction of the composite beam an increase in the mean temperature increase leads to larger deflections and compressions as shown in Fig. 3.11. Tensile membrane action develops in the ribs earlier as the composite beam applies more load to them. This also causes large sagging moments to develop. A reduction in the mean temperature increase results in lower deflections and forces in both directions.

If the mean temperature is increased in the direction of the ribs then the resistance to the composite beam is less resulting in larger deflections. This leads to the compressive forces in the slab in the direction of the composite beam reducing. The moment in the composite beam was found to double as the development of tensile membrane action

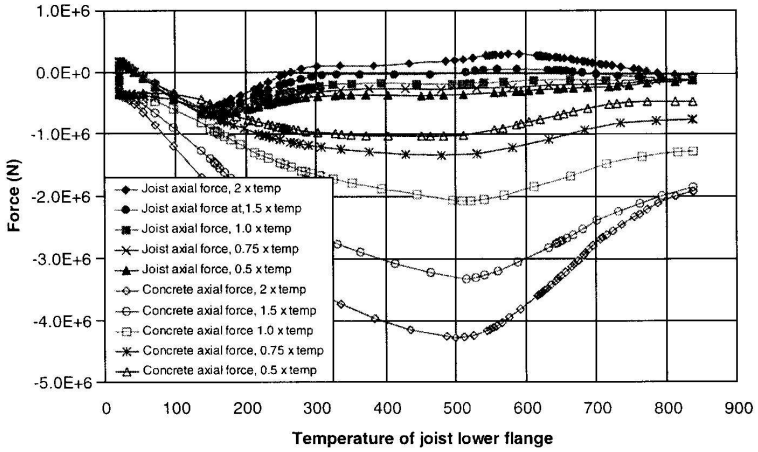

Figure 3.11: Axial force in the slab and composite beam due to varying temperature in the longitudinal direction [13]

in the ribs is delayed due to the extra expansion (see Fig. 3.12).

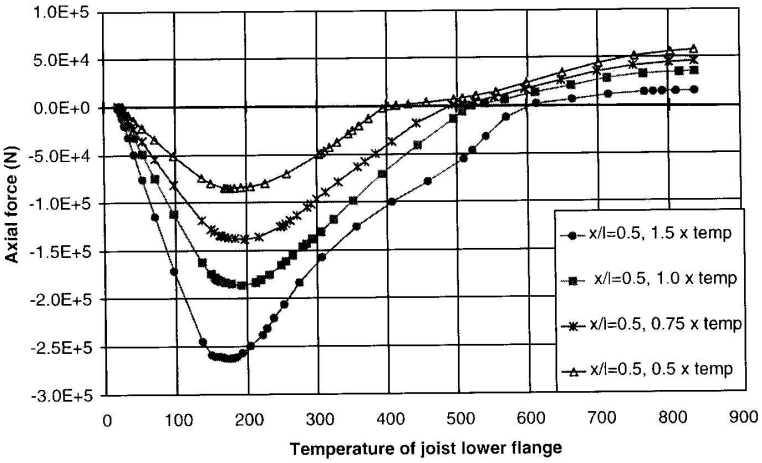

Figure 3.12: Axial force in the ribs due to varying temperature in the transverse direction [13]

The temperature study showed that the choice of mean temperature is the most significant factor in terms of the behaviour of the structure as it affects both the displacement and the internal forces generated. Varying the thermal gradient will affect the internal forces but will not have a significant impact on the displacement.

Modelling of tensile membrane action

The availability of tensile membrane action as a load carrying mechanism was investigated in heated and unheated structures by Gillie [14]. He used the numerical model of the first British Steel test to compare the tensile membrane behaviour observed when it was heated and unheated. For the unheated model the load applied was ten times that used in the test so that membrane action would occur. The largest difference in behaviour occurred in the direction parallel to the secondary beams. In the heated case the reinforcement remained mostly in compression due to thermal expansion. With no heating, the reinforcement strain was tensile and greater than the yield strain of 0.2%. Perpendicular to the secondary beam both cases produced tensile strains but the patterns were very different. Tensile strains occurred over the full width of the compartment in the heated case as shown in Fig. 3.13. This was very different to the unheated case where large tensile strains developed due to sagging between the secondary beams and compressive strains occurred over them. This study showed that tensile membrane action is much more reliable in a heated structure. In particular tensile strains do not peak locally in the heated compartment but develop evenly over the entire area.

3.4.4 Theoretical analyses

To provide a greater understanding of structural behaviour in fire a number of theoretical studies were carried out [85–87]. These also provided another source of verification for the numerical models produced. Intentionally simple, the models illustrated the extremely complex behaviour that occurs even in a single structural element subjected to thermal effects. The studies examined:-

- thermal expansion
- thermal bowing
- the effect of restraint

All of these were shown to have a significant impact on the displacement but more importantly on the pattern of internal forces in the beam studied.

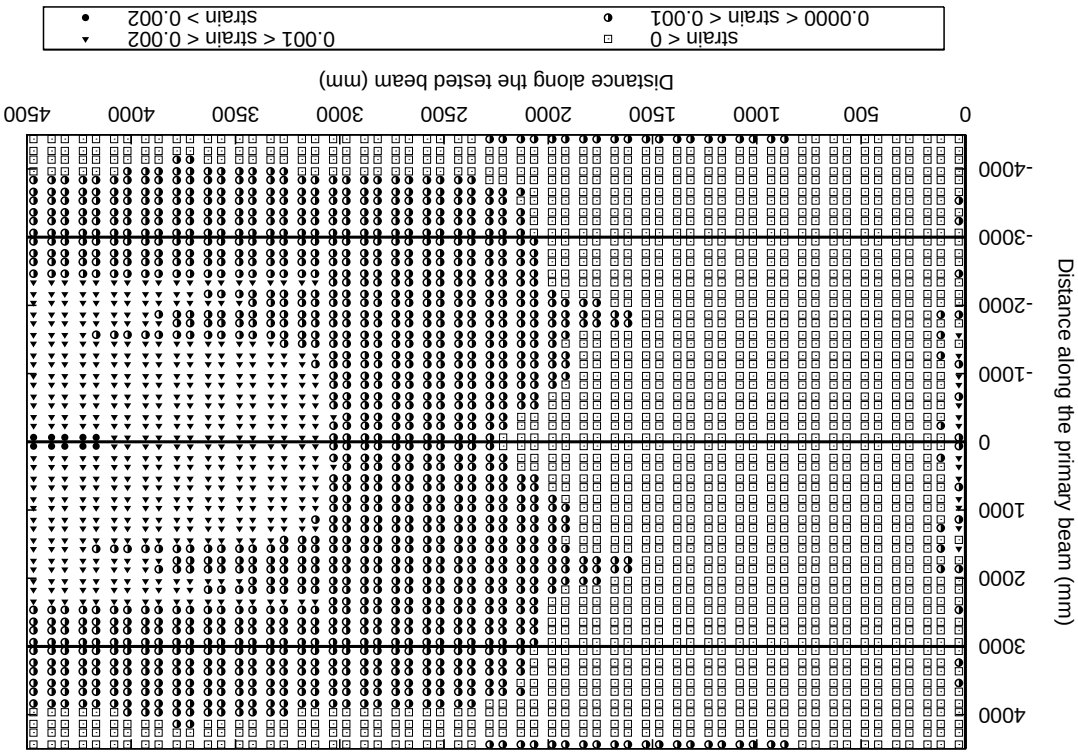

Figure 3.13: Reinforcement mechanical strains in the direction of the ribs at the end of British Steel Test 1 [14]

The most important equation governing the behaviour of structures exposed to fire was found to be:

$$\epsilon_{total} = \epsilon_{thermal} + \epsilon_{mechanical} \tag{3.1}$$

The displaced shape of the structure is governed by the total strain whilst the internal stress is governed by the mechanical strain. If there is no restraint to thermal expansion then all of the thermal strain will produce deflections as there is no mechanical strain. By contrast, if there is restraint, then some or all of the thermal strain will produce mechanical strain.

Thermal expansion

If a beam is subject to a uniform temperature rise this will cause a thermal expansion strain ϵ_T:

$$\epsilon_T = \alpha \Delta T \tag{3.2}$$

With no lateral restraint all of this this will go into deflections and the beam will move laterally by $\alpha \Delta T l$. Restraint will cause the beam to either yield or buckle. If the beam is stocky then it will yield before buckling can occur. The temperature at which it will yield can be calculated from:

$$\Delta T_y = \frac{\sigma_y}{E\alpha} \tag{3.3}$$

A slender beam will buckle before its yield stress is reached and this will occur at a temperature of:

$$\Delta T_{cr} = \frac{\pi^2}{\alpha} \left(\frac{r}{l} \right)^2 \tag{3.4}$$

where r is the radius of gyration.

Above this temperature the force at the supports will remain constant and all of the additional thermal strain will go into deflection. As the temperature increases sufficiently that the material properties start to degrade then the restraining force will fall as the yield stress reduces. After the beam has buckled the P-Δ moments generated increase. They do not start to reduce until degradation of the material properties starts to occur.

In an actual building it is unlikely that a beam would have perfect lateral restraint. If the restraint stiffness, k_t, can be calculated then a revised critical buckling temperature can be calculated:

$$\Delta T_{cr} = \frac{\pi^2}{\alpha \lambda^2} \left(1 + \frac{EA}{k_t L}\right) \tag{3.5}$$

Figure 3.14 shows the effect of varying the axial restraint on buckling temperature. It can be seen that the degree of restraint required for a beam to buckle due to thermal expansion is small.

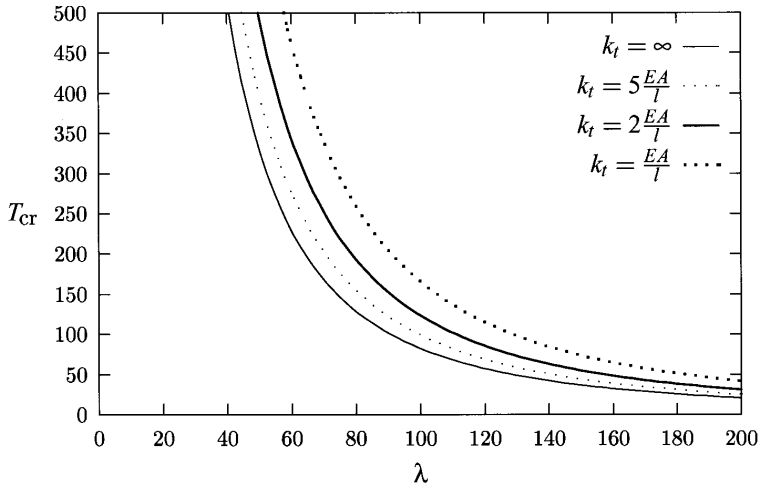

Fig. 9. Buckling temperatures for thermal expansion against finite lateral restraint.

Figure 3.14: Buckling temperatures for thermal expansion against varying lateral restraint [15]

Thermal bowing

The situation where a beam will be subject to a completely uniform temperature rise is unlikely to happen. In a real fire the temperature distribution will vary through the depth causing a thermal gradient to develop. The temperature difference between the surfaces will lead to thermal bowing. Considering a simply supported beam of length l and depth d, the thermal gradient in the beam can be calculated from:

$$T_{,y} = \frac{T_2 - T_1}{d} \tag{3.6}$$

where T_1 is the temperature on the top surface and is greater than that of the lower surface T_2. This will produce a uniform curvature over the length of the beam:

$$\phi = \alpha T_{,y} \tag{3.7}$$

As the beam has no restraint to this curvature the ends will move in to accommodate it. This produces a strain which can be considered a contraction strain and is calculated:

$$\epsilon_\phi = 1 - \frac{sin(\frac{l\phi}{2})}{l\phi 2} \tag{3.8}$$

If the beam has lateral restraint then the deflection can be determined from the induced P-Δ moment. The tensile force P_t in the beam can be calculated by solving the quadratic equation:

$$P_t = \left(\sqrt{\frac{1}{2}\left(\frac{\pi\delta}{l}\right)^2 + 1} - 1 \right) EA \tag{3.9}$$

Where a beam is subject to a thermal gradient and is fixed at both ends a constant moment of M=EIϕ will develop along its length.

In reality the temperature distribution in a beam will be a combination of both thermal expansion and a through depth thermal gradient. The deflection and internal stresses in the beam depend on whichever phenomenon is the most dominant. Figure 3.15 shows the temperature-deflection response of a beam for combinations of thermal expansion strain ϵ_T and thermal contraction strain ϵ_ϕ. Where thermal expansion is dominant the deflection response is characterised by the pre- and post-buckling regions and the beam is in compression. As the effect of a thermal gradient becomes more important the temperature-deflection curve becomes smoother and the compressive forces reduce before eventually becoming tensile.

Put in figure 19 from principles paper.....

The preceding theory was all developed for application to beams or one-way spanning slabs. Usmani [70] applied the one-dimensional theory to the two-dimensional problem of the Cardington restrained beam test (British Steel test 1). The longitudinal and transverse directions were treated individually and then appropriate stiffnesses were chosen to determine the combined state using compatibility. Theoretical results agreed both quantitatively and qualitatively with the experimental and numerical results.

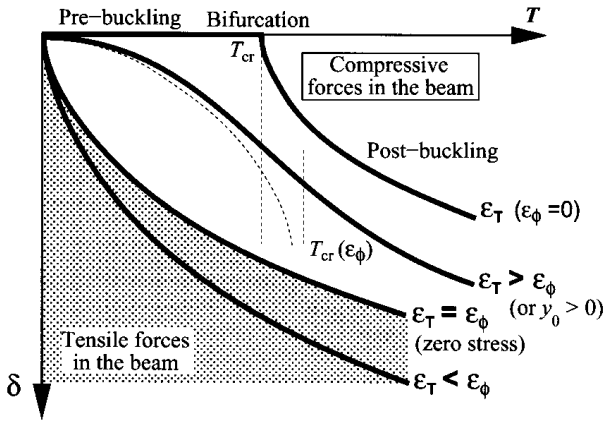

Fig. 19. Temperature deflection responses for combinations of ε_T and ε_ϕ.

Figure 3.15: Temperature deflection response of beam with varying combinations of thermal expansion and thermal gradient [15]

Restraint

A numerical study was carried out to further examine the behaviour of a single beam subject to varying thermal loads [87]. The results confirmed those from the theory and highlighted the importance of restraint to structural behaviour in fire. Figure 3.16 contains results from two analyses of the same beam, one with simply supported ends and one that was laterally restrained. The effect of restraint is illustrated in the different temperatures at which runaway starts to occur. Initially the deflections of the laterally restrained beam are slightly higher due to the restraint, however, runaway does not start to happen until a temperature of approximately 750^oC is reached. The simply supported beam starts to runaway at a much lower temperature of 450^oC. This is when material degradation starts to weaken the beam such that it can no longer carry the load through bending but with no lateral restraint it cannot use catenary action to carry the load.

Put in figure 6.24 from Susan's thesis.....

To summarise, the conclusions of the theoretical study were:-

- restraint conditions significantly effect the deflection and internal stresses
- restraint to thermal expansion produces compression forces leading to yielding or

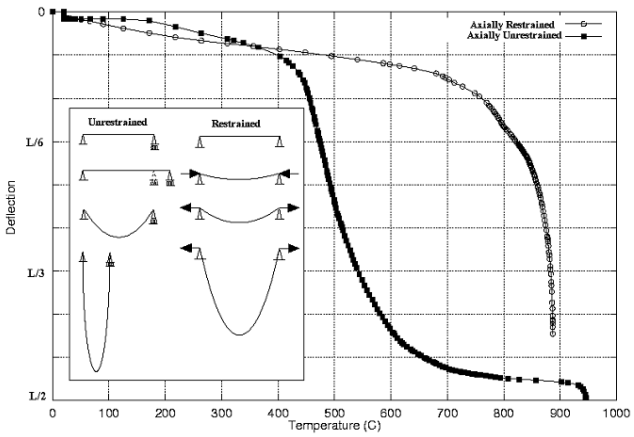

Figure 3.16: Runaway in an axially restrained and unrestrained beam [?]

buckling

- very little restraint is required for slender sections to reach their buckling temperature
- restraint to thermal bowing produces tensile forces
- a combination of thermal expansion and thermal bowing can produce a wide range of deflections and internal stress distributions governed by restraint conditions
- restraint allows the load to be carried through catenary action at high temperatures

3.4.5 Conclusions of the project

The key findings of the PIT project were:-

- due to the high degree of redundancy that composite steel-framed buildings possess they are extremely stable in fire and have a large reserve of strength
- the behaviour of such buildings is dominated by their response to the thermal load, in particular the effect of restrained thermal expansion
- material degradation is of secondary importance to thermal effects

These conclusions mean that structural engineers must change their approach to designing for fire. Previously no consideration was given to thermal loads and it was assumed that failure occurs solely due to material degradation. Thermal loads can be beneficial as restrained thermal expansion allows concrete floors to develop a deflected shape very efficient at transferring load through membrane action. The elevated temperatures mean that this shape can be obtained without large and damaging mechanical strains in the reinforcement. The implications for a structural engineer designing for fire are that a composite building is capable of resisting fire, however, the correct behaviour and load carrying mechanisms must be accounted for i.e. thermal effects should be considered and concrete floor slabs should be designed to carry load through membrane action rather than bending.

3.5 Performance-based design methods for composite floor slabs in fire

3.5.1 SCI Design Guide

Say this is useful.....

The Steel Construction Institute published a 'Level 1' design guide for use in the fire engineering of low risk buildings [45]. It was produced based on the results from full-scale fire tests, observations from real building fires and computer modelling. The guidance was prepared with two safety considerations in mind:

1. There should be no increased risk to life safety of occupants, fire fighters and others in the vicinity of the building, relative to current practice
2. On the floor exposed to fire, excessive deformation should not cause failure of compartmentation i.e. the fire will be contained within its compartment of origin and should not spread horizontally or vertically

These recommendations can only be applied to structures similar to the Cardington building i.e. braced, non-sway composite steel frames. The design method is based on a theoretical study of the tensile membrane behaviour of simply supported composite

slabs carried out by Bailey [88] from observations of an ambient test conducted at the Building Research Establishment [89]. He adopted a yield line approach whereby an enhancement factor due to membrane forces is calculated and applied to the yield-line capacity of the slab. To predict the ultimate failure point a limiting strain in the reinforcement was defined. It was assumed that the strain in the reinforcement was the same value over the entire length of the slab and limited to that which occurs at a maximum stress in the reinforcement of $0.5f_y$.

Bailey extended the previous method so that it could be applied to the fire situation [**?**, **?**]. In doing so a number of assumptions were made. A linear temperature distribution through the depth of the slab was assumed with the temperature difference between the top and bottom faces of the slab a constant 770^oC. It was further assumed that all of the reinforcement around the slab edges had fractured and so boundary conditions could be treated as simply supported, even for internal panels. For the fire scenario it was necessary to alter the failure criterion to consider the extra deflections induced by thermal bowing due to the temperature difference between the top and bottom faces of the slab. This is added to the allowable mechanical strain to give a total strain which is used to calculate the failure deflection. A safety factor of 2.4 was applied to the thermally induced deflection. This is an empirically determined factor based on the results from the Cardington tests. To determine the ultimate capacity the moment capacity of the slab, calculated using reduced material properties, should be multipled by the enhancement factor based on this limiting deflection. The most significant omission is thermal expansion strain as these have been shown to contribute significantly to the large deflections that occurred in the Cardington tests [90, 91]. Despite this, however, the method provides a quick and efficient method for engineers to use in a design office.

To apply the design method every floor in the building should be divided into floor design zones. Each zone must be rectangular with beams on every side. Within a zone beams must only span in one direction and there should be no columns. Normally the beams on the boundary of a floor design zone will be protected, however, they may be left unprotected provided they are designed so. By using the design tables in the SCI guide if the floor is found to have sufficient strength then all beams within a design zone may be left unprotected.

The SCI guide states that the designer must ensure that on the outside of a building the floor slab must be adequately anchored to the edge beams. This is not consistent with the theory used to produce the design charts as Bailey assumes that complete fracture of reinforcement will occur along along all four edges thus leaving the slab simply supported and with no lateral restraint.

A study undertaken at the University of Sheffield showed that this design method over-predicted the tensile membrane action of concrete slabs [92]. This was in comparison to results from their Vulcan finite element package [93] when used to analyse a 9m x 9m ribbed concrete slab. The largest discrepancy between the theoretical and numerical results was for heavily reinforced slabs. For slabs with light reinforcement the difference was not so large. The study only looked at one square slab with a 9m span and so did not investigate the effect of geometry on the results.

Bailey extended his original method so that it could be used for the design of slabs with orthotropic reinforcement [94]. He states that membrane action is significant in slabs with an aspect ratio equal to or less than three. It is suggested that for slabs with an aspect ratio of less than three that the most efficient method of increasing the tensile membrane capacity of the slab is to increase the area of reinforcement in the longer span. This is because along the edge of the longer span the slab boundaries move towards the centre of the slab and so the strains in the reinforcement are smaller.

3.5.2 HERA Design Guide

In 2001 the Heavy Engineering Research Association of New Zealand (HERA) published design guidelines for the design of multi-storey steel framed buildings [60]. The guide is intended for the design of structures exposed to severe fires where any unprotected steel member will reach very high temperatures and the building is exhibiting severe inelastic behaviour. Referred to as the Slab Panel Method of design the guide is based on the work of Bailey [?] but with a number of developments made by Clifton [95].

The most significant development is in the temperature distribution of the structural members. Bailey assumes a linear temperature distribution between the top and bottom surfaces of the slab with a temperature difference of 770^{o}C. He does not take account of the fire load, compartment geometry, available ventilation or the slab

geometry. By comparison, the New Zealand guide presents concrete and reinforcement temperatures based on natural fire curves from a series of parametric studies on different compartments. These curves were used as input for heat transfer analyses to provide concrete and reinforcement temperatures for a wide range of possible fire scenarios. The second significant difference is in the calculation of the yield line capacity of the slab. Bailey considered the individual bending capacity of unprotected steel beams but did not consider them to act compositely with the slab. Clifton assumes a perfect shear connection between the slab and beams thus allowing him to include the secondary beams in the calculation of the moment capacity of the slab. He states that although the tensile contribution will be small due to the high temperatures the moment contribution will be high due to the large lever arm. Once the yield-line capacity has been calculated it is multiplied by an enhancement factor to account for the tensile membrane action. The enhancement factors are those calculated by Bailey [45].

To ensure that the load capacity calculated using the design method can be achieved a number of guidelines are given. These specify ductility and lapping requirements for the reinforcement and shear capacity checks at all connections. It is assumed that the steel decking of the floor will ensure that compartmentation breach does not occur. When there is no deck then crack control is achieved by adopting the 'strong crack control' provisions described in AS 3600 [96].

3.6 Conclusion

A number of fire tests and in particular those carried out at Cardington have been described. The findings of the subsequent numerical and theoretical studies which highlighted the most influential factors affecting structural behaviour in fire have been discussed and the importance of tensile membrane action in maintaining structural integrity highlighted. Particular attention has been given to the theoretical studies which were undertaken as part of the PIT project as they form the background to this piece of research. They illustrated that by returning to fundamental principles to describe structural behaviour it is possible to achieve accurate results without the need to resort to complicated and time-consuming computer analyses.

The performance-based design methods developed for the UK and New Zealand based

on the results of the Cardington studies have been described. Their shortcomings have been explained with reference to the real structural behaviour observed from the studies of the Cardington fire tests.

Chapter 4

Analytical Methods to Describe the Behaviour of Structures subject to Thermal Effects

4.1 Introduction

Many analytical methods for the small-deflection analysis of plates subjected to heating are available [97–100]. Studies of the large-deflection analysis of plates are more limited [101–104] and tend to consider either thermal bending or thermal expansion but do not consider both phenomena at the same time. Biswas [105] considered both, however, his solution for anisotropic plates does not deal with the thermal loading correctly.

Analytical studies of the thermal behaviour of beams are similarly limited. The majority of the work is concerned with stability issues relating to the buckling of beams at elevated temperature. Boley and Weiner [106] produced a solution for a beam subject to uniform temperature increase. Birman [107] considered the effect of material non-linearity on the behaviour of beams subject to either a thermal gradient or thermal expansion. Usmani et. al. [?] have investigated the behaviour of beams under varying support conditions and temperature distributions, however, the equations are not suitable for dealing with both a through depth gradient and a mean temperature rise.

To analyse structural members in a fire, and in particular concrete members, any solution must be capable of considering both a through depth thermal gradient and a mean temperature increase. In this chapter equations are developed to describe the behaviour of laterally restrained beams and plates subject to such a temperature distribution. The solutions obtained are geometrically non-linear but assume elastic material properties invariant with temperature.

4.2 Theory of thermal stresses applied to beams

4.2.1 Classical beam theory

Classical beam theory is based on the assumption that straight lines normal to the middle surface before deformation remain straight, normal to the middle surface and unchanged in length after deformation. This approximate assumption was initially applied to beams by Bernoulli and subsequently applied to plates and shells by Love and Kirchhoff.

Stress-strain-displacement relationships

Considering Fig. 4.1 the strain at any point in the beam can be described as:

$$\epsilon_x = \epsilon_{xm} - z\frac{d^2w}{dx^2} \tag{4.1}$$

where ϵ_{xm} is the membrane strain and z is the distance from the middle surface. The stresses at this point are obtained by multiplying Eqn. 4.1 by the Young's modulus of the material E:

$$\sigma_x = \sigma_{xm} + \sigma_{xf} = E\epsilon_{xm} - Ez\frac{d^2w}{dx^2} \tag{4.2}$$

where σ_{xm} is the membrane stress, which is uniform over the length of the beam, and σ_{xf} the bending stress, which is linearly varying through the depth of the beam.

Stress resultants

Appropriate integration of Eqn. 4.2 through the depth of the beam allows the calculation of the stress resultants acting on the beam. This provides the resultant

membrane force F_x and bending moment M_x:

$$F_x = \int_{-h/2}^{h/2} \sigma_x dz \tag{4.3}$$

$$M_x = \int_{-h/2}^{h/2} \sigma_x z dz \tag{4.4}$$

Substituting Eqn. 4.2 into Eqns. 4.3 and 4.4 gives:

$$F_x = EA\epsilon_{xm} = \sigma_{xm} A \tag{4.5}$$

and:

$$M_x = -EI\frac{d^2w}{dx^2} \tag{4.6}$$

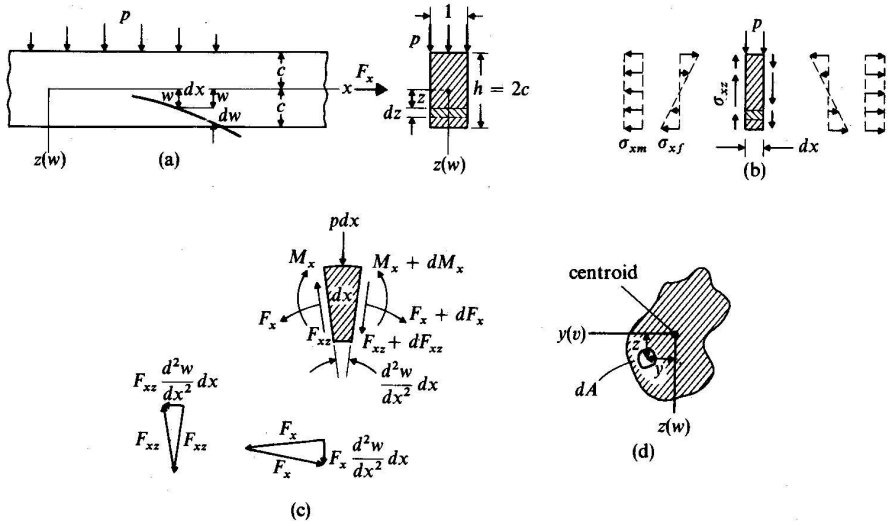

Figure 4.1: Geometry and internal forces of a deflected beam [16]

Equation of moment equilibrium

Consider the equilibrium of the moments of the forces acting on the element in Fig. 4.1. As the limit dx tends to zero the moment dF_{xz} can be ignored as it will tend to zero giving:

$$F_{xz}dx - (M_x + dM_x) + M_x = 0 \tag{4.7}$$

$$F_{xz} = \frac{dM_x}{dx} \tag{4.8}$$

Equation of transverse equilibrium

Considering equilibrium of forces on the element in the transverse z direction:

$$dF_{xz} + pdx + F_x \frac{d^2w}{dx^2} dx = 0 \tag{4.9}$$

which can be re-arranged to give:

$$-\frac{dF_{xz}}{dx} = -\frac{d^2M_x}{dx^2} = p + F_x \frac{d^2w}{dx^2} \tag{4.10}$$

Making use of Eqn. 4.6:

$$EI\frac{d^4w}{dx^4} = p + F_x \frac{d^2w}{dx^2} \tag{4.11}$$

Where the beam is subject to transverse loading only and there is no axial force applied then $F_x = 0$ and Eqn. 4.11 simplifies to:

$$EI\frac{d^4w}{dx^4} = p \tag{4.12}$$

The first term in Eqn. 4.11 represents the flexural resistance to deflection and is proportional to the flexural stiffness of the beam EI. The third term represents the transverse component of any axial force caused by the curvature of the beam $\frac{d^2w}{dx^2}$. In the case of compressive forces this increases the deflection whereas in the case of tensile forces it will resist deflection. When the deflection of the beam is small then the transverse component of any horizontal force will be small. In the situation that F_x is not proportional to the deflection i.e. there are external loads applied to the end of the beam then the third term is linear in w. When F_x is proportional to w such as when the ends of the beam are laterally restrained and a restraining force is developed due to large deflections, then the equation is non-linear in w.

4.2.2 Classical beam theory incorporating thermal effects

In applying the preceding theory to the situation where a beam is subject to thermal effects it is necessary to alter the stress-strain relationship. The strain induced by the change in temperature is superimposed onto that caused by mechanical loading.

The thermal strains are expressed:

$$\epsilon_t = \alpha \Delta T(z) \tag{4.13}$$

where α is the coefficient of thermal expansion for the material being considered and $\Delta T(z)$ is the temperature increase at depth z.

Thermal strains will produce thermal stresses when there is restraint to expansion, the temperature field is non-uniform or the material properties are anisotropic.

Incorporating Eqn. 4.13, Eqns 4.1 and 4.2 become:

$$\epsilon_x = \epsilon_{xm} - z\frac{d^2w}{dx^2} - \alpha \Delta T \tag{4.14}$$

$$\sigma_x = \sigma_{xm} + \sigma_{xf} = E\epsilon_{xm} - Ez\frac{d^2w}{dx^2} - E\alpha \Delta T \tag{4.15}$$

where ΔT is the temperature increase at the point of the beam being considered. Substituting Eqn. 4.15 into 4.3 and 4.4 gives revised stress resultants:

$$F_x = EA\epsilon_{xm} - N^T \tag{4.16}$$

and:

$$M_x = -EI\frac{d^2w}{dx^2} - M^T \tag{4.17}$$

Where the thermal force N^T and the thermal moment M^T are given by:

$$N^T = E\alpha \int_{-h/2}^{h/2} \Delta T dz \tag{4.18}$$

$$M^T = E\alpha \int_{-h/2}^{h/2} \Delta T z dz \tag{4.19}$$

Substituting Eqns. 4.16 and 4.17 into 4.10 gives the governing equation of equilibrium for a beam subject to a transverse load p, a thermal moment M^T and a thermal force N^T:

$$EI\frac{\partial^4 w}{\partial x^4} = p + \frac{\partial^2 M^T}{\partial x^2} + EA\epsilon_{xm}\frac{\partial^2 w}{\partial x^2} - N^T\frac{\partial^2 w}{\partial x^2} \tag{4.20}$$

4.3 Solution for a laterally restrained beam subject to thermal effects

4.3.1 Beam idealisation

Geometry

The beam to be analysed is as shown in Fig. 4.2. It is of length L and can be of any cross sectional configuration of area A and second moment of area I about the axis of bending.

Figure 4.2: Beam geometry

Material properties

The analysis assumes that the material is linear elastic and has equivalent properties in both tension and compression. Further, material properties are not allowed to vary through the section i.e. they do not vary with temperature.

Boundary conditions

The beam being analysed is laterally restrained against translation but free to rotate which leads to the end conditions at $x = 0$ and $x = L$ being:

$$w = 0 \quad u = 0 \quad M_x = 0 \tag{4.21}$$

where u is the horizontal displacement of the beam in the x direction.

Temperature distribution

The temperature distribution through the section can be obtained by heat transfer analysis. It is assumed that the distribution obtained is constant along the length and breadth of the beam so that the temperature is solely a function of the depth z. As the temperature varies only in z it can be represented as a thermal gradient $T_{,z}$ and a mean temperature increase ΔT [70].

Load application

Loading on the beam consists of two components; the normal transverse load defined as p and the thermal load due to the temperature distribution through the depth $T(z)$. The thermal load can be represented by a thermal moment M^T and a thermal force N^T calculated using Eqns. 4.18 and 4.19. For this solution the transverse load will be ignored so that the only load applied to the beam is the thermal load.

4.3.2 Determination of the deflection profile

The thermal moment M^T and the deflection w will be represented by the first term of a single Fourier sine series:

$$w(x) = w_T \sin \frac{\pi x}{L} \tag{4.22}$$

$$M^T(x) = M_1^T \sin \frac{\pi x}{L} \tag{4.23}$$

The Fourier coefficient M_1^T in Eqn. 4.23 is calculated by performing a Fourier integration:-

$$\begin{aligned} M_m^T &= \frac{2}{L}\int_0^L M^T \sin \frac{m\pi x}{a}\,\mathrm{d}x \\ &= \frac{4M^T}{\pi m} \\ M_1^T &= \frac{4M^T}{\pi} \end{aligned} \tag{4.24}$$

which allows the thermal moment to be described as:-

$$M^T(x) = \frac{4M^T}{\pi} \sin \frac{\pi x}{L} \tag{4.25}$$

As the beam is laterally restrained a membrane stress σ_{xm} will develop along its length. The value of σ_{xm} is a function of the deflection of the beam w_T and the mean temperature increase ΔT. The total membrane strain ϵ_{xm} can be calculated from [16]:

$$\epsilon_{xm} = \frac{\pi^2 w_T^2}{4L^2} \tag{4.26}$$

The thermal stress resultant N^T can be calculated using Eqn. 4.18. Substituting Eqns. 4.22, 4.25 and 4.26 into 4.20, dividing by $\sin\frac{\pi x}{L}$ and rearranging the terms provides a cubic equation with respect to the deflection w_T:-

$$w_T^3 + \left(\frac{4I}{A} - \frac{4N^T L^2}{\pi^2 EA}\right) w_T + \frac{16M^T L^2}{\pi^3 EA} = 0 \tag{4.27}$$

This can be solved to determine the deflection of the beam due to thermal loading.

4.3.3 Calculation of membrane forces

The membrane force in the beam F_x can be calculated by substituting Eqn. 4.5 into 4.16 and inserting the deflection w_T calculated from Eqn. 4.27:

$$F_x = EA\frac{\pi^2 E w_T^2}{4L^2} - N^T \tag{4.28}$$

4.3.4 Verification against finite element analyses

To determine the accuracy of the proposed solution i.e. Eqns. 4.27 and 4.28, a series of finite element analyses were carried out. The analyses considered different values of thermal moment and thermal force. For each analysis the membrane stresses and maximum deflections were compared with the theoretical predictions.

The beam being considered consisted of a 10m long rectangular section, 100mm deep and of unit width. A thermal expansion coefficient α of 8E-6 was taken and a Young's modulus value E of 40,000N/mm^2. Two values of thermal gradient through the depth of the beam were considered, $T_{,z} = 1^oC/mm$ and $4^oC/mm$, while the mean temperature increase was varied between 0^oC and 300^oC in increments of 50^oC.

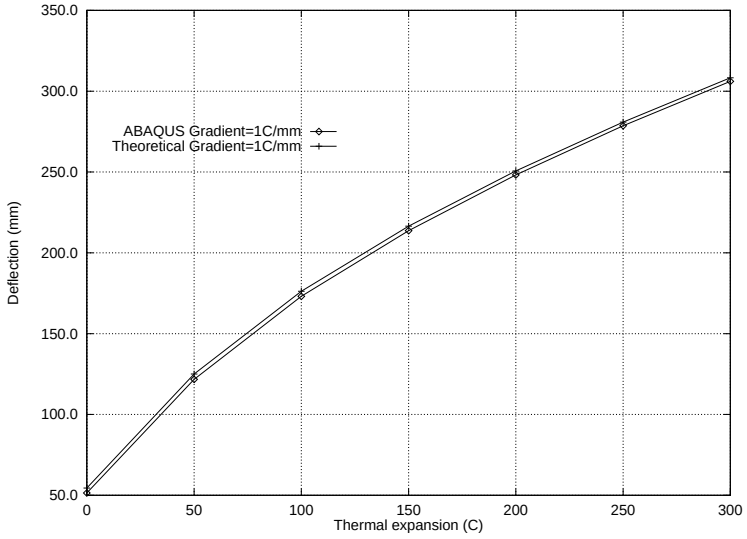

Figure 4.3: Deflections with thermal gradient $T_{,z}$ of $1^oC/mm$

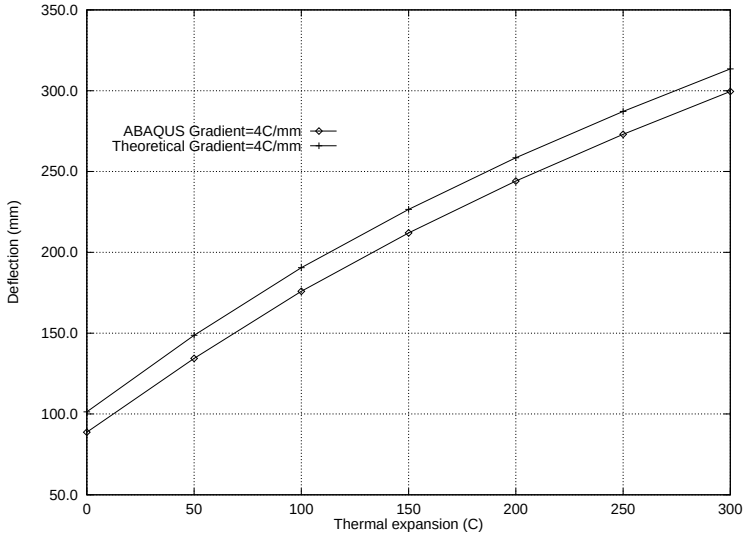

Figure 4.4: Deflections with thermal gradient $T_{,z}$ of $4^oC/mm$

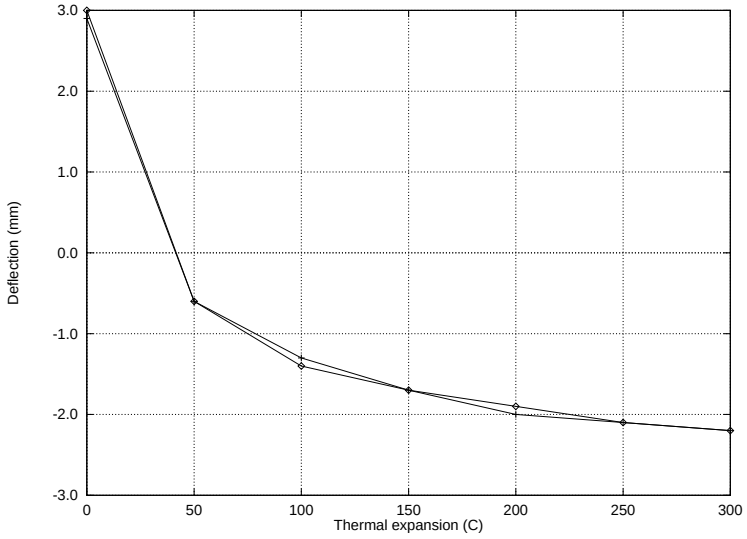

Figure 4.5: Membrane stresses with thermal gradient $T_{,z}$ of $1^oC/mm$

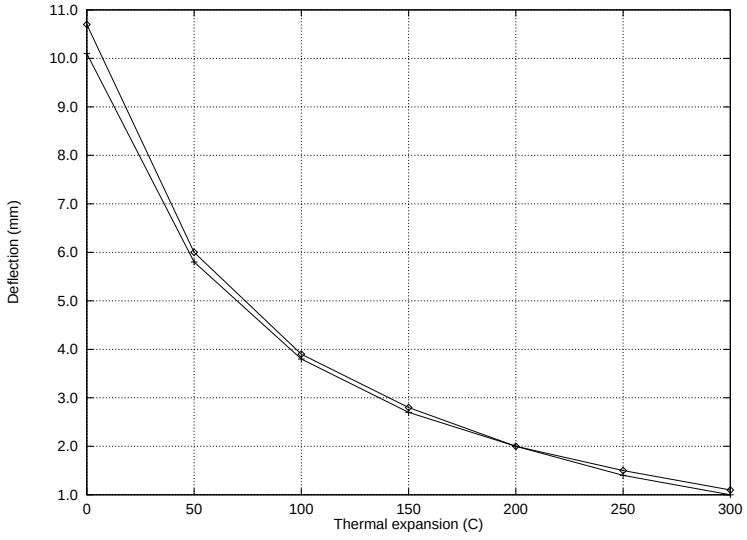

Figure 4.6: Membrane stresses with thermal gradient $T_{,z}$ of $4^oC/mm$

Deflection results

The theoretical deflections compared well against those obtained from the numerical results as shown in Figs. 4.3.4 and 4.3.4. When the beam is only subject to a thermal gradient with no mean temperature increase the deflection predictions are most accurate for the smaller gradient. As the gradient was increased to 4^oC/mm the theoretical deflection was larger than that obtained from the finite element analysis. The results are still acceptable, however.

When the gradient is maintained at a constant value and the mean temperature increased the deflection behaviour is accurately predicted. The difference between the theoretical and numerical results remains constant and is due to any error caused by the bending deflection from the thermal gradient. It can therefore be concluded that the solution can cope with large thermal forces due to a mean temperature increase ΔT better than moments caused by the gradient $\mathrm{T}_{,z}$.

Membrane stress results

The membrane stresses in the beam are more accurately predicted than the deflections. Figures 4.3.4 and 4.3.4 show the membrane stresses in the beam for the same analyses as previously. With a relatively low thermal gradient of 1^oC/mm the stresses are accurately predicted at all values of mean temperature increase ΔT. When the thermal gradient is increased to 4^oC/mm the difference between the theoretical and numerical stresses is more noticeable but still extremely small. It can be seen for the 4^oC/mm analysis that as the mean temperature increases and the thermal expansion force becomes the governing load as opposed to the thermal gradient that the membrane stress very rapidly tends towards that predicted numerically.

4.4 Theory of thermal stresses applied to plates

4.4.1 Classical plate theory

The fundamental assumptions that form the basis of classical plate theory for homogeneous, isotropic, elastic, thin plates are based on the geometry of the

deformation of a plate of uniform thickness h such as shown in Fig. 4.7. These assumptions are:

1. The deflection of the midsurface is small compared to the depth of the plate.
2. After deformation has taken place the midsurface is unstrained.
3. Plane sections normal to the midsurface remain plane.
4. The stress normal to the midplane is small and may be ignored.

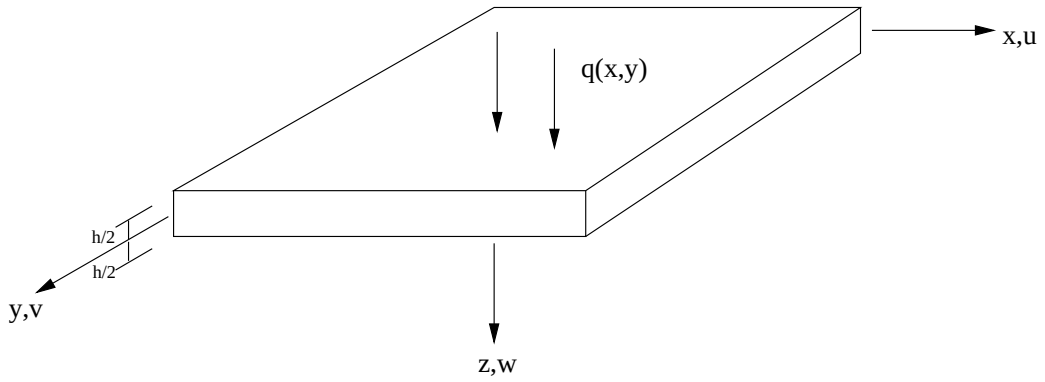

Figure 4.7: Coordinate system of a plate

Stress-strain-displacement relationships

The stress-strain relationships for a plate may be written as:

$$\epsilon_{xx} = \frac{1}{E}(\sigma_{xx} - \nu\sigma_{yy}) \tag{4.29}$$

$$\epsilon_{yy} = \frac{1}{E}(\sigma_{yy} - \nu\sigma_{xx}) \tag{4.30}$$

$$\epsilon_{xy} = \frac{2(1+\nu)}{E}\sigma_{xy} \tag{4.31}$$

Rearranging Eqns. 4.29-4.31 provides the stresses:

$$\sigma_{xx} = \frac{E}{1-\nu^2}(\epsilon_{xx} + \nu\epsilon_{yy}) \tag{4.32}$$

$$\sigma_{yy} = \frac{E}{1-\nu^2}(\epsilon_{yy} + \nu\epsilon_{xx}) \tag{4.33}$$

$$\sigma_{xy} = G\epsilon_{xy} \tag{4.34}$$

The classical theory of plates assumes that the deflection of the plate is small compared to the thickness such that the influence of membrane forces on the equilibrium of the plate can be ignored. When considering the large-deflection behaviour of plates this is not true and assumptions 1 and 2 of the classical theory do not hold. Von Karman [108] proposed a theory using the non-linear strain-displacement relations that gave consideration to the membrane forces. Quadratic terms in the slopes $\frac{\partial w}{\partial x}$ and $\frac{\partial w}{\partial y}$ are retained whilst higher order non-linear terms are ignored. The membrane strains can therefore be described as:

$$\epsilon_{xx} = \frac{\partial u}{\partial x} + \frac{1}{2}\left(\frac{\partial w}{\partial x}\right)^2 \tag{4.35}$$

$$\epsilon_{yy} = \frac{\partial v}{\partial y} + \frac{1}{2}\left(\frac{\partial w}{\partial y}\right)^2 \tag{4.36}$$

$$\gamma_{xy} = \frac{\partial u}{\partial y} + \frac{\partial v}{\partial x} + \frac{\partial w}{\partial x}\frac{\partial w}{\partial y} \tag{4.37}$$

Including bending strains the above equations are revised to:

$$\epsilon_{xx} = \frac{\partial u}{\partial x} + \frac{1}{2}\left(\frac{\partial w}{\partial x}\right)^2 - z\frac{\partial^2 w}{\partial x^2} \tag{4.38}$$

$$\epsilon_{yy} = \frac{\partial v}{\partial y} + \frac{1}{2}\left(\frac{\partial w}{\partial y}\right)^2 - z\frac{\partial^2 w}{\partial y^2} \tag{4.39}$$

$$\epsilon_{xy} = \frac{\partial u}{\partial y} + \frac{\partial v}{\partial x} + \frac{\partial w}{\partial x}\frac{\partial w}{\partial y} - 2z\frac{\partial^2 w}{\partial x \partial y} \tag{4.40}$$

Stress resultants

Stress resultants may be obtained by integration of Eqns. 4.32-4.34 through the depth of the plate h. The resultant membrane forces per unit length N_x, N_y and N_{xy} are calculated:

$$N_x = \int_{-h/2}^{h/2} \sigma_{xx} dz; \quad N_y = \int_{-h/2}^{h/2} \sigma_{yy} dz; \quad N_{xy} = \int_{-h/2}^{h/2} \sigma_{xy} dz; \tag{4.41}$$

Bending moments per unit length M_x and M_y, and the twisting moment per unit length M_{xy} are determined from:

$$M_x = \int_{-h/2}^{h/2} \sigma_{xx} z dz; \quad M_y = \int_{-h/2}^{h/2} \sigma_{yy} z dz; \quad M_{xy} = \int_{-h/2}^{h/2} \sigma_{xy} z dz; \tag{4.42}$$

Introducing Eqns. 4.32-4.34 into 4.42 provides the following set of equations describing the bending moments in the plate:

$$M_x = -D\left(\frac{\partial^2 w}{\partial x^2} + \nu\frac{\partial^2 w}{\partial y^2}\right) \tag{4.43}$$

$$M_y = -D\left(\frac{\partial^2 w}{\partial y^2} + \nu\frac{\partial^2 w}{\partial x^2}\right) \tag{4.44}$$

$$M_{xy} = -(1-\nu)D\frac{\partial^2 w}{\partial x \partial y} \tag{4.45}$$

The membrane stresses in the plate can be described in terms of an Airy stress function $F(x, y)$:

$$\sigma_{xx} = \frac{\partial^2 F}{\partial y^2}; \quad \sigma_{yy} = \tfrac{\partial^2 F}{\partial x^2}; \quad \tau_{xy} = \frac{\partial^2 F}{\partial x \partial y}; \tag{4.46}$$

Thus the membrane stress resultants N_x, N_y and N_{xy} can be described:

$$N_x = \frac{\partial^2 F}{\partial y^2}h; \quad N_y = \tfrac{\partial^2 F}{\partial x^2}h; \quad N_{xy} = \frac{\partial^2 F}{\partial x \partial y}h; \tag{4.47}$$

4.4.2 Equation of membrane equilibrium

By differentiating Eqn. 4.35 twice with respect to y, Eqn. 4.36 twice with respect to x and Eqn. 4.37 with respect to x and y and summing all three results the equation of compatibility for a plate is obtained:

$$\frac{\partial^2 \epsilon_{xx}}{\partial y^2} + \frac{\partial^2 \epsilon_{yy}}{\partial x^2} - \frac{\partial^2 \gamma_{xy}}{\partial xy} = \frac{\partial^2 w}{\partial x \partial y} - \frac{\partial^2 w}{\partial x^2}\frac{\partial^2 w}{\partial y^2} \tag{4.48}$$

Hooke's law allows the strains to be described in terms of the stress resultants acting on the plate:

$$\epsilon_{xx} = \frac{1}{Eh}(N_x - \nu N_y) \tag{4.49}$$

$$\epsilon_{yy} = \frac{1}{Eh}(N_y - \nu N_x) \tag{4.50}$$

$$\gamma_{xy} = \frac{N_{xy}}{Gh} \tag{4.51}$$

Putting Eqns. 4.47 into 4.49-4.51 gives:

$$\epsilon_{xx} = \frac{1}{E}\left(\frac{\partial^2 F}{\partial y^2} - \nu\frac{\partial^2 F}{\partial x^2}\right) \tag{4.52}$$

$$\epsilon_{yy} = \frac{1}{E}\left(\frac{\partial^2 F}{\partial x^2} - \nu\frac{\partial^2 F}{\partial y^2}\right) \tag{4.53}$$

$$\gamma_{xy} = \frac{-2(1+\nu)}{E}\frac{\partial^2 F}{\partial x \partial y} \tag{4.54}$$

Substituting Eqns. 4.52-4.54 into 4.48 yields:

$$\frac{\partial^4 F}{\partial x^4} + 2\frac{\partial^4 F}{\partial x^2 y^2} + \frac{\partial^4 F}{\partial y^4} - E\left[\left(\frac{\partial^2 w}{\partial x \partial y}\right)^2 - \frac{\partial^2 w}{\partial x^2}\frac{\partial^2 w}{\partial y^2}\right] = 0 \tag{4.55}$$

which is the equation of membrane equilibrium for a plate.

4.4.3 Equation of bending equilibrium

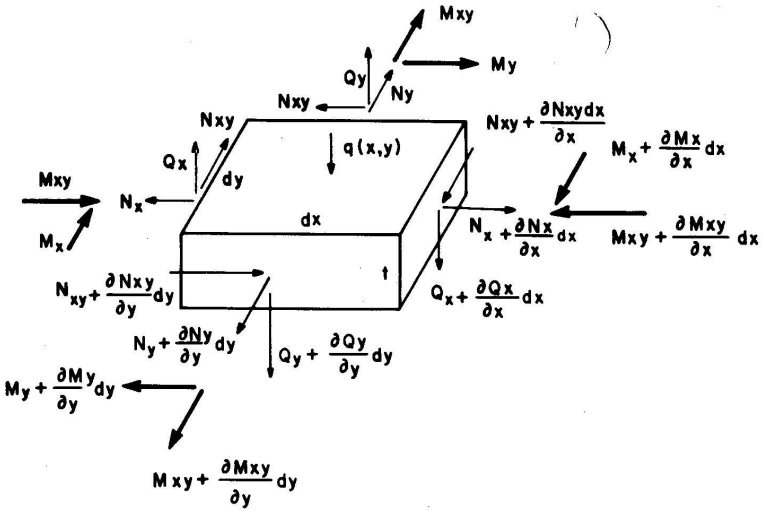

Figure 4.8: Stress resultants acting on a plate element [17]

Considering moment equilibrium about the $x-$ and $y-$axes from Fig. 4.8:

$$\frac{\partial M_x}{\partial x} + \frac{\partial M_{xy}}{\partial y} = Q_x \tag{4.56}$$

$$\frac{\partial M_y}{\partial y} + \frac{\partial M_{xy}}{\partial x} = Q_y \tag{4.57}$$

When considering the force equilibrium in the z-direction it is necessary to modify the classical plate theory equation to include the transverse component of any membrane forces N_x, N_y and N_{xy}. Considering Fig. 4.8 this results in the equation of equilibrium being:

$$\frac{\partial}{\partial x}\left(Q_x + N_x\frac{\partial w}{\partial x} + N_{xy}\frac{\partial w}{\partial y}\right) + \frac{\partial}{\partial y}\left(Q_y + N_{xy}\frac{\partial w}{\partial x} + N_y\frac{\partial w}{\partial y}\right) + q = 0 \tag{4.58}$$

which becomes:

$$\frac{\partial Q_x}{\partial x} + \frac{\partial Q_y}{\partial y} + N_x\frac{\partial^2 w}{\partial x^2} + 2N_{xy}\frac{\partial^2 w}{\partial x \partial y} + N_y\frac{\partial^2 w}{\partial y^2} + q = 0 \tag{4.59}$$

Q_x and Q_y can be eliminated by making use of Eqns. 4.56 and 4.57 such that Eqn. 4.59 becomes:

$$\frac{\partial^2 M_x}{\partial x^2} + 2\frac{\partial^2 M_{xy}}{\partial x \partial y} + \frac{\partial^2 M_y}{\partial y^2} + N_x \frac{\partial^2 w}{\partial x^2} + N_{xy}\frac{\partial^2 w}{\partial x \partial y} + N_y \frac{\partial^2 w}{\partial y^2} + q = 0 \tag{4.60}$$

Placing Eqn. 4.47 into 4.60 and using 4.43 and 4.44 leads to:

$$\frac{\partial^4 w}{\partial x^4} + 2\frac{\partial^4 w}{\partial x^2 y^2} + \frac{\partial^4 w}{\partial y^4} = \frac{h}{D}\left[\frac{q}{h} + \frac{\partial^2 F}{\partial y^2}\frac{\partial^2 w}{\partial x^2} + \frac{\partial^2 F}{\partial x^2}\frac{\partial^2 w}{\partial y^2} - 2\frac{\partial^2 F}{\partial x \partial y}\frac{\partial^2 w}{\partial x \partial y}\right] \tag{4.61}$$

Equations 4.55 and 4.61 are the governing non-linear differential equations describing the large-deflection response of a thin plate subject to a transverse load q. Based on the boundary conditions the equations can be solved for the deflection w and the stress function F. Once these are known the membrane stress distributions can be calculated using Eqns. 4.47.

4.4.4 Classical plate theory incorporating thermal effects

Stress-strain relationship

The membrane strains are obtained by adding the thermal strains of Eqn. 4.13 to those produced by mechanical stresses:

$$\epsilon_{xx} = \frac{1}{E}(\sigma_{xx} - \nu\sigma_{yy}) + \alpha\Delta T \tag{4.62}$$

$$\epsilon_{yy} = \frac{1}{E}(\sigma_{yy} - \nu\sigma_{xx}) + \alpha\Delta T \tag{4.63}$$

$$\gamma_{xy} = \frac{\tau_{xy}}{G} \tag{4.64}$$

Rearranging Eqns. 4.62-4.64 provides the stress components:

$$\sigma_{xx} = \frac{E}{1-\nu^2}[\epsilon_{xx} + \nu\epsilon_{yy} - (1-\nu)\alpha\Delta T] \tag{4.65}$$

$$\sigma_{yy} = \frac{E}{1-\nu^2}[\epsilon_{yy} + \nu\epsilon_{xx} - (1-\nu)\alpha\Delta T] \tag{4.66}$$

$$\tau_{xy} = G\gamma_{xy} \tag{4.67}$$

Strain-displacement relationship

The membrane strains in an isotropic plate of temperature T are expressed as:

$$\epsilon_{xx} = \frac{\partial u}{\partial x} + \frac{1}{2}\left(\frac{\partial^2 w}{\partial x^2}\right) + \alpha\Delta T \tag{4.68}$$

$$\epsilon_{yy} = \frac{\partial v}{\partial y} + \frac{1}{2}\left(\frac{\partial^2 w}{\partial y^2}\right) + \alpha\Delta T \tag{4.69}$$

$$\gamma_{xy} = \frac{\partial u}{\partial y} + \frac{\partial v}{\partial x} + \frac{\partial w}{\partial x}\frac{\partial w}{\partial y} \tag{4.70}$$

The strains at a distance z from the mid-layer of the plate are:

$$\epsilon_{xx} = \frac{\partial u}{\partial x} + \frac{1}{2}\left(\frac{\partial^2 w}{\partial x^2}\right) - z\frac{\partial^2 w}{\partial x^2} + \alpha\Delta T \tag{4.71}$$

$$\epsilon_{yy} = \frac{\partial v}{\partial y} + \frac{1}{2}\left(\frac{\partial^2 w}{\partial y^2}\right) - z\frac{\partial^2 w}{\partial y^2} + \alpha\Delta T \tag{4.72}$$

$$\gamma_{xy} = \frac{\partial u}{\partial y} + \frac{\partial v}{\partial x} + \frac{\partial w}{\partial x}\frac{\partial w}{\partial y} - 2\frac{\partial^2 w}{\partial x \partial y}z \tag{4.73}$$

Stress Resultants

Substituting Eqns. 4.71-4.73 into 4.42 gives revised bending stress resultants incorporating the effects of any thermal moment in the plate:

$$M_x = -D\left(\frac{\partial^2 w}{\partial x^2} + \nu\frac{\partial^2 w}{\partial y^2}\right) - M^T \tag{4.74}$$

$$M_y = -D\left(\frac{\partial^2 w}{\partial y^2} + \nu\frac{\partial^2 w}{\partial x^2}\right) - M^T \tag{4.75}$$

$$M_{xy} = -(1-\nu)D\frac{\partial^2 w}{\partial x \partial y} \tag{4.76}$$

Compatibility equation incorporating thermal effects

Incorporating thermal effects into the stress-strain relationships results in Eqn. 4.52-4.54 changing to:

$$\epsilon_x = \frac{1}{E}\left(\frac{\partial^2 F}{\partial y^2} - \nu\frac{\partial^2 F}{\partial x^2}\right) + \frac{N^T}{Eh} \tag{4.77}$$

$$\epsilon_y = \frac{1}{E}\left(\frac{\partial^2 F}{\partial x^2} - \nu\frac{\partial^2 F}{\partial y^2}\right) + \frac{N^T}{Eh} \tag{4.78}$$

$$\gamma_{xy} = \frac{-2(1+\nu)}{E}\frac{\partial^2 F}{\partial x \partial y} \tag{4.79}$$

Substituting Eqns. 4.77-4.79 into 4.48 provides a revised membrane equilibrium equation considering the effects of temperature:

$$h\left(\frac{\partial^4 F}{\partial x^4} + 2\frac{\partial^4 F}{\partial x^2 y^2} + \frac{\partial^4 F}{\partial y^4}\right) - Eh\left[\left(\frac{\partial^2 w}{\partial x \partial y}\right)^2 - \frac{\partial^2 w}{\partial x^2}\frac{\partial^2 w}{\partial y^2}\right] + \frac{\partial^2 N^T}{\partial x^2} + \frac{\partial^2 N^T}{\partial y^2} = 0 \tag{4.80}$$

Equilibrium equation incorporating thermal effects

Inserting the revised bending stress resultants of Eqns. 4.74-4.76 into 4.61 leads to:

$$D\left(\frac{\partial^4 w}{\partial x^4}+2\frac{\partial^4 w}{\partial x^2 y^2}+\frac{\partial^4 w}{\partial y^4}\right) - h\left(\frac{\partial^2 F}{\partial y^2}\frac{\partial^2 w}{\partial x^2}+\frac{\partial^2 F}{\partial x^2}\frac{\partial^2 w}{\partial y^2}-2\frac{\partial^2 F}{\partial x \partial y}\frac{\partial^2 w}{\partial x \partial y}\right) + \frac{1}{1-\nu}\left(\frac{\partial^2 M^T}{\partial x^2}+\frac{\partial^2 M^T}{\partial y^2}\right)=0 \quad (4.81)$$

Thus the governing equations describing the large deflection behaviour of a plate under thermal effects are Eqns. 4.80 and 4.81.

4.5 Solution for a laterally restrained plate subject to thermal effects

4.5.1 Plate idealisation

Geometry

Figure 4.9 shows the plate to be analysed. The length and breadth are L and B in the x and y directions respectively whilst the thickness is of constant value h over the entire area.

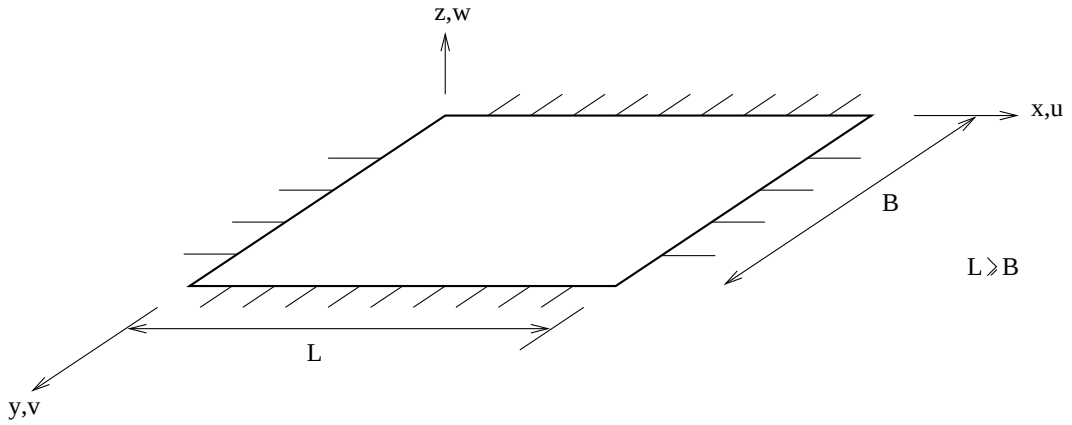

Figure 4.9: Plate geometry

Material properties

The plate being considered is constructed of homogeneous, isotropic material with the the assumptions made about the material properties of the beam in Section 4.3.1 being similarly applied i.e. linear elasticity invariant with temperature.

Boundary conditions

It is assumed that the plate is laterally restrained against translation but free to rotate along all four edges. This leads to boundary conditions at $x = 0$ and $x = L$:

$$w = 0 \quad u = 0 \quad M_x = 0 \tag{4.82}$$

and at $y = 0$ and $y = B$:

$$w = 0 \quad v = 0 \quad M_y = 0 \tag{4.83}$$

Where u and v are the horizontal displacements of the plate in the x and y directions respectively.

Temperature distribution

The temperature distribution through the plate can be obtained by a heat transfer analysis. It is assumed that the distribution obtained is constant over the entire area of the plate so that the temperature is a function of the depth z i.e. there is no spatial variation in the x and y directions. As the temperature varies only in z it can be represented as a thermal gradient $T_{,z}$ and a mean temperature increase ΔT.

Load application

The load acting on the plate consists of two components; the normal transverse load defined as p and the thermal load which can be further split into a thermal moment M^T and a thermal force N^T. Equations 4.18 and 4.19 can be used to calculate the thermal loading.

4.5.2 Determination of the deflection profile

In obtaining a solution to the governing differential equations it is necessary to represent the deflection of the slab and the thermal moment as double Fourier series:

$$w_{\mathrm{T}}(x,y) = \sum_{m=1}^{\infty}\sum_{n=1}^{\infty} w_{mn} \sin\frac{m\pi x}{L}\sin\frac{n\pi y}{B} \tag{4.84}$$

$$M^T(x,y) = \sum_{m=1}^{\infty}\sum_{n=1}^{\infty} M^T_{mn} \sin\frac{m\pi x}{L}\sin\frac{n\pi y}{B} \tag{4.85}$$

The Fourier coefficients M^T_{mn} are calculated by performing the Fourier integration:

$$M^T_{mn} = \frac{4}{LB}\int_0^L\int_0^B M^T \sin\frac{m\pi x}{L}\sin\frac{n\pi y}{B}dxdy \tag{4.86}$$

$$= \frac{16M^T}{\pi^2 mn} \tag{4.87}$$

The thermal moment Fourier series can therefore be written as:

$$M^T(x,y) = \sum_{m=1}^{\infty}\sum_{n=1}^{\infty} \frac{16M^T_{mn}}{\pi^2 mn} \sin\frac{m\pi x}{L}\sin\frac{n\pi y}{B} \tag{4.88}$$

In obtaining a solution only the first term in the Fourier series' will be considered:

$$w_{\mathrm{T}}(x,y) = w_T \sin\frac{\pi x}{L}\sin\frac{\pi y}{B} \tag{4.89}$$

$$M^T(x,y) = M^T \sin\frac{\pi x}{L}\sin\frac{\pi y}{B} \tag{4.90}$$

Substituting Eqn. 4.89 into that for compatibility, Eqn. 4.80, results in:

$$\frac{1}{E}\left(\frac{\partial^4 F}{\partial x^4} + 2\frac{\partial^4 F}{\partial x^2 y^2} + \frac{\partial^4 F}{\partial y^4}\right) = \frac{w_T^2\pi^4}{2L^2B^2}\left(\cos\frac{2\pi x}{L} + \cos\frac{2\pi y}{B}\right) \tag{4.91}$$

The general solution of the Airy stress function F consists of two parts, a homogeneous solution F_H and a particular solution F_P:

$$F = F_H + F_P \tag{4.92}$$

The particular solution F_P is obtained by solving Eqn. 4.91:

$$F_P = \frac{w_T^2 E}{32}\left(\frac{L^2}{B^2}\cos\frac{2\pi x}{L} + \frac{B^2}{L^2}cos\frac{2\pi y}{B}\right) \tag{4.93}$$

The general solution of Eqn. 4.80 can be described as:

$$F = P\frac{x^2}{2} + Q\frac{y^2}{2} + \frac{w_T^2 E}{32}\left(\frac{L^2}{B^2}\cos\frac{2\pi x}{L} + \frac{B^2}{L^2}\cos\frac{2\pi y}{B}\right) \tag{4.94}$$

For this analysis it was assumed that the plate was laterally restrained along all of its edges. Considering this statement the values of P and Q can be calculated to be:

$$P = \frac{w_T^2 \pi^2 E}{8\left(1-\nu^2\right)}\left(\frac{1}{B^2}+\nu\frac{1}{L^2}\right) - \frac{E\alpha\Delta T}{1-\nu} \tag{4.95}$$

$$Q = \frac{w_T^2 \pi^2 E}{8\left(1-\nu^2\right)}\left(\frac{1}{L^2}+\nu\frac{1}{B^2}\right) - \frac{E\alpha\Delta T}{1-\nu} \tag{4.96}$$

The final solution for the Airy stress function F satisfying the equation of compatibility Eqn. 4.80 can therefore be written as:

$$\begin{aligned} F = &\frac{w_T^2 \pi^2 E}{8\left(1-\nu^2\right)}\left(\frac{1}{B^2}+\nu\frac{1}{L^2}\right)\frac{x^2}{2} + \frac{w_T^2 \pi^2 E}{8\left(1-\nu^2\right)}\left(\frac{1}{L^2}+\nu\frac{1}{B^2}\right)\frac{y^2}{2} \\ &+\frac{w_T^2 E}{32}\left(\frac{L^2}{B^2}cos\,\frac{2\pi x}{L}+\frac{B^2}{L^2}cos\,\frac{2\pi y}{B}\right) - \frac{E\alpha\Delta T}{1-\nu}\frac{x^2}{2} - \frac{E\alpha\Delta T}{1-\nu}\frac{y^2}{2} \end{aligned} \tag{4.97}$$

Substituting Eqns. 4.89, 4.90 and 4.97 into the equation for equilibrium Eqn. 4.81 and applying the Galerkin procedure [109] the following equation is obtained:

$$\begin{aligned} \int_0^L \int_0^B \; & D\left(\tfrac{\partial^4 w}{\partial x^4} + 2\tfrac{\partial^4 w}{\partial x^2 y^2} + \tfrac{\partial^4 w}{\partial y^4}\right) - h\left(\tfrac{\partial^2 F}{\partial y^2}\tfrac{\partial^2 w}{\partial x^2} + \tfrac{\partial^2 F}{\partial x^2}\tfrac{\partial^2 w}{\partial y^2} - 2\tfrac{\partial^2 F}{\partial x \partial y}\tfrac{\partial^2 w}{\partial x \partial y}\right) \\ &+\tfrac{1}{1-\nu}\left(\tfrac{\partial^2 M^T}{\partial x^2} + \tfrac{\partial^2 M^T}{\partial y^2}\right)\sin\tfrac{\pi x}{L}\sin\tfrac{\pi y}{B}dxdy = 0 \end{aligned} \tag{4.98}$$

Carrying out the integration of Eqn. 4.98 over the entire area of the plate produces a non-linear cubic equation with respect to the deflection w_T:-

$$\begin{aligned} &\frac{3}{4}\left\{\left(3-\nu^2\right)\left(1+\frac{L^4}{B^4}\right)+4\nu\frac{L^2}{B^2}\right\}\left(\frac{w_{\mathrm{T}}}{h}\right)^3 \\ &\left\{\left(1+\frac{L^2}{B^2}\right)^2 - 12\frac{L^2\left(1+\nu\right)N^T}{\pi^2 E h^3}\left(1+\frac{L^2}{B^2}\right)\right\}\left(\frac{w_{\mathrm{T}}}{h}\right) \\ &-192\frac{L^2\left(1+\nu\right)M^T}{\pi^4 E h^4}\left(1+\frac{L^2}{B^2}\right) = 0 \end{aligned} \tag{4.99}$$

The cubic equation can then be solved to determine the deflection of the plate due to the two components of the thermal load.

4.5.3 Calculation of membrane forces

The membrane stress distribution along the boundary of the slab for any deflection w_T can be calculated by inserting the solution obtained for the Airy stress function of Eqn.

4.97 into Eqns. 4.46:

$$\sigma_{xx} = \frac{\partial^2 F}{\partial y^2} = \frac{w^2\pi^2 E}{8(1-\nu^2)}\left(\frac{1}{L^2}+\frac{\nu}{B^2}\right) - \frac{w^2\pi^2 E}{8L^2}\cos\frac{2\pi y}{B} - \frac{E\alpha\Delta T}{1-\nu} \quad (4.100)$$

$$\sigma_{yy} = \frac{\partial^2 F}{\partial x^2} = \frac{w^2\pi^2 E}{8(1-\nu^2)}\left(\frac{1}{B^2}+\frac{\nu}{L^2}\right) - \frac{w^2\pi^2 E}{8B^2}\cos\frac{2\pi x}{L} - \frac{E\alpha\Delta T}{1-\nu} \quad (4.101)$$

4.5.4 Verification against finite element results

To determine the accuracy of Eqns. 4.97 and 4.100 in describing the behaviour of a plate under thermal loading a series of finite element analyses were undertaken. Varying loads of thermal moment and thermal force were considered and the membrane stresses and maximum deflections of the theoretical and numerical solutions compared.

The plate being considered is of 100mm depth, has a thermal expansion coefficient α of 8E-6 and a Young's modulus of 40,000N/mm^2. A constant breadth B of 5,000mm was chosen. Two values were considered for the length L, 5,000mm and 7,500mm giving aspect ratios of 1 and 1.5 so that the ability of the equations to deal with plates of different geometries was also investigated.

Deflection results

For all of the analyses the theoretical deflections from Eqn. 4.99 agree well with those obtained from the finite element analyses. When the plate is loaded by a thermal moment only and with no thermal expansion force the results match extremely closely. Figures 4.10 and 4.11 show the results for a plate with an aspect ratio of 1 whilst Figs. 4.16 and 4.17 those for a plate with an aspect ratio of 1.5. The results for small thermal moments i.e. with a thermal gradient of 1^oC/mm match better than those for the larger thermal moment produced by a gradient 4^oC/mm. The error between the results is small however. Similar results were noticed for the beam in Section 4.3.4.

As the thermal expansion force in the plate increases with the mean temperature increase ΔT the deflections obtained match very closely. When the plate has an aspect ratio of 1 the difference between the theoretical and numerical results remains constant over the entire range of temperatures considered. The error is caused by the thermal moment loading as opposed to the thermal expansion force loading. If the plate aspect

ratio is increased to 1.5 the deflections agree well for both cases where there is a thermal moment but no thermal force. However, as the thermal force is increased the difference between the theoretical and numerical results increases slightly. This is due to the assumption that the plate follows the sinusoidal deflection in Eqn. 4.89. The actual deflected shape of a plate as the aspect ratio increases above 1 resembles that of a 'bath tub' as described by Paik [110]. The deflection in the middle part of the plate is almost flat and although the maximum deflection can be calculated reasonably closely the actual deflected shape is not accurately represented by a double sine curve. As the aspect ratio increases this becomes more noticeable. The 'bath tub' effect and the impact of the aspect ratio becomes more apparent when the membrane stresses along the plate boundary are examined.

Membrane stress results

To determine the accuracy of the Eqns. 4.100 and 4.101 in describing the membrane stress distribution along the boundary of the plate the theoretical and numerical stresses will be compared at the midpoint of the plate edges and, for certain examples, the distribution along the edges. Figures 4.12 and 4.13 show the stresses at the middle of an edge of a square plate subject to different thermal loadings. The stresses are more accurately calculated for lower thermal gradients. When the plate is subject to both a thermal gradient and thermal expansion the trend of the stresses is captured but the error between the theoretical and numerical results increases. Examining the membrane stress distribution along the entire edge of the plate it can be seen that the trend of the distribution is closely followed by Eqns. 4.100 and 4.101 as shown in Figs. 4.14 and 4.15. The theoretical results are closer to the numerical results for a thermal gradient of $1^oC/mm$ than for $4^oC/mm$.

Although Eqn. 4.100 can accurately predict the maximum deflection for a plate with an aspect ratio of 1.5 it would be expected that the membrane stress distribution would not be so accurately represented. This is demonstrated in Figs. 4.18 and 4.19 where it can be seen that above a mean temperature increase of approximately 100^oC the theoretical membrane stress at the centre of the short edge diverges from the numerical result. The theoretical result produces increasing compressive stresses due to the assumption of the deflected surface shape, whereas, due to the bath tub effect in the numerical result the

compressive stresses are lower due to larger strains. At the centre of the long edge the stresses can be more accurately calculated as seen in Fig. 4.18, this is because across the shortest span the sine curve approximation is still valid.

Figures 4.20 and 4.21 show the stress distribution along the edges of the plate. Although not as accurate as for a square plate the results still follow the general trend and are reasonable. The largest discrepancy between the theoretical and numerical results is in the membrane stress at the middle of the shortest span. This would be expected as it is at this point that the effect of the deflected shape becomes most influential on the stress distribution.

Above an aspect ratio of 1.5 the accuracy of the results obtained reduces. Although Eqn. 4.100 can still continue to predict the deflection, albeit with decreasing accuracy, Eqns. 4.100 and 4.101 are not capable of accurately representing the membrane stress distribution due to the double sine curve approximation.

4.6 Conclusions

The analytical methods presented in this chapter have been shown to accurately predict the deflection and membrane stress distributions in both beams and plates subjected to thermal loading. In comparison with results obtained from non-linear finite element analyses the results agree well. The plate analysis method has been shown to produce the most accurate results for aspect ratios close to 1. Beyond an aspect ratio of approximately 1.5 the accuracy of the membrane stress distribution reduces due to assumptions regarding the shape of the deflected surface.

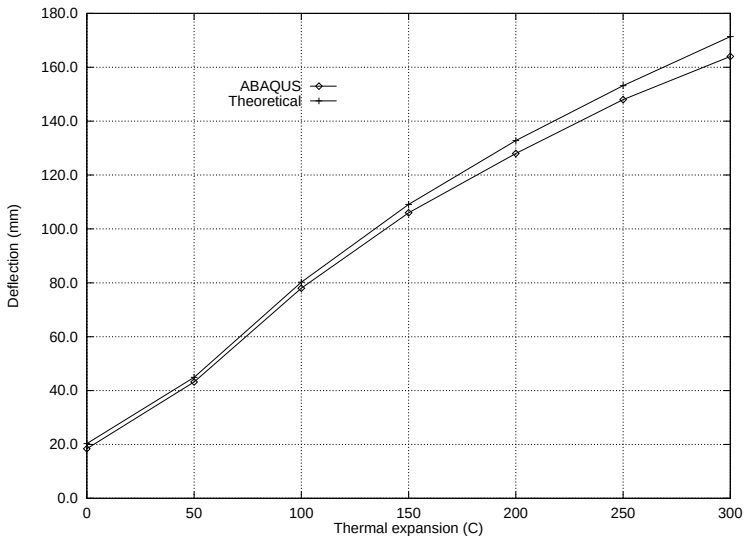

Figure 4.10: Centre deflections for L/B=1 with thermal gradient $T_{,z}$ of $1^oC/mm$

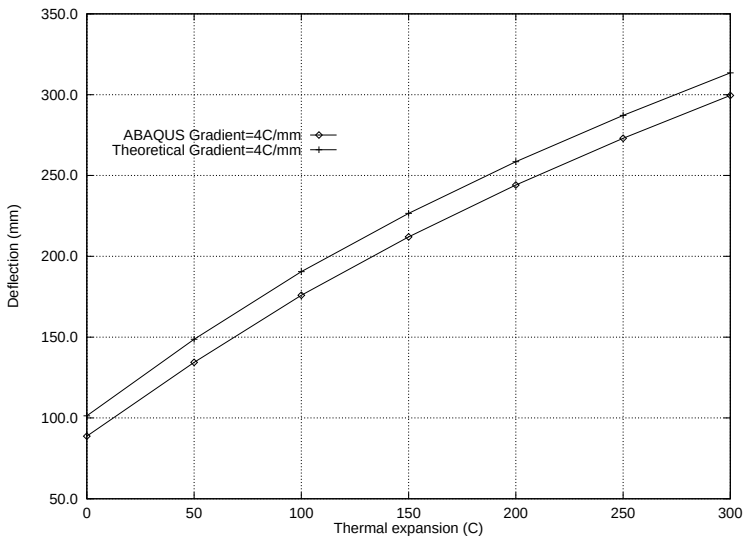

Figure 4.11: Centre deflections with L/B=1 thermal gradient $T_{,z}$ of $4^oC/mm$

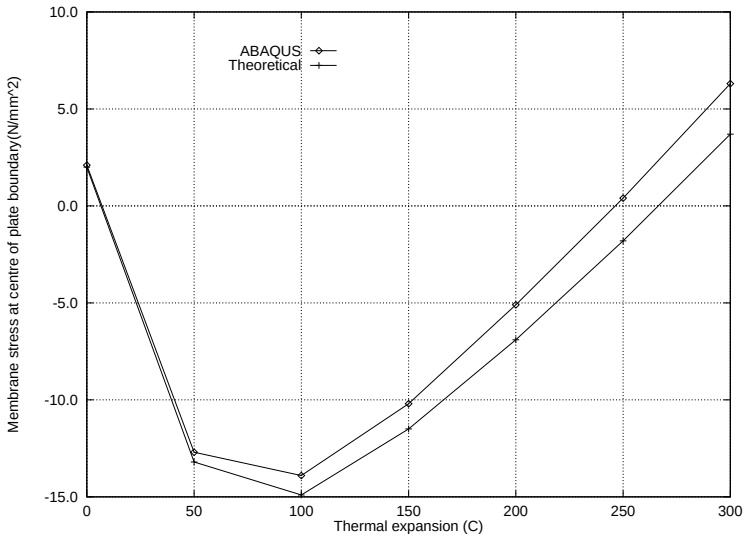

Figure 4.12: Membrane stresses at x=$L/2$ for L/B=1 with thermal gradient $T_{,z}$ of $1^oC/mm$

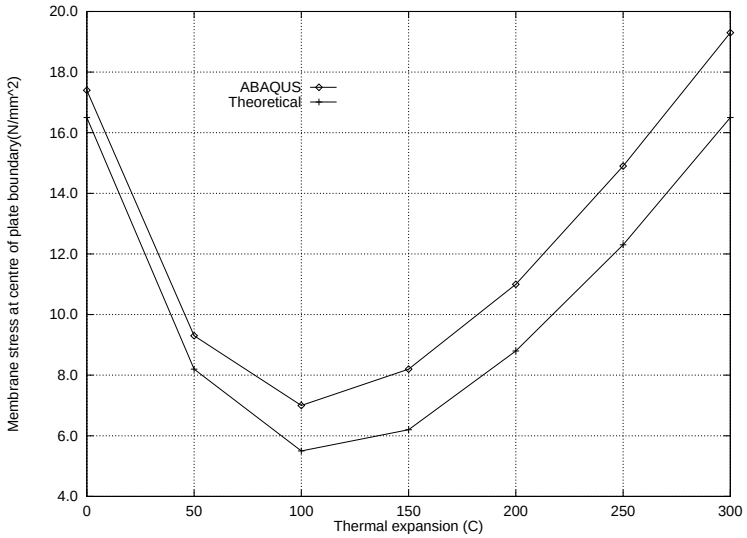

Figure 4.13: Membrane stresses at x=$L/2$ for L/B=1 with thermal gradient $T_{,z}$ of $4^oC/mm$

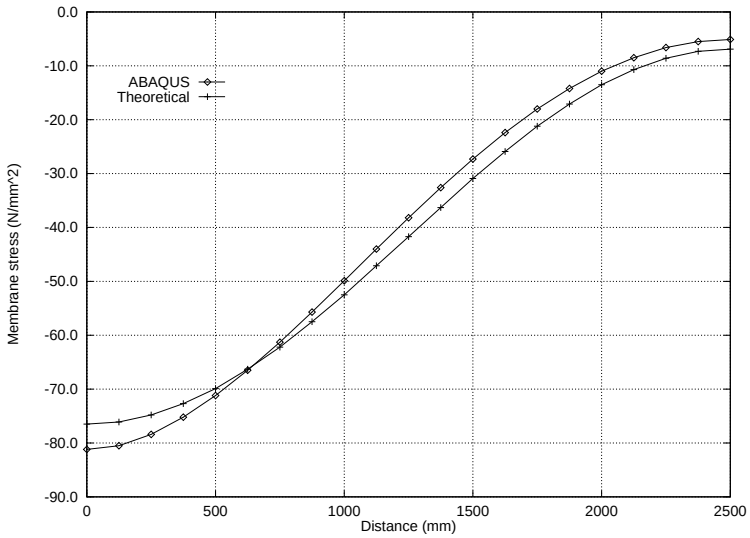

Figure 4.14: Membrane stresses along breadth B for L/B=1 with thermal gradient $T_{,z}$ of $1^oC/mm$ and thermal expansion ΔT of 200^oC

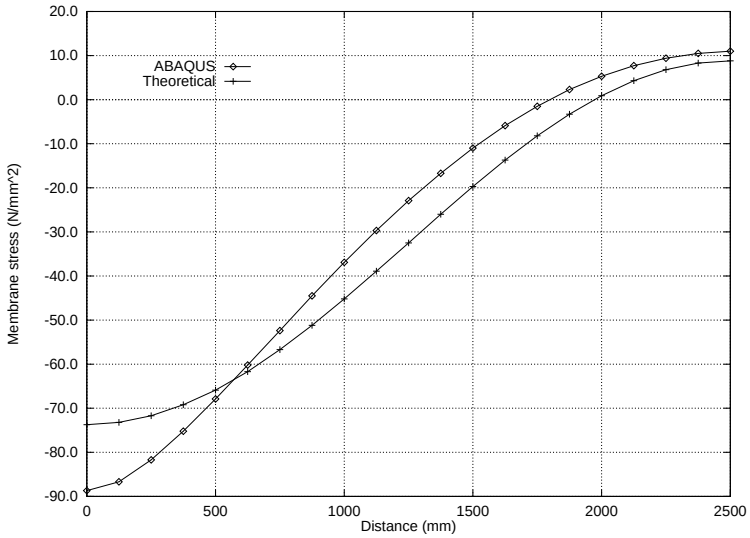

Figure 4.15: Membrane stresses along breadth B for L/B=1 with thermal gradient $T_{,z}$ of $4^oC/mm$ and thermal expansion ΔT of 200^oC

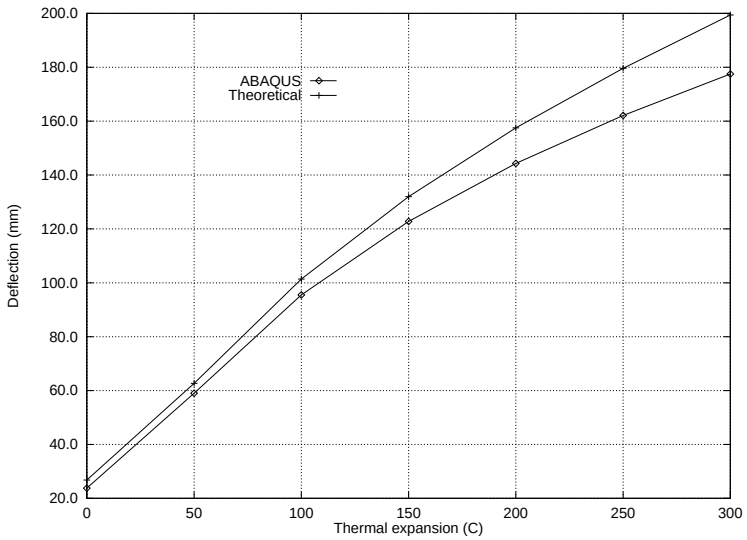

Figure 4.16: Centre deflections for L/B=1.5 with thermal gradient $T_{,z}$ of $1^oC/mm$

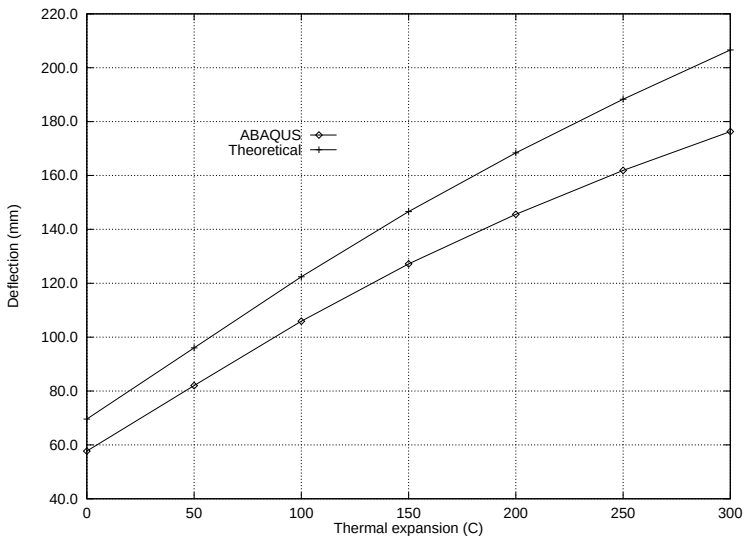

Figure 4.17: Centre deflections L/B=1.5 with thermal gradient $T_{,z}$ of $4^oC/mm$

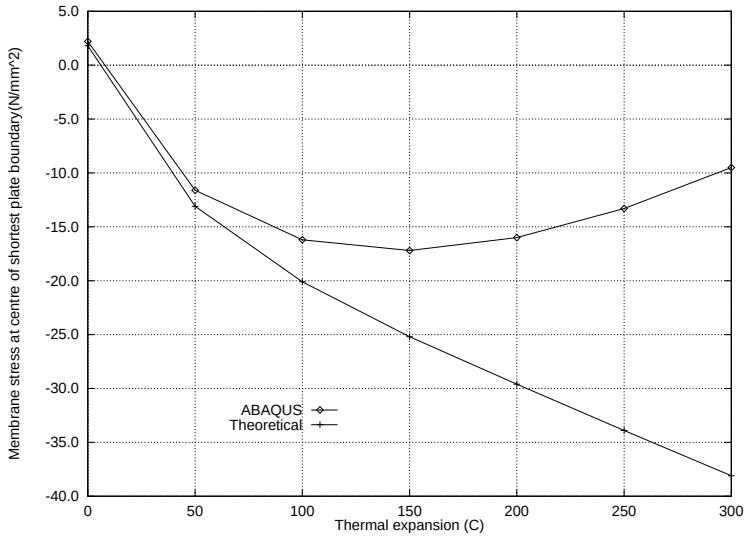

Figure 4.18: Membrane stresses at centre of short edge y=$B/2$ for L/B=1.5 with thermal gradient $T_{,z}$ of $1^oC/mm$

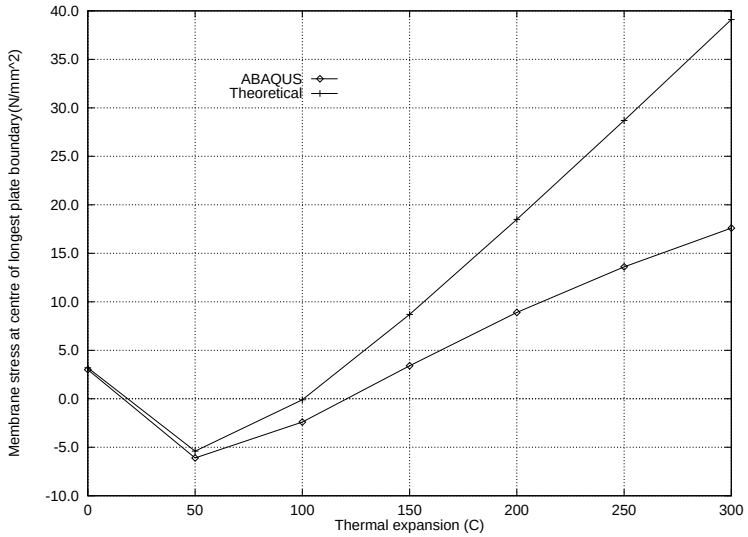

Figure 4.19: Membrane stresses at centre of long edge x=$L/2$ for L/B=1.5 with thermal gradient $T_{,z}$ of $1^oC/mm$

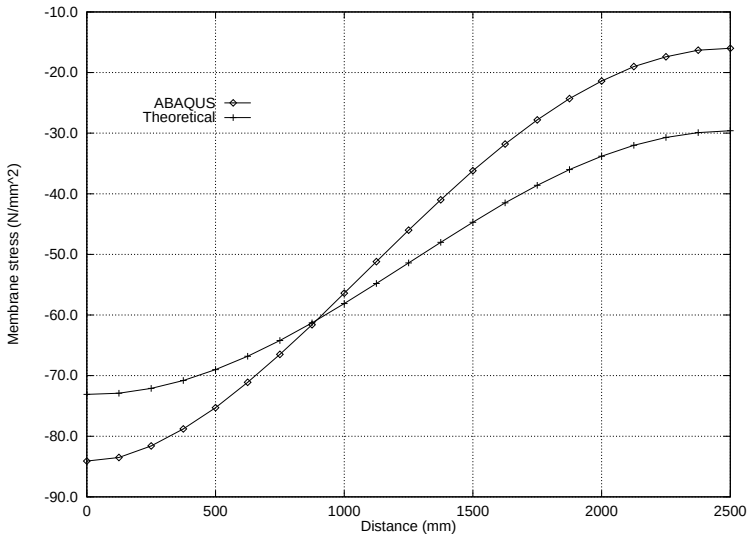

Figure 4.20: Membrane stresses along breadth B for L/B=1.5 with thermal gradient $T_{,z}$ of $1^oC/mm$ and thermal expansion ΔT of 200^oC

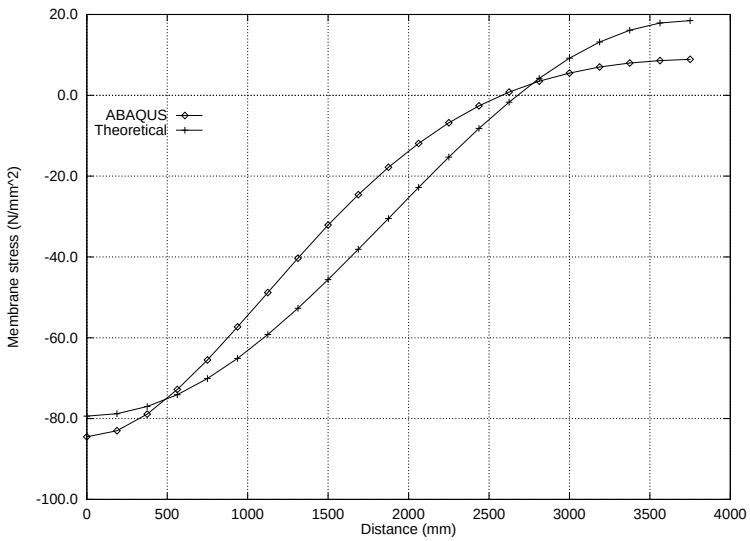

Figure 4.21: Membrane stresses along length L for L/B=1.5 with thermal gradient $T_{,z}$ of $1^oC/mm$ and thermal expansion ΔT of 200^oC

Chapter 5

Proposed Method for Ultimate Limit State Design of Concrete Floor Slabs in Fire

5.1 Introduction

Observations from the test on the Cardington building and numerical modelling have shown that in a fire the load transfer mechanism is membrane action in the slab. At the centre of the slab where the deflections are largest there will be tensile membrane action whilst nearer the boundaries there will be compressive membrane action. Whereas compressive membrane action is an unstable mechanism tensile membrane action, where the load is carried solely through the steel reinforcing bars, is stable. Existing methods for the design of floor slabs in fire that consider membrane action rely on extending approaches intended for ambient conditions. The load capacity is still calculated based on the yield-line approach utilising the bending capacity of the slab but with an enhancement based on the size of the membrane forces and the maximum deflection. This is not appropriate for fire design where the deflected shape of the slab is not suitable for developing yield lines and failure will occur by rupture of the reinforcement along the slab boundaries. This chapter details a proposed design method which considers the true behaviour and load carrying mechanism of the slab. It is assumed that all of the load is being carried through membrane action and any contribution

from bending strength is ignored.

5.2 Design method

5.2.1 Design philosophy

In producing a design method for floor slabs in fire there were two main points which had to be considered:

1. The slab must be designed for the correct load carrying mechanism.
2. The thermally induced loads (because of restrained thermal expansion) and their effects must be accounted for.

As stated previously the load carrying mechanism of a slab in a fire is membrane action. Although compressive membrane action along the slab boundaries will allow some of the load to be carried through bending, particularly in the corners where there are massive compression forces due to restrained thermal expansion, the majority of the load will be transferred through tensile membrane action. This is particularly true at the ultimate load capacity where deflections will be large. In this design method any bending capacity is ignored and it is assumed that the only reliable load carrying method is tensile membrane action.

In a fire the loading on a structural element is much more complex than in ambient conditions. The temperature distribution within an element produces thermal loads consisting of a thermal expansion force and a thermal moment which must be considered in design. These loads create internal forces and can cause deflections depending on the degree of restraint along the slab boundaries. When designing for fire, the structural engineer must therefore consider not only the dead and imposed loads on the slab but also the thermal forces.

5.2.2 Assumptions

To simplify the analysis procedure a number of assumptions were made. These are as follows:

1. The slab is assumed to be rectangular in plan.

2. The slab is assumed to be restrained against lateral translation along all boundaries but free to rotate.

   This is reasonable given very little restraint to lateral translation is actually required for slender members [15] such as slabs. Thermal gradients will cause large hogging moments at supports if rotations are restrained. With no reinforcement against these moments at the supports, rotations will freely occur in regions away from the stiff corners.

3. Anchorage to tensile membrane forces in the slab is available along the slab boundaries.

   To ensure that the tensile membrane mechanism can develop it is essential that the floor slab reinforcement is anchored at the compartment perimeter. Internally continuity could be provided by lapping of reinforcement. Compartments with exterior beams will require the reinforcement to be sufficiently anchored to the edge beams to ensure that there is sufficient restraint available. In addition to the detailing, this assumption is further helped by the development of compressive membrane behaviour in the slab along the perimeter supports. This 'compression ring' [**?**] occurs in ambient conditions but in a fire the compressive forces will be much larger due to restrained thermal expansion.

4. The temperature distribution in the slab varies only through the depth of the slab i.e. $T = f(z)$

5. The material behaviour for the reinforcing steel is considered temperature dependent.

   In this instance they are considered uniaxial and properties based on Eurocode 2 [5] are used. The Eurocode properties are further simplified as elastic perfectly plastic with infinite ductility unless a rupture strain is specified. This assumption is reasonable based on high temperature properties of steel.

6. It is assumed that failure during the heating phase of the fire is ductile with no localisation of strain occurring in the reinforcement.

   Observations from the Cardington tests and numerical modelling have shown that this is a reasonable assumption. Although there was localised straining and

rupture in the reinforcement over the supports in the Cardington tests [111], modelling work [10] has suggested that this did not take place during the heating phase. Tensions caused during cooling may be sufficient to fracture reinforcement at several locations over the supports in a similar fashion to the beam connections in the Cardington tests. This method is suitable for calculating the load capacity during the heating phase of the fire only.

7. The fire limit state is assumed to have reached when any part of the reinforcement achieves a mechanical strain equal to a limiting mechanical strain.

   In the case of cold rolled steel with a diameter of 12mm or less typical of slab reinforcement this would occur at a strain of 2.5%.

8. Compartment perimeter beams are assumed to deflect much less than the centre of the slab ($\delta_b << \delta_S$).

9. The deflected shape is governed entirely by the temperature distribution in the slab.

10. Membrane capacity is derived solely from the reinforcement

11. The temperature of the reinforcement and surrounding concrete are identical as are their thermal expansion coefficients such that no slippage occurs.

5.3 Analysis procedure

The proposed analysis consists of three separate stages:

1. **Thermal input:** Determine the likely fire scenario (unless given), and calculate the temperature distribution over the depth, $T(z)$. From this the equivalent thermal expansion ΔT and equivalent thermal gradient $T_{,z}$ of the slab can be calculated.

2. **Mechanical response:** For the given temperature distribution calculate the deflection of the reference surface of the slab $w(x, y)$ and the associated stress and strain states at the reference surface $\sigma(x, y)$ and $\epsilon(x, y)$ coincident with the plane of reinforcement.

3. **Load capacity:** Using an energy method determine ultimate membrane capacity.

Each stage is discussed separately in the following sections.

5.3.1 Determination of thermal loading

Fire scenario

There are a number of methods which can be used to determine the design fire. The simplest approach is the use of a standard fire curve such as BS476 or ASTME119, however, these are unlikely to be representative of a fire that would actually occur. If details such as the fuel load, available ventilation and thermal properties of the wall linings are known then a natural fire curve can be calculated using curves such as those found in Eurocode 1 [112].

Temperature distribution through the slab depth

When the temperature-time curve of the fire is known then any numerical procedure can be used to calculate the temperature distribution that this causes through the depth of the slab.

Estimation of equivalent temperature effects on the model

The temperature distribution through the depth of the slab will follow a parabolic curve and be highly non-linear. To simplify the calculation of the thermal loading to be applied to the slab an equivalent temperature distribution consisting of an equivalent mean temperature ΔT and an equivalent thermal gradient $T_{,z}$ are calculated using a method developed previously by Usmani [82]. The method divides the slab into a number of layers such as is used to estimate the effects of temperature on bridge decks [113] and allows the effects of different fires to be easily compared e.g. does a fire have a high mean temperature and low gradient or vice versa.

5.3.2 Determination of the mechanical response of the slab

Calculation of the deflection profile due to thermal loading

The deflection of the slab due to the equivalent temperature distributions is calculated using the method presented in Chapter 4. Using Eqn.4.100:

$$\begin{aligned} \frac{3}{4}\left\{\left(3-\nu^2\right)\left(1+\frac{L^4}{B^4}\right)+4\nu\frac{L^2}{B^2}\right\}\left(\frac{w_{\mathrm{T}}}{h}\right)^3 \\ \left\{\left(1+\frac{L^2}{B^2}\right)^2-12\frac{L^2\left(1+\nu\right)N^T}{\pi^2Eh^3}\left(1+\frac{L^2}{B^2}\right)\right\}\left(\frac{w_{\mathrm{T}}}{h}\right) \\ -192\frac{L^2\left(1+\nu\right)M^T}{\pi^4Eh^4}\left(1+\frac{L^2}{B^2}\right)=0 \end{aligned} \tag{5.1}$$

Calculation of stress-strain distribution in the reinforcement due to thermal loading

The membrane stress distribution along the boundary of the slab for any deflection w can be calculated using Eqns. 4.100 and 4.101:

$$\sigma_{xx} = \frac{w^2\pi^2E}{8(1-\nu^2)}\left(\frac{1}{L^2}+\frac{\nu}{B^2}\right)-\frac{w^2\pi^2E}{8L^2}\cos\frac{2\pi y}{B}-\frac{E\alpha\Delta T}{1-\nu} \tag{5.2}$$

$$\sigma_{yy} = \frac{w^2\pi^2E}{8(1-\nu^2)}\left(\frac{1}{B^2}+\frac{\nu}{L^2}\right)-\frac{w^2\pi^2E}{8B^2}\cos\frac{2\pi x}{L}-\frac{E\alpha\Delta T}{1-\nu} \tag{5.3}$$

In this instance we are interested in the stress in the reinforcement so the the Young's modulus should be that of the steel E_s.

Equations 5.2 and 5.3 can be rearranged to provide the mechanical membrane strains. When calculating ϵ_{xx} then x=0 or L and when calculating ϵ_{yy} then y=0 or B such that:

$$\epsilon_{xx,\mathrm{mech}} = \frac{w^2\pi^2}{8L^2}\left(1-\cos\frac{2\pi y}{B}\right)+\nu\frac{w^2\pi^2}{8B^2}-\alpha\Delta T \tag{5.4}$$

$$\epsilon_{yy,\mathrm{mech}} = \frac{w^2\pi^2}{8B^2}\left(1-\cos\frac{2\pi x}{L}\right)+\nu\frac{w^2\pi^2}{8L^2}-\alpha\Delta T \tag{5.5}$$

By removing the thermal components the total membrane strains can be calculated:

$$\epsilon_{xx,\mathrm{total}} = \frac{w^2\pi^2}{8L^2}\left(1-\cos\frac{2\pi y}{B}\right)+\nu\frac{w^2\pi^2}{8B^2} \tag{5.6}$$

$$\epsilon_{yy,\mathrm{total}} = \frac{w^2\pi^2}{8B^2}\left(1-\cos\frac{2\pi x}{L}\right)+\nu\frac{w^2\pi^2}{8L^2} \tag{5.7}$$

Ductility Class	ϵ_{uk} (%)
H	>5
N	>2.5

Table 5.1: EC2 ductility classes

The values of x and y chosen should correspond to the positions of the reinforcement along the edge so that a mechanical stress and mechanical strain are calculated for each bar. These will be defined as $\sigma_{w_{\mathrm{T}}}$, $\epsilon_{w_{\mathrm{T}}}$. Should the calculated mechanical stress be greater than the yield stress then it is necessary to define the stress as $\sigma_{w_{\mathrm{T}}} = \sigma_{y,T}$ where $\sigma_{y,T}$ is the yield stress of the reinforcement at a temperature T.

5.3.3 Failure criterion

To obtain a value for the ultimate load it is necessary to define a point at which failure is said to have been reached. Geometrical limits such as $span/30$ should not be applied in a situation such as this where, due to thermal expansion, large deflections do not necessarily mean the structure is near failure. A better approach is to apply a limiting value for the mechanical strain based on the ductility of the reinforcing bars. EC2 [114] recognises two classes of ductility, high ductility (H) and normal ductility (N). Table 5.1 shows the ductility properties given in EC2 where ϵ_{uk} is the characteristic value of the elongation at maximum load. EC2 states that reinforcement with a bar size of 16mm or above can be treated as being highly ductile whereas if the bar size is 12mm or less then normal ductility should be assumed.

For the purposes of this design method it will be assumed that the ultimate load has been reached when any of the reinforcing bars reaches this mechanical strain limit. In practice this will always occur in the reinforcing bars at the centre of the slab across the shortest span over supports. This is where the greatest tensile stresses occur. The total strain $\epsilon_{\mathrm{total}}$ at which this point is reached is calculated by considering the ductility class and the thermal expansion such that:

$$\epsilon_{\mathrm{total}} = \epsilon_{uk} + \alpha \Delta T \tag{5.8}$$

The limiting deflection w_{t} at which this total strain value is reached can be calculated using Eqn. 5.5 as the shortest span will reach the mechanical yield strain limit first.

By setting $\epsilon_{\text{mech}} = \epsilon_{uk}$ and $w = w_{\text{t}}$ and rearranging:

$$w_{\text{t}} = \frac{B}{\pi}\sqrt{4(\epsilon_{uk} + \alpha\Delta T)} \tag{5.9}$$

5.3.4 Determination of the ultimate membrane capacity

Calculation of stress-strain distribution due to combined loading

At the ultimate limit deflection w_{t} there will be tensile membrane forces throughout most of the slab and so some cracking of the concrete will occur. EC2 [114] states that for concrete in tension with cracks that Poisson's ratio should be taken as zero. In calculating the stress in the reinforcement at the deflection w_{t} it is therefore necessary to modify Eqns. 5.2 and 5.3 slightly to take account of this such that:

$$\sigma_{xx} = \frac{w_t^2 \pi^2 E_s}{8L^2}\left(1 - \cos\frac{2\pi y}{B}\right) - E_s\alpha\Delta T \tag{5.10}$$

$$\sigma_{yy} = \frac{w_t^2 \pi^2 E_s}{8B^2}\left(1 - \cos\frac{2\pi x}{L}\right) - E_s\alpha\Delta T \tag{5.11}$$

If the reinforcement bars are at a temperature that will cause the steel properties to degrade then appropriate reduced values of E_s and $\sigma_{y,T}$ should be chosen. The mechanical strains can be calculated using Eqns. 5.4 and 5.5. Again, a mechanical strain and mechanical stress should be calculated for every reinforcing bar and values of x and y should be chosen accordingly. The mechanical stress and mechanical strain at this deflection will be defined as $\sigma_{w_{\text{t}}}$, $\epsilon_{w_{\text{t}}}$.

Calculation of internal work done

To determine the internal work done as the slab moves through the deflection w_{q} is a complicated procedure. The internal work must be calculated for every reinforcing bar as they are all different. Initially the stress strain states in the reinforcement caused by the thermal loading are considered. Due to the deflection w_{T} caused by the thermal load each bar will have a particular mechanical stress and strain $\sigma_{w_{\text{T}}}$, $\epsilon_{w_{\text{T}}}$. These have been calculated in Section 5.3.2 using Eqns.5.2, 5.3, 5.4 and 5.5.

If a square slab under thermal loading is considered then the largest deflections will occur at its centre. Figure 5.1 shows a typical membrane stress distribution along the

boundary of a laterally restrained slab with an aspect ratio close to one. It would be possible, however, for the membrane stresses at midspan to be compressive depending on the temperature distribution within the slab and the aspect ratio.

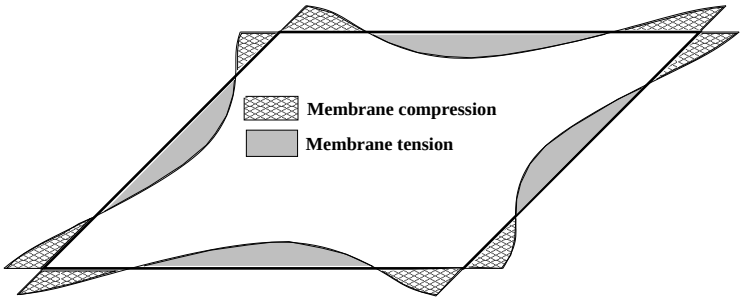

Figure 5.1: Typical normal membrane stress distribution along slab boundary due to fire

The failure point of the slab has been defined as when the slab has a total deflection of w_{t} corresponding to a limiting mechanical strain ϵ_{uk} in the reinforcement. Due to this deflection each reinforcing bar will have a mechanical stress and strain $\sigma_{w_{\mathrm{t}}}$,$\epsilon_{w_{\mathrm{t}}}$ as calculated in Section 5.3.4. At the deflection w_{t} the magnitude of the membrane stress distribution normal to the slab edge has changed. Figure 5.2 shows a typical membrane stress distribution due to a thermal load and also a combined load in the reinforcing bars along the boundary, the points represent the position of the reinforcing bars. It can be seen that under the combined loading more of the reinforcing bars are in tension. Near the middle of the slab boundary the reinforcing bars have reached yield such that $\sigma_{w_{\mathrm{t}}} = \sigma_{y,T}$ and $\epsilon_{w_{\mathrm{t}}} > \epsilon_{y,T}$.

The internal work done is defined as the energy required to move from the stress-strain state $\sigma_{w_{\mathrm{T}}}$, $\epsilon_{w_{\mathrm{T}}}$ at a deflection of w_{T} due to the thermal loading to the stress-strain state $\sigma_{w_{\mathrm{t}}}$, $\epsilon_{w_{\mathrm{t}}}$ at a deflection of $w_{\mathrm{t}} = w_{\mathrm{T}} + w_{\mathrm{q}}$ due to the combined loading. Figure 5.3 shows a typical change in the stress-strain state for a reinforcing bar. The shaded area represents the internal work done.

Considering the differing stress-strain states in each reinforcing bar it can be seen that to calculate the internal work done is a complicated process. If V is the volume of a reinforcing bar then the total internal work done can be defined as:

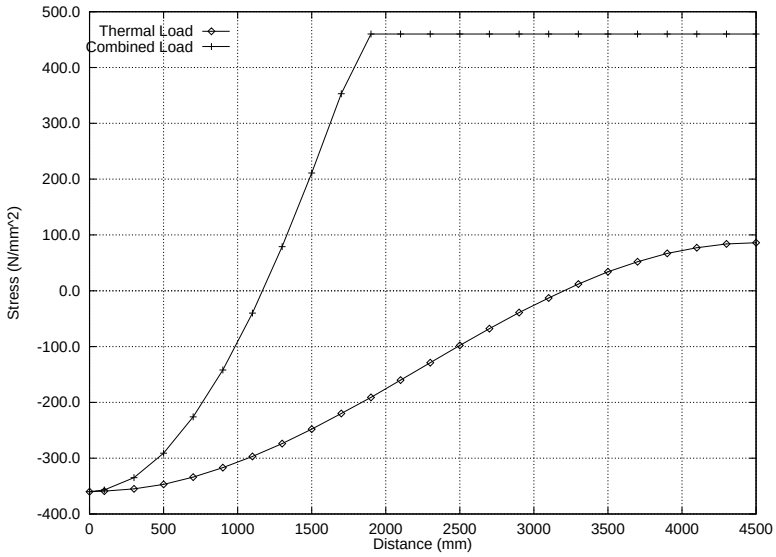

Figure 5.2: Membrane stress in reinforcing mesh along slab boundary

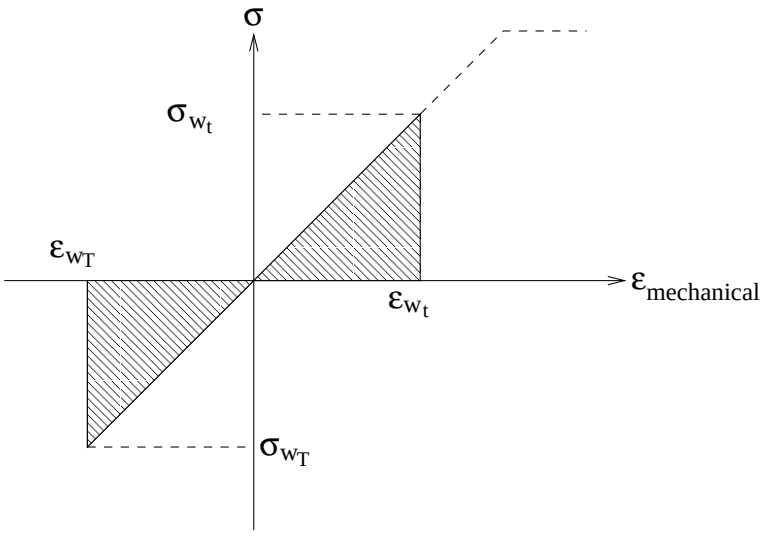

Figure 5.3: Mechanical stress-strain in reinforcing bar

$$\Pi_{int} = \sum_{n=1}^{\text{no. rebar}} \int_V \Delta\sigma\Delta\epsilon \, \mathrm{d}V \tag{5.12}$$

where

$$\Delta\sigma = \sigma_{w_\mathrm{t}} - \sigma_{w_\mathrm{T}} \tag{5.13}$$

$$\Delta\epsilon = \epsilon_{w_\mathrm{t}} - \epsilon_{w_\mathrm{T}} \tag{5.14}$$

It is necessary, however, to divide the distance w_q into increments and calculate the internal energy at these points.

Calculation of external work done

Calculation of the external work done by the load is straightforward. Keeping the assumption that the deflected shape forms a double Fourier sine surface then the external work done is that of the load moving through a deflection increase Δw and can be calculated:

$$\begin{aligned} \Pi_{ext} &= \int_0^L \int_0^B q_\mathrm{ult} \Delta w \sin \frac{\pi x}{L} \sin \frac{\pi y}{B} \, \mathrm{d}x \, \mathrm{d}y \\ &= q_\mathrm{ult} \Delta w \frac{4LB}{\pi^2} \end{aligned} \tag{5.15}$$

Calculation of ultimate membrane capacity of slab

Comparing the internal and external work done the load q that the slab is capable of carrying at any deflection can then be calculated. Over any increment the load that the slab is capable of carrying can be calculated:

$$q_\mathrm{ult} = \frac{\Delta\Pi_{int}}{\Delta\Pi_{ext}} \tag{5.16}$$

It is possible to construct a plot of the load-deflection response of the slab and the smaller the size of the increment chosen the more accurate the answer obtained will be. At the maximum allowable deflection w_t the load calculated from Eqn. 5.16 will be the ultimate load capacity of the slab q_ult.

5.3.5 Contribution of unprotected composite secondary beams

At the limit state it can be reasonably assumed that unprotected secondary beams will retain very little flexural stiffness due to material degradation. Axial stiffness will provide the only available contribution. Furthermore, it can be assumed that the deflection profile of unprotected secondary beams will depend entirely on the profile of the much stiffer slab. It can also be conservatively assumed that the mean temperature of the unprotected beam is close to the atmosphere temperature during the heating phase of the fire. As the beam is constrained to the deflection profile imposed by the slab, it is reasonable to assume that the additional load capacity provided by the beam is governed by the compatibility principle. These assumptions provide a simple modification of the internal work expression of Eqn. 5.12 to:

$$\Pi_{int} = \sum_{n=1}^{\text{no. rebar}} \int^{V} \Delta\sigma\Delta\epsilon \, \mathrm{d}V + \sum_{n=1}^{\text{no. beams}} \int^{V} \Delta\sigma_B\Delta\epsilon_B \, \mathrm{d}V \tag{5.17}$$

where

$$\Delta\sigma_B = \sigma_{beam,w_t} - \sigma_{beam,w_T} \tag{5.18}$$

$$\Delta\epsilon_B = \epsilon_{beam,w_t} - \epsilon_{beam,w_T} \tag{5.19}$$

Calculation of stress-strain in unprotected composite secondary beams

The equations below are written assuming the secondary beams span across the short direction (B). If the thermal expansion of the beam is defined as ΔT_b, the mechanical stress and strain in the secondary beams after the thermal loading can be calculated:

$$\sigma_{beam,w_T} = \frac{w_t^2\pi^2 E_b}{8B^2}\left(1 - \cos\frac{2\pi x}{L}\right) - E_b\alpha_b\Delta T_b \tag{5.20}$$

$$\epsilon_{beam,w_T} = \frac{w^2\pi^2}{8B^2}\left(1 - \cos\frac{2\pi x}{L}\right) - \alpha_b\Delta T_b \tag{5.21}$$

At the limiting deflection the mechanical stress and strain can be calculated as:

$$\sigma_{beam,w_t} = \frac{w_t^2\pi^2 E_b}{8B^2}\left(1 - \cos\frac{2\pi x}{L}\right) - E_b\alpha_b\Delta T_b \tag{5.22}$$

$$\epsilon_{beam,w_t} = \frac{w^2\pi^2}{8B^2}\left(1 - \cos\frac{2\pi x}{L}\right) - \alpha_b\Delta T_b \tag{5.23}$$

An appropriate reduced value of E_b and yield stress σ_{y,T_b} should be chosen based on the temperature T_b of the secondary beams. The value of x chosen should correspond to the position of the secondary beams under the slab. By applying Eqns. 5.20, 5.21, 5.22 and 5.22 in Eqn. 5.17, the contribution of the beam to the limit capacity can be calculated.

5.4 Additional design considerations

5.4.1 Internal beam connections

At the fire limit state the vertical shear force acting on a connection will be different to that at ambient. This is because of the change in the load-carrying mechanism and the likelihood that the applied load will be smaller due to evacuation. Whereas at ambient a composite floor slab is designed as one-way spanning, in a fire this may change such that it may be acting as two-way spanning depending on the aspect ratio of the fire compartment considered. A larger amount of the vertical shear force may therefore be transferred to connections on secondary beams thus reducing the shear load on the primary beam connections.

For internal boundaries the horizontal force from the membrane action will be transmitted from the reinforcement directly into the surrounding composite floor and would not need to be considered in the design of connections. It would be necessary however to ensure that there is sufficient lapping and anchorage to be capable of transferring the force from a bar at tensile yield.

5.4.2 Lateral restraint on exterior compartments

When an outer compartment is subjected to a fire the lateral restraint assumed at the panel boundary must be provided by the composite action of the edge beam and the floor slab. At the fire limit state the forces acting on the edge beam and its connections will be larger than at ambient conditions and this must be accounted for in the design process. Figure 5.2 shows a typical membrane stress distribution along the edge of a panel. The edge beam will therefore need to be capable of carrying both the standard vertical load as well as the additional horizontal load due to the membrane forces.

As shown in Fig. 5.2 the actual stress distribution along the panel boundary is complex. At the centre of the edge tensile yield will have been reached, however, at the corners there will be large compressive forces due to restrained thermal expansion. This stress distribution will create a complicated distribution of forces along the length of the beam. Near to the column supports where the floor is very stiff the compressive forces will be transmitted as shear. Towards the centre of an external edge beam where there is less restraint the forces will be tensile and could create a torsional moment acting on the beam. However, the slab and beam will be acting compositely due to the connecting shear studs and so will have considerable rotational stiffness to resist this force. The issue for the designer therefore becomes one of shear with the beam-column connections having to resist a double shearing action. A connection will need to be designed for both the vertical shear force:

$$S_v = \frac{wL}{2} \tag{5.24}$$

where w is the load per unit length acting on the beam at the fire limit state and also a horizontal shear force from the membrane forces:

$$S_h = \sum_{n=1}^{\text{no. rebar}} \frac{A_s \sigma}{2} \tag{5.25}$$

Five of the six tests carried out on the Cardington building were on compartments with external beams and none of the edge beams appeared to be affected by torsional forces. Not all of the beams had fire protection applied and although they did deflect they provided sufficient strength for the slab to transmit load through membrane action.

5.5 Limitations of the design method

There are a number of limitations to the proposed design method that has been presented. The assumptions made in Section 5.2.2 impose a number of limitations whilst others are due to limits in the current theory. The three main limitations are:-

1. Any bending or membrane strength in the concrete is currently ignored
2. Profiled decks are not explicitly dealt with
3. Slab perimeter beams must be protected so their deflection is low

Bending and membrane strength of concrete

Ignoring any bending or membrane strength in the concrete allows a conservative estimation of the slab capacity to be determined. The effect of ignoring the concrete can best be quantified if the potential internal energy available in the slab is considered. This can be considered to consist of two components, the energy available in the steel and that in the concrete. As has been shown the calculation of the energy in the steel is relatively straightforward, this is helped by the fact that it can be assumed that all the steel is at the one temperature. Given the relative volumes of the concrete and steel the available potential energy in the concrete is extremely large even though it is much weaker than the steel. Calculation of the energy in the concrete is complicated by a number of issues:

1. the temperature in the concrete varies through the depth in the z-direction
2. the stress and strain distribution varies in the x-, y- and z-directions
3. cracking of the concrete will occur

As the concrete will crack at relatively low strains the majority of the concrete energy will be developed at small deflections. After a crack has developed then that concrete can contribute no more energy and all of the internal energy will be developed in the steel. The result of this is that for a required load capacity, by including the concrete energy, the deflection at which the slab can carry this load will be much lower than if only the steel contribution was considered. With regards to the fire situation this is important when considering compartmentation issues. The highly complex stress-strain distribution which varies in three-dimensions means that calculation of the concrete internal energy is only practical by computer. It is possible, however, to perform the necessary calculations for the design method by hand when only steel is considered. It can therefore be concluded that the current method is suitable for calculation of a conservative value for the load capacity at the structural limit state.

Profiled decking

The cubic equation Eqn. 4.100 for calculating the deflection of the slab under the thermal loading currently assumes that the slab is of constant depth. In the situation

where the floor is profiled such as at Cardington then an approximation for the depth of the slab would need to be made. Bailey [40] assumes a depth based on the average height of the troughs and the ribs. Other types of profiled decks such as dovetails might be better dealt with by assuming the slab to be the full depth of the rib. This would seem reasonable as the profiling is much less significant than in other types of decking system.

Including profiled decks explicitly in an analytical solution is difficult. This is due to the thermal loading which should be applied. The thermal loading depends on the temperature distribution through a section and if a floor is profiled then the temperature distribution can not be assumed to be only a function of the depth. To describe analytically a thermal loading distribution where the load is a function varying in the x-, y- and z- directions would be extremely difficult and an approximation for average loading values would be required.

Slab perimeter beam protection

Although the design method presented allows some beams to be left without fire protection applied it still requires beams on the perimeter of the slab being considered to be protected. There are good reasons for this the most important being compartmentation issues. If beams deflect significantly then holes will develop in walls which would allow the escape of hot gases and flames. Fire could then spread to the next compartment. However, the need for protection on these beams increases construction costs. There is the cost and application of the materials themselves and the need for a site engineer to verify that the correct beams have been protected. If the wrong beams were protected then it could prove disastrous in the event of a fire. Another issue stems from the possible need to increase the size of the compartment perimeter beams to ensure they retain sufficient strength. With no protection applied they would quickly reach high temperatures and become very weak. Removing the need for protection on compartment perimeter beams would undoubtedly reduce costs and eliminate the potential danger of the wrong beams being protected, however, it may not be possible given compartmentation requirements and the need to resize the beams.

Cooling capacity

As it stands the method can be applied to structures during the heating phase of a fire. The structural behaviour during the cooling phase is equally complex and the issue of whether the calculated capacity is available at this time is extremely important. As the intensity of the fire starts to reduces the compartment temperatures fall and the steel beams will immediately start to cool. They will quickly regain strength. The slab, however, will still be absorbing heat and trying to deflect. This generates large tensile forces in the beams as they are forced to adopt the deflection profile imposed by the slab. If the unprotected secondary beams are being relied upon to help carry the required load then their connections must be capable of withstanding these tensile forces.

5.6 Conclusion

The procedure presented in this chapter provides a robust and scientific method of calculating the membrane load capacity of a composite floor slab. Both the thermal and applied loads acting on the slab are considered and the ultimate load capacity of the slab calculated using an energy method. It is assumed that all of the load is carried through membrane action in the steel reinforcement. Rather than impose geometrical limits such as span/20 a limiting value of mechanical strain is used to define failure. The contribution of any unprotected secondary beams to the load capacity can be included by treating them in a similar fashion to a reinforcing bar. Perimeter beams in internal compartments may have an increased shear load at the beam-column connections due to the change in the load transfer mechanism from one-way bending action to two-way membrane action. This may require an increase in the connection strength. Similarly, an external edge beam will require the beam-column connections to be designed to carry both the standard vertical shear force and also the additional horizontal shear force due to the membrane forces in the slab.

Currently compressive membrane action in areas of the floor with low deflections are not considered. Profiled steel decks are not explicitly considered and it is necessary to make an approximation for the depth and the temperature distribution through the section. It is required that perimeter steel beams have protection applied, however, it

may be possible to remove this if deflections can be shown to be low and there are no compartmentation issues.

Chapter 6

Numerical Analysis of Concrete Floor Slabs in Fire

6.1 Introduction

The method presented in Chapter 5 for the analysis of composite floor slabs under thermal effects was developed entirely from structural mechanics. This chapter presents the results of a series of parametric studies that were carried out using numerical models of a range of slabs to determine how accurately the analysis method can predict the structural behaviour of laterally restrained floor slabs.

6.2 Slab properties

6.2.1 Geometry

A number of different slab geometries were considered. The first model consisted of a one-way spanning slab with a span of 6m, the aim of this initial study was to investigate how the theoretical solution deals with pure catenary action. This would provide confidence that the method can accurately predict the load carried through tensile membrane action such that any difference in the solution for the two-way spanning slabs would be due to other load-carrying mechanisms or assumptions in obtaining the solution.

Two different geometries were analysed for the two-way spanning slabs. Firstly a square 6m x 6m slab was modelled. Subsequently a 6m x 9m slab was analysed to provide a slab with a larger aspect ratio. A standard A142 mesh was used for all analyses and the slab depth was kept constant at 100mm.

6.2.2 Loading

To ensure that the loading in the finite element model represented that which would occur in reality it was separated into two stages. In stage one the dead and imposed loads were applied to the slab, in stage two the thermal load caused by the fire was applied. The thermal load was represented by specifying the temperature distribution through the depth of the slab at the end of the fire. To ensure that the highly non-linear nature of the temperature distribution was captured, the temperatures were specified at twenty-one separate points through the depth of the slab, this gave a reading every 5mm. During the analysis the temperature at each point increases linearly from zero at the beginning to its final value.

The actual temperature distribution applied was that calculated previously in Section 5.3.1. It is based on the Eurocode 1 parametric fire and produced a temperature variation through the slab as shown in Fig. 6.1.

The maximum temperature of the reinforcement that is reached in a fire depends on its position within the slab. As the position of the reinforcement is lowered towards the fire exposed face the maximum temperature reached increases. Although it is unlikely that in a fire the reinforcement temperature would go above 400^oC analyses were run with temperatures up to 700^oC to give confidence over a wide range of temperatures. The reinforcement height was varied to give maximum temperatures between 100^oC and 700^oC in increments of 100^oC.

6.2.3 Material properties

The concrete was taken to have an ambient crushing strength of $30N/mm^2$. Variation of the concrete properties with temperature were based on the values given in Eurocode 2 [5]. Reinforcement was taken as having an ambient yield stress of $460N/mm^2$ and

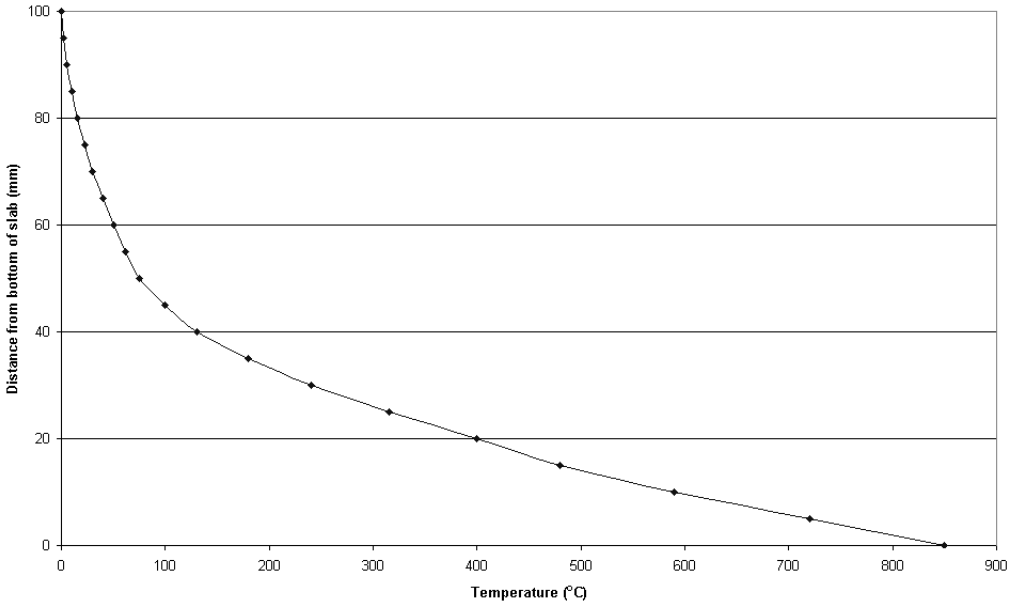

Figure 6.1: Temperature distribution through a 100mm slab

the material properties were assumed to follow the rules given in Eurocode 2. For all analyses the area of reinforcement was 142mm^2/m.

6.3 Numerical model

6.3.1 Element selection

The concrete slab was modelled using the S4R element. This is a four-noded shell element with reduced integration. The steel reinforcing mesh was represented as a smeared layer i.e. of constant thickness equal to the area of one reinforcing bar divided by its spacing.

6.3.2 Material models

Steel

The stress-strain curves of the reinforcing steel were described by inputing values of stress and strain at discrete points along the curve over a range of temperatures at

increments of 100^{o}C. Between the defined temperature values the stress and strain are interpolated linearly.

Concrete

The material model used to describe the concrete behaviour was the concrete damaged plasticity model [115] within the ABAQUS finite element package [116]. It is a continuum, plasticity-based damage model that assumes the two main failure mechanisms of the concrete are tensile cracking and compressive crushing. Under compression the stress-strain curve is linear up to the initial yield point. Beyond the ultimate stress strain softening reduces the allowable compressive stress to zero. The tensile portion of the behaviour is linear to the failure stress beyond which the cracks which would develop are represented by strain-softening.

If unloading occurs from a part of the stress-strain curve which has been affected by strain-softening then the elastic stiffness is reduced due to either tensile or compressive plastic straining. This is defined by introducing a damage variable which is a function of plastic strain and temperature.

Typically concrete will fail in tension at a stress that is approximately 10% of its compressive strength, however, the Eurocodes allow the tensile strength of concrete to be ignored. To aid convergence in a numerical model it is often necessary to introduce some tension stiffening to represent the transfer of load from the concrete to the reinforcement. This was done by defining a post-failure stress-strain relationship for the concrete. The result of this was that once the concrete had reached its ultimate tensile stress this value was maintained regardless of the strain i.e. the concrete is assumed to be capable of transferring this stress across cracks. At large strains this introduces an artificial strength to the system. With a reinforcement temperature below 400^{o}C it was possible to have a low failure tensile stress, 0.01N/mm^2. This did not significantly affect the result as the majority of the strength came from the reinforcement. At higher reinforcement temperatures, however, convergence became more difficult as the reinforcement which was being used to transfer load across the cracks was becoming weaker. To obtain a solution it became necessary to increase the tensile stress remaining across any cracks to 0.1N/mm^2. Although still a low value it becomes more significant

when the size of force which can be developed in the reinforcement is considered. It therefore became necessary to include the additional internal energy that this strength introduces to the system in some of the theoretical calculations so that a reasonable comparison could be made between results.

6.4 Analysis of a one-way spanning slab

The theoretical analyses using the energy method in Chapter 5 produced results which closely followed those from the numerical models (see Figs. 6.2-6.8). Up to a reinforcement temperature of 400^oC the theory overpredicts the load capacity at lower deflections. This is probably due to the sequence in which the loads are applied. In the theoretical solution the thermal load is applied first and then the normal load is applied whereas in the numerical model the thermal load is applied last.

As the deflections increase and the limiting deflection (calculated from the thermal strain plus the allowable mechanical strain of 2.5%) is reached the theoretical and numerical results converge and the results agree very closely. This is demonstrated in Fig. 6.9 which shows the failure envelope of the slab i.e. membrane load capacity against reinforcement temperature. Values of the numerical load capacity were based on the load required to achieve the limiting deflection. The largest error between the results occurs at a temperature of 400^oC where the theory overpredicts the numerical result for the ultimate load by 5%.

Above 400^oC the theory underpredicts the load capacity. This is because it was necessary to increase the tensile strength of the concrete to achieve convergence as described in Section 6.3.2. The additional internal energy which this creates leads to the difference between the results. As the steel yield stress reduces with increasing temperature the concrete contributes a higher percentage of the internal energy. Below a reinforcement temperature of 400^oC the steel contributes 94% of the internal energy, however, at higher temperatures this value reduces until at 700^oC the steel is contributing only 66%. Table 6.1 shows the percentage of the total energy content in the numerical model that comes from the steel reinforcement at different reinforcement temperatures, this is assuming that tensile yield has been reached over the entire concrete section.

Temperature (^oC)	Limiting deflection (mm)	Theoretical ultimate load (kN/m^2)	Numerical ultimate load (kN/m^2)	Theoretical ultimate load/ Numerical ultimate load	Steel energy (%)
100	614	8.57	8.52	1.01	93.8
200	621	8.66	8.55	1.01	93.8
300	634	8.85	8.54	1.04	93.8
400	641	8.94	8.49	1.05	93.8
500	649	7.47	7.77	0.96	89.0
600	658	4.32	5.63	0.77	82.6
700	670	1.93	3.37	0.57	66.1

Table 6.1: Summary of analyses of one-way spanning slab

To confirm that the error between the results was due to the concrete tensile strength a second theoretical analysis with a reinforcement temperature of 700^oC was carried out which accounted approximately for the additional energy in the concrete. It was assumed that the concrete had reached tensile yield throughout its entire depth. The results, which produced a close match to the numerical model, are shown in Fig. 6.8.

Table 6.1 summarises the theoretical and numerical results. The errors between the theoretical and numerical results are small and show that the theoretical design method accurately describes the tensile membrane behaviour of a one-way spanning composite floor slab.

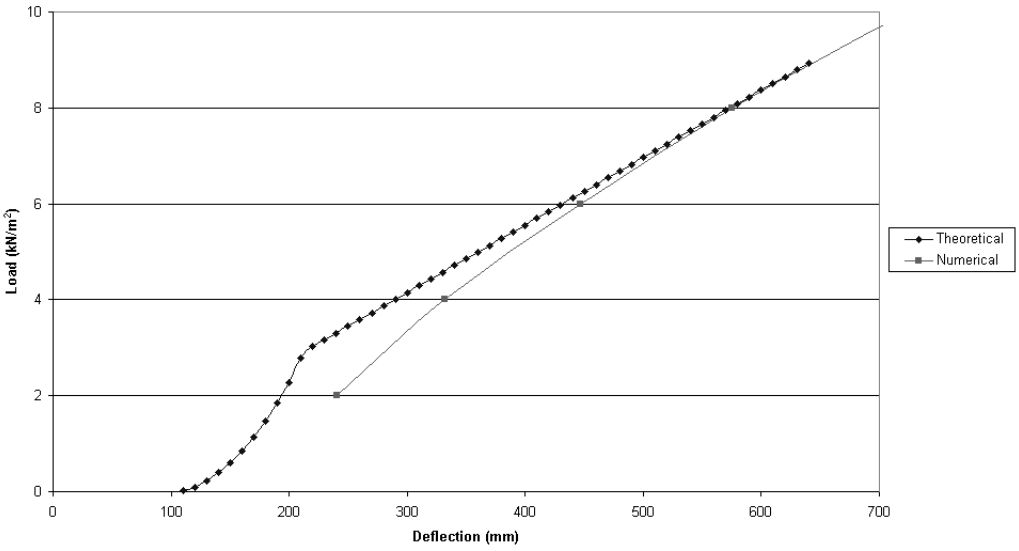

Figure 6.2: Load-deflection relationship for one-way spanning slab with reinforcement temperature of 100^oC

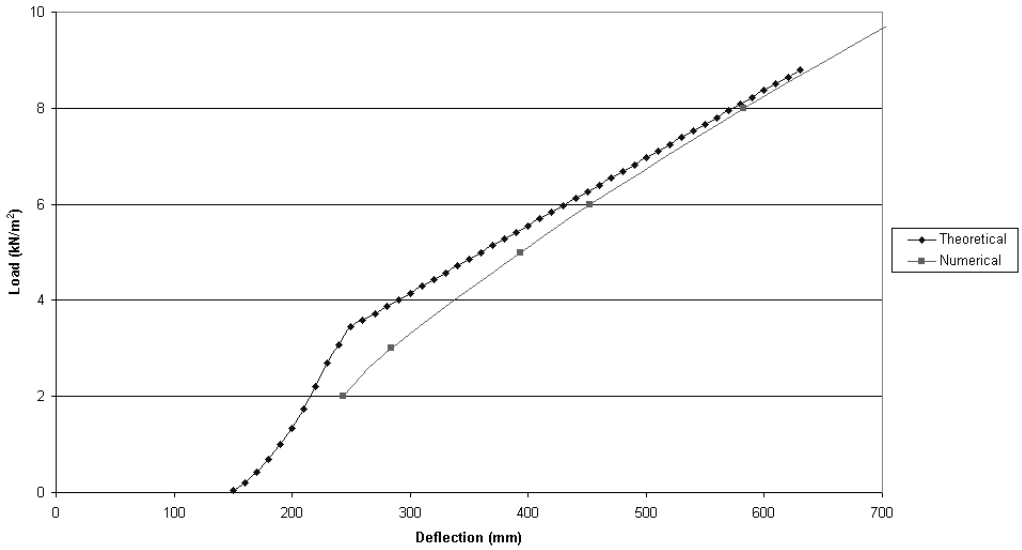

Figure 6.3: Load-deflection relationship for one-way spanning slab with reinforcement temperature of 200^oC

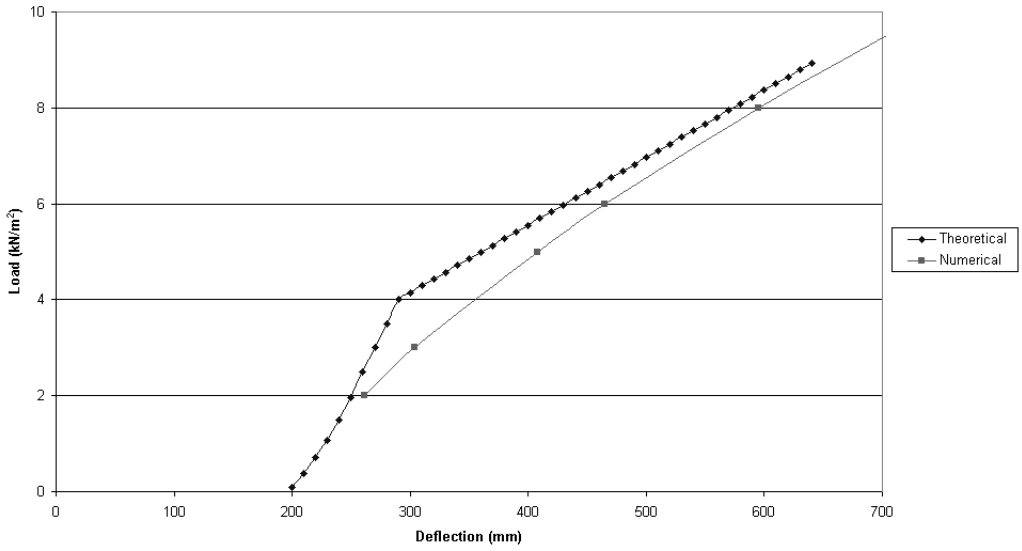

Figure 6.4: Load-deflection relationship for one-way spanning slab with reinforcement temperature of 300^oC

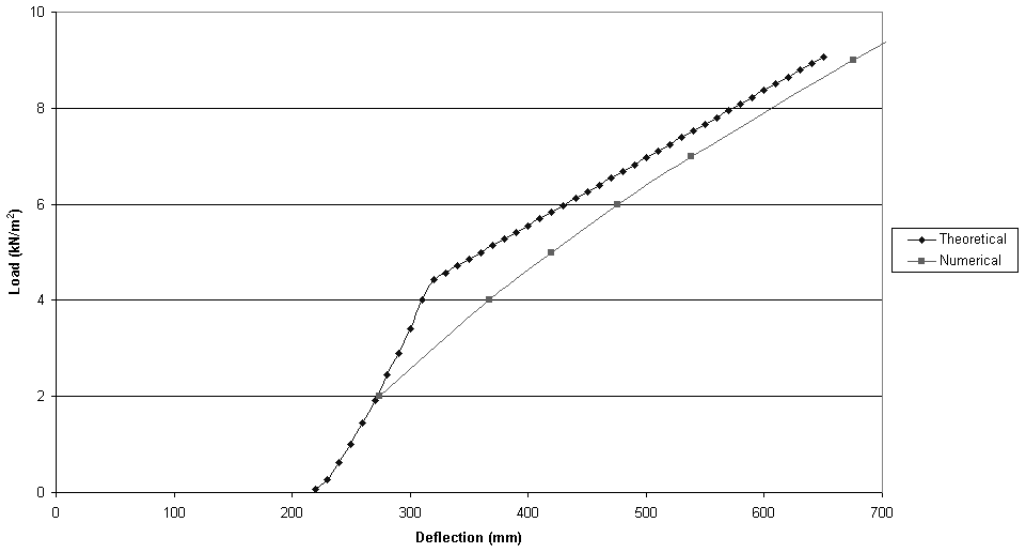

Figure 6.5: Load-deflection relationship for one-way spanning slab with reinforcement temperature of 400^oC

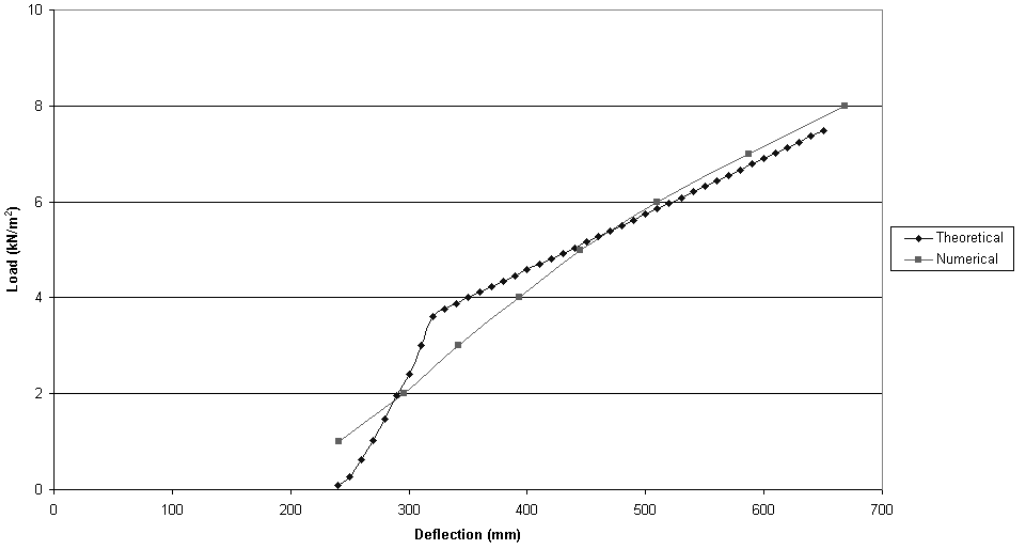

Figure 6.6: Load-deflection relationship for one-way spanning slab with reinforcement temperature of 500^oC

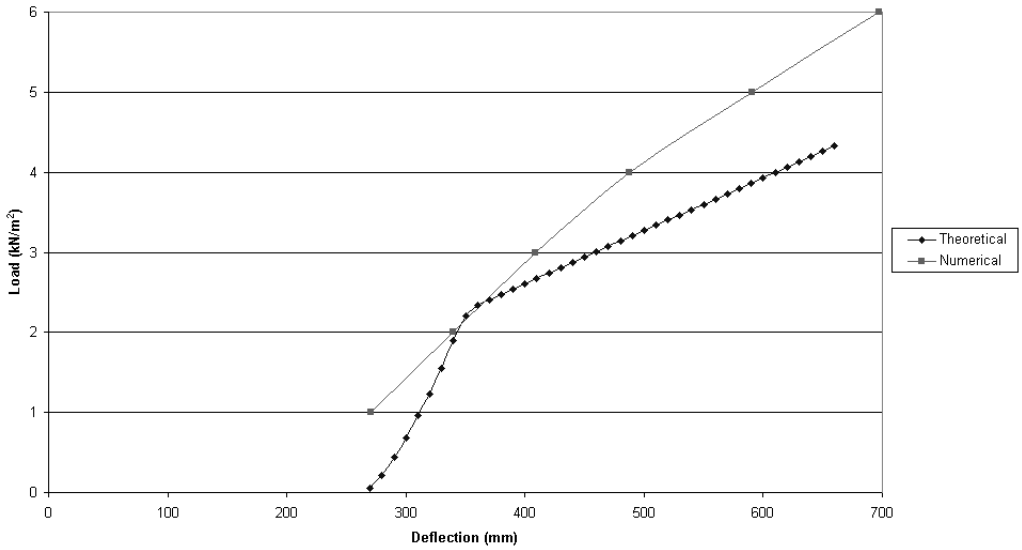

Figure 6.7: Load-deflection relationship for one-way spanning slab with reinforcement temperature of 600^oC

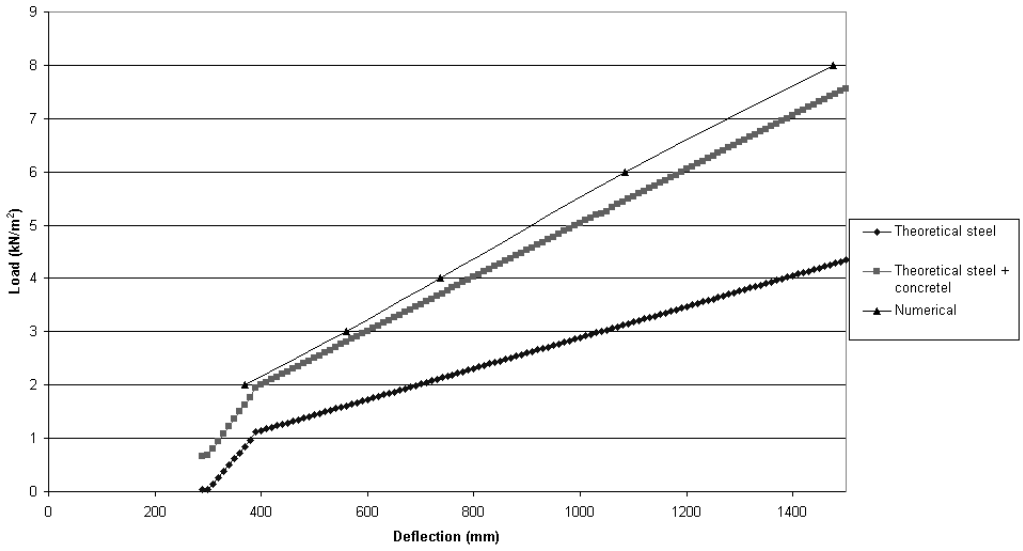

Figure 6.8: Load-deflection relationship for one-way spanning slab with reinforcement temperature of 700^oC

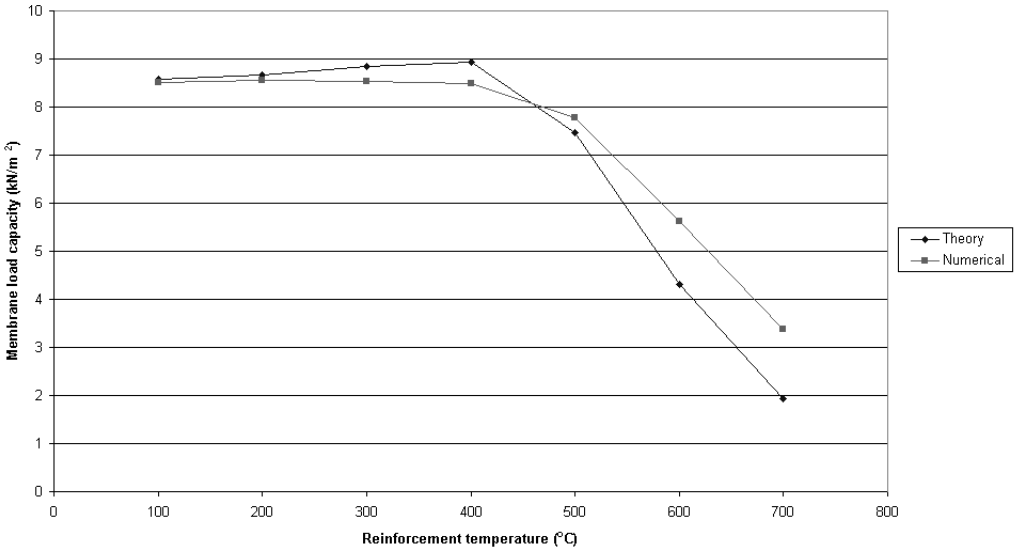

Figure 6.9: Failure envelope for a one-way spanning slab with a span of 6m

6.5 Analysis of two-way spanning slabs

6.5.1 Slab with an aspect ratio of 1

The first two-way spanning slab to be analysed was a 6m x 6m slab with lateral restraint along all four boundaries.

Deflection response

Similar trends to those seen in the analyses of the one-way spanning slab were observed. With reinforcement temperatures of 100^oC and 200^oC the theory overpredicted the load at small deflections as shown in Figs. 6.10 and 6.11 but as the limiting deflection was approached the results converged and agreed well. Between 200^oC and 400^oC (see Figs. 6.12 and 6.13) the results are virtually identical for all loads.

Above a reinforcement temperature of 400^oC there are differences between the theoretical and numerical results. This is due to the required increase in the concrete tensile strength necessary to achieve convergence as described previously for the one-way spanning slab. Below 400^oC the steel is contributing 98.5% of the internal

Temperature (^oC)	Limiting deflection (mm)	Theoretical ultimate load (kN/m^2)	Numerical ultimate load (kN/m^2)	Theoretical ultimate load/ Numerical ultimate load	Steel energy (%)
100	614	14.23	14.00	1.02	98.5
200	621	14.34	14.23	1.01	98.5
300	634	14.51	14.92	0.97	98.5
400	641	14.63	15.08	0.97	98.5
500	649	12.22	14.22	0.86	81.0
600	658	7.33	8.62	0.85	72.3
700	670	3.11	5.31	0.59	52.1

Table 6.2: Summary of analyses of two-way spanning slab with aspect ratio of one

energy (assuming the entire section has reached tensile yield) but by 500^oC this has reduced to 81% and at 700^oC the steel and concrete are contributing equally. This makes it difficult to draw a comparison between the results at such high temperatures. In addition, compressive membrane action will be occurring in regions of the slab where the deflection is less than the slab depth. Due to the large deflections of the slab, however, this will only contribute a small amount of the total load capacity. At any given deflection as the steel weakens the load capacity from compressive membrane action will remain the same but as a percentage of the total it will increase as the tensile membrane capacity of the steel reduces due to degradation. It would appear from the results at lower temperatures (¡400^oC) that the contribution from compressive membrane action is low and can therefore be ignored. The effect of these error sources are seen particularly in Fig. 6.16 where the numerical result for the load capacity is 66% higher than the theoretical at the limiting deflection. Unlike the one-way spanning slab it is not straightforward to account for the internal energy in the concrete as the stress pattern over the volume of the slab will be very complex with regions of both tension and compression and so it could not be assumed that the entire section is at tensile yield.

Figure 6.17 shows the failure envelope for the 6m x 6m slab. There is close agreement between the theoretical and numerical results up to a temperature of 400^oC. Before degradation of the steel begins to occur at 400^oC the maximum error between the theoretical and numerical results is only 3%, however, above this temperature the error increases due to the reasons given above. Table 6.2 summarises the results for the two-way spanning square slab.

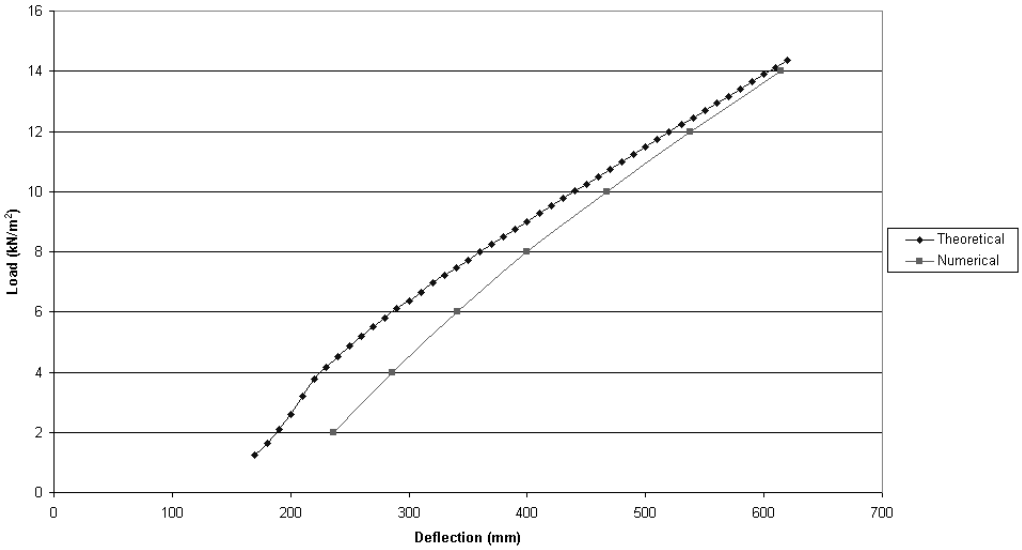

Figure 6.10: Load-deflection relationship for two-way spanning slab with reinforcement temperature of 100^oC

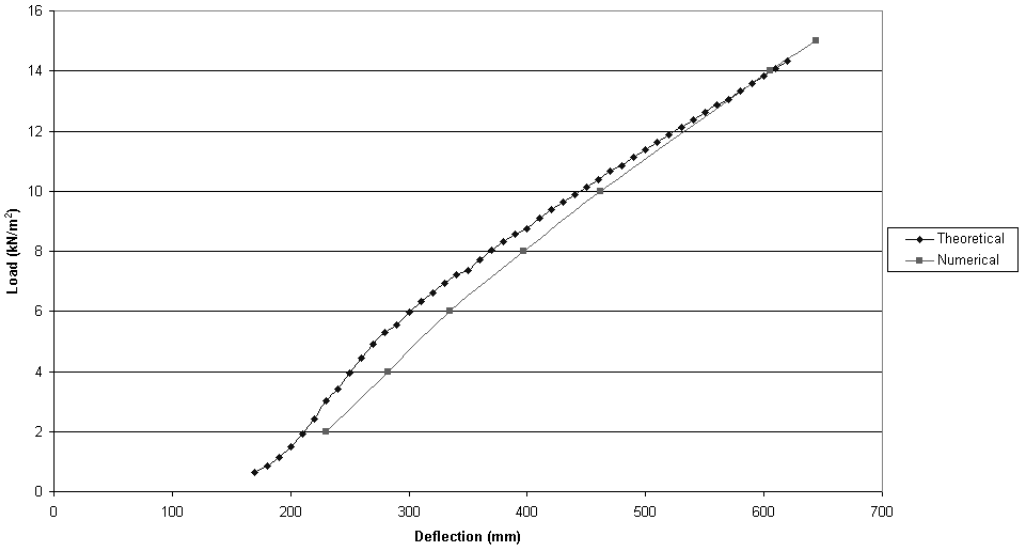

Figure 6.11: Load-deflection relationship for two-way spanning slab with reinforcement temperature of 200^oC

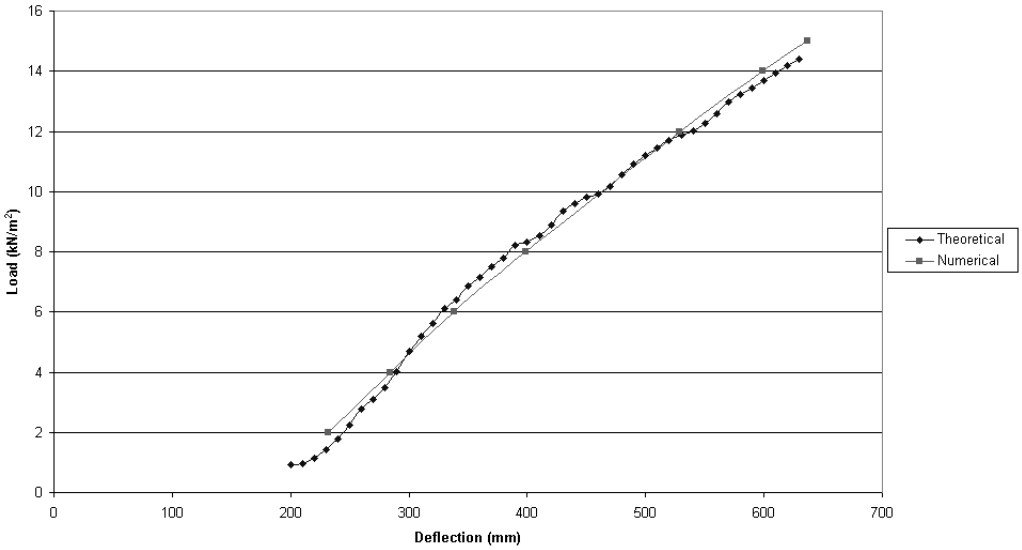

Figure 6.12: Load-deflection relationship for two-way spanning slab with reinforcement temperature of 300^oC

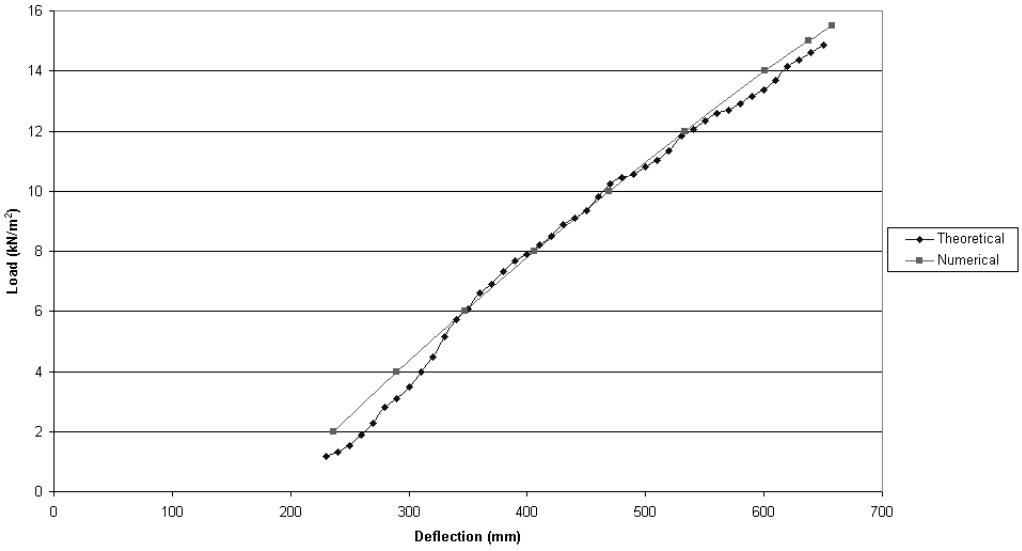

Figure 6.13: Load-deflection relationship for two-way spanning slab with reinforcement temperature of 400^oC

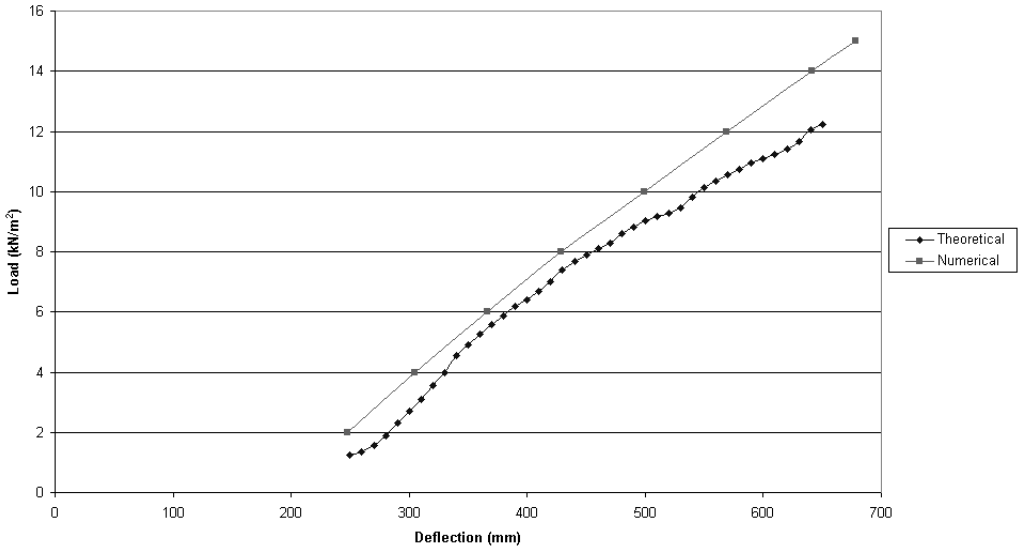

Figure 6.14: Load-deflection relationship for two-way spanning slab with reinforcement temperature of 500^oC

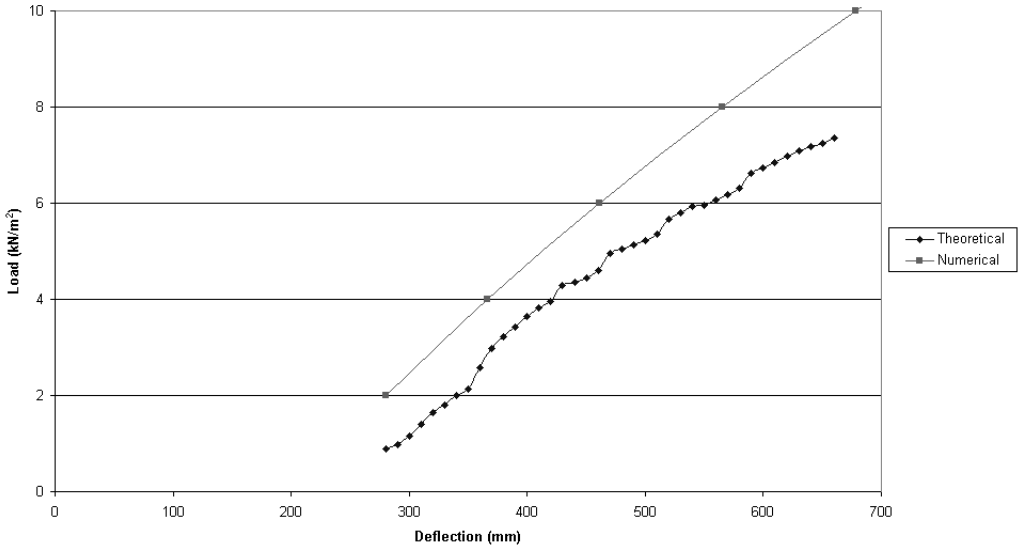

Figure 6.15: Load-deflection relationship for two-way spanning slab with reinforcement temperature of 600^oC

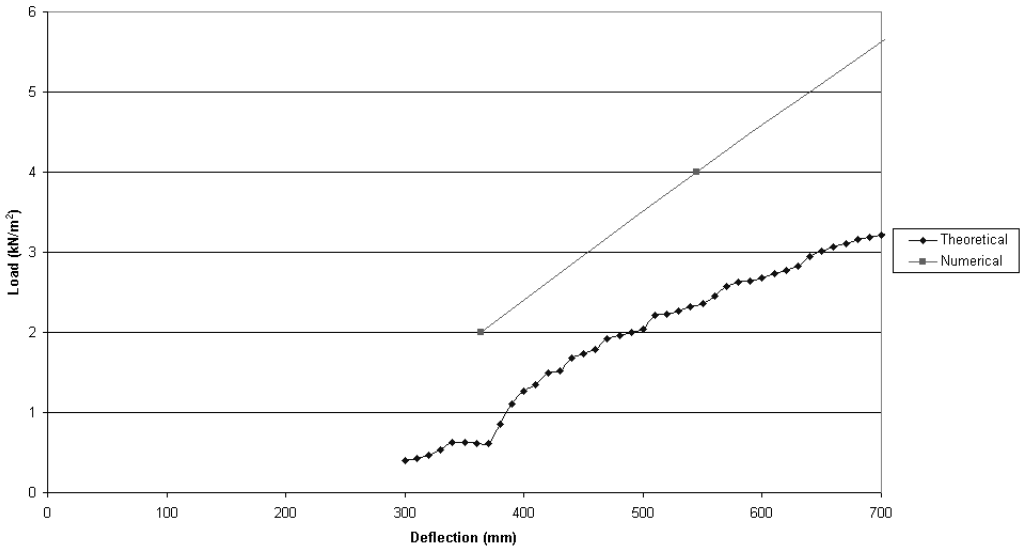

Figure 6.16: Load-deflection relationship for two-way spanning slab with reinforcement temperature of 700^oC

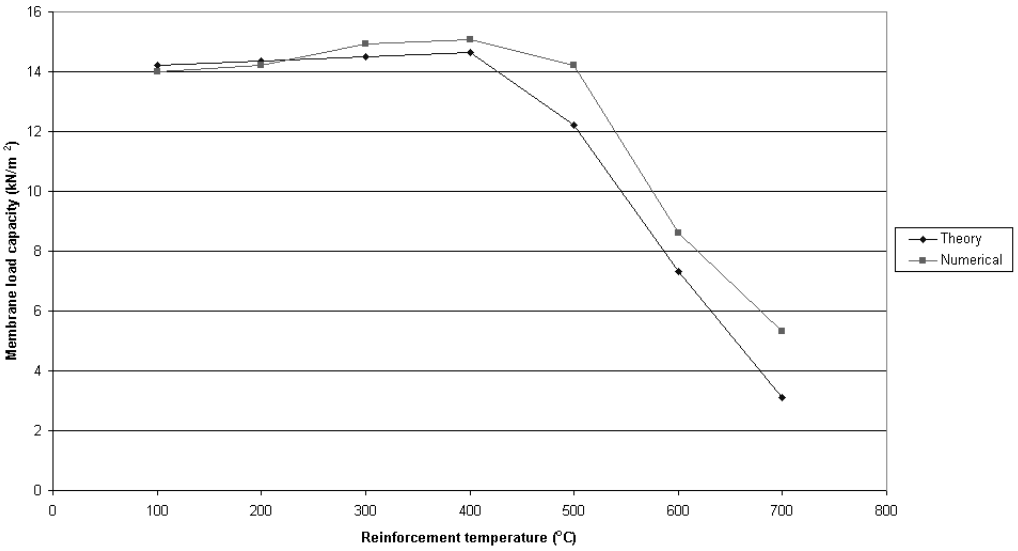

Figure 6.17: Failure envelope for a two-way spanning slab with a span of 6m

Reinforcement force response

Examining the forces in the reinforcement provides further confidence that the theoretical equations are capturing the structural behaviour of the slab. Figures 6.18-6.22 show the forces in the reinforcement along the boundary of the slab at x=0.1L, 0.2L, 0.3L, 0.4L and 0.5L. Values are those found at the limiting deflection (i.e. at "failure") and at all of the reinforcement temperatures considered.

In Figs 6.19-6.22 the theoretical values closely follow the numerical values over the entire range of reinforcement temperatures. At the limiting deflection the reinforcement is in tension at all four of these positions and in the centre 60% of the slab yield has been reached. As would be expected the forces reduce as degradation occurs. From the graphs it can be seen that in the numerical model the forces are generally less than those produced by the theoretical solution. This is because at the large deflections corresponding to a mechanical strain of 2.5% the theory overpredicts the strain i.e. for a given deflection the theory will calculate a strain larger than that in the numerical model. As the stress-strain curve for the steel reinforcement is highly non-linear this leads to the stresses being underpredicted in the numerical model. In obtaining the theoretical solution the stress-strain curve was idealised as being elastic-plastic with a clearly defined yield point. In reality beyond a temperature of approximately 200^oC this is not the case. In this instance the values chosen for the theoretical solution have led to the forces in the reinforcement being overestimated. This in turn would result in the calculated internal energy being larger than it actually was. Although this could lead to a non-conservative solution the results show that this is not the case as other load carrying mechanisms are not considered so there is additional capacity which is being ignored.

The only significant difference between the theoretical and numerical results occurs in the corner of the slab. Figure 6.18 shows the forces at a position of 0.1L. Although the general trend of the forces is followed the error is large. This is because in the corners the slab actually has significant bending strength which comes from two sources; this area is restrained on two adjacent edges and subject to large compression forces developed from restrained thermal expansion. Calculating the stresses in the reinforcement based purely on membrane action will therefore lead to errors. The numerical results show that the reinforcement is in tension up to a temperature of approximately 450^oC. This

is because the large deflections the slab is undergoing result in the corners wanting to rise up but as they are restrained vertically they must stay in position leading to large hogging moments. Despite the difference between the results in this section of the slab it will not significantly affect the results of the theoretical analysis because the majority of the internal energy is developed in the reinforcement bars at tensile yield in the middle section of the slab. Those bars at the edge of the slab contribute relatively little energy as their deflections are much smaller.

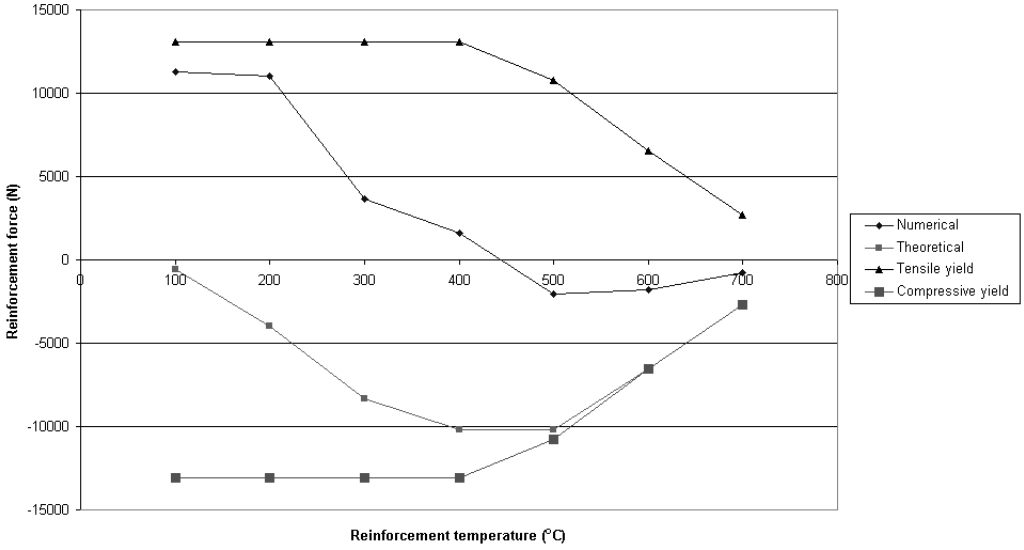

Figure 6.18: Forces in reinforcement in square slab at x=0.1L

6.5.2 Slab with an aspect ratio of 1.5

The second slab to be analysed had dimensions of 6m x 9m giving an aspect ratio of 1.5. All other variables such as the height and the temperature distribution remained the same as for the one-way spanning and the square two-way spanning slabs analysed previously.

Deflection response

The failure envelope for a slab with an area of 6m x 9m is shown in Fig. 6.23. At all temperatures the theoretical values for the ultimate load are always less than that

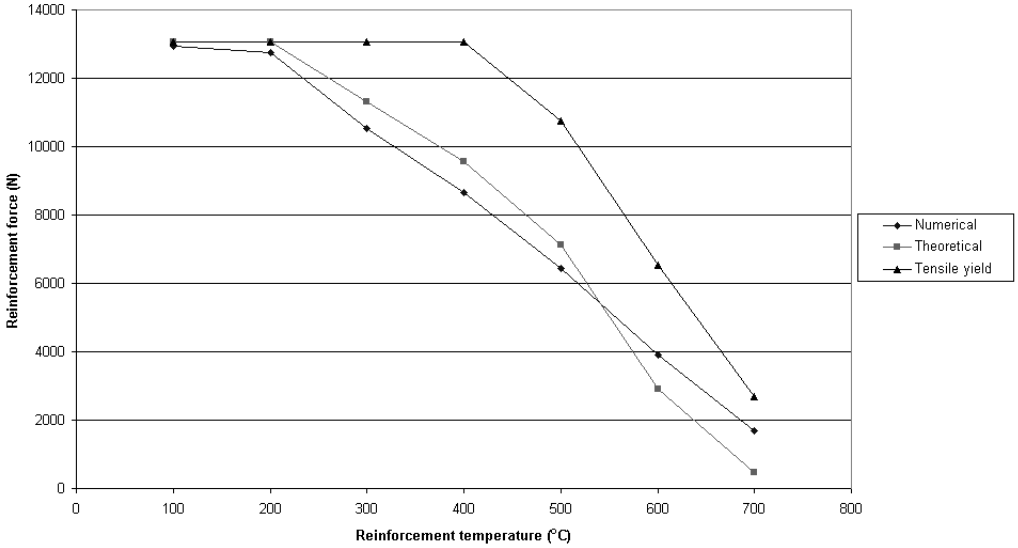

Figure 6.19: Forces in reinforcement in square slab at x=0.2L

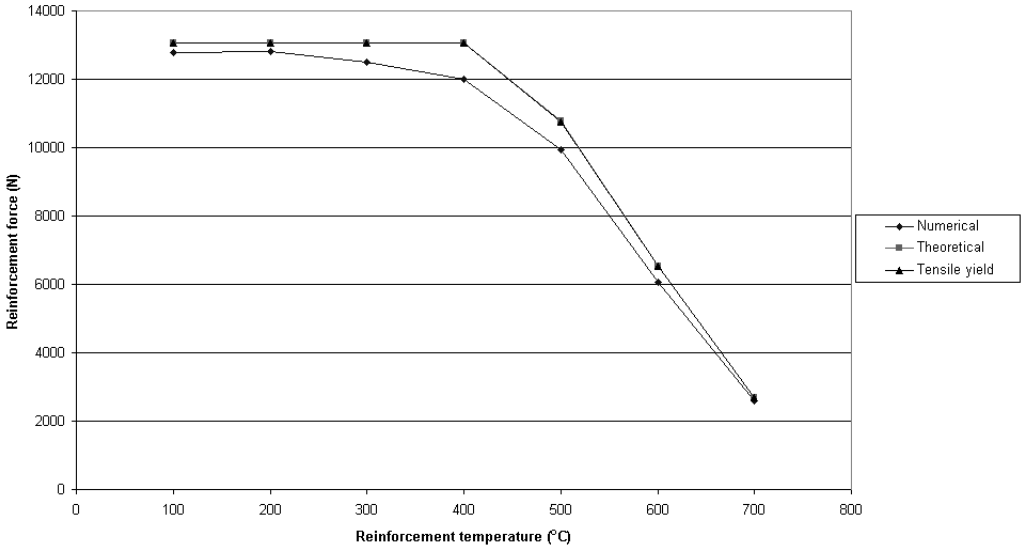

Figure 6.20: Forces in reinforcement in square slab at x=0.3L

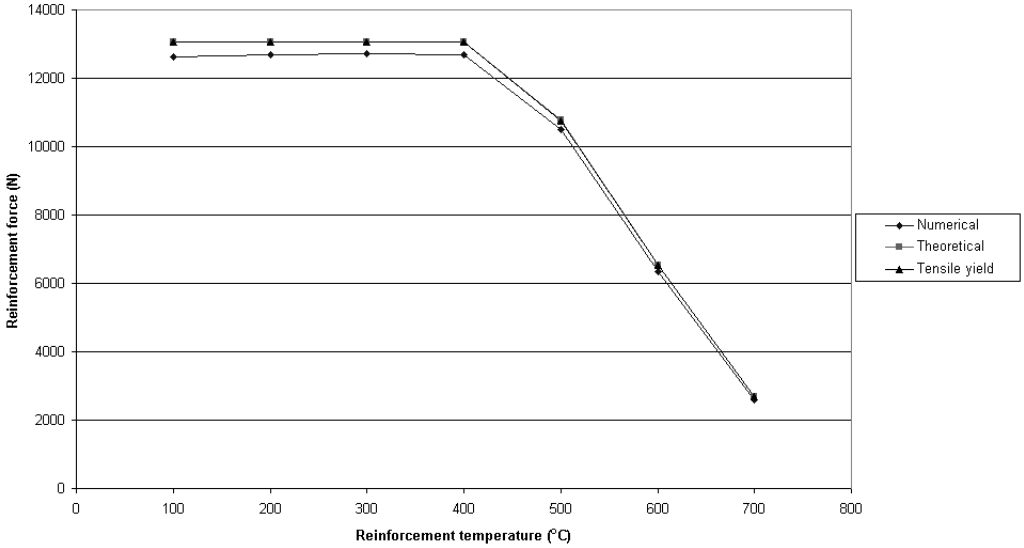

Figure 6.21: Forces in reinforcement in square slab at x=0.4L

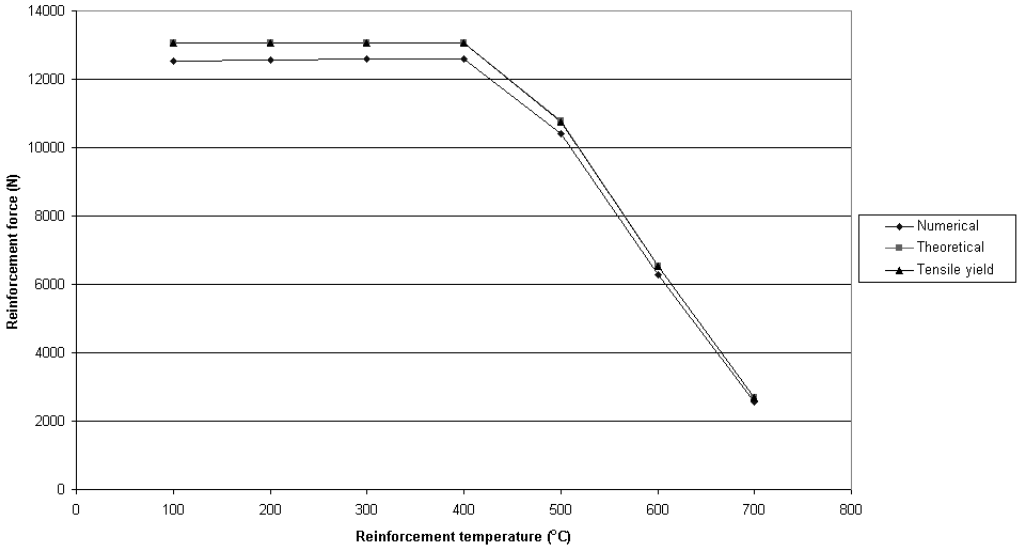

Figure 6.22: Forces in reinforcement in square slab at x=0.5L

predicted by the numerical model. With reinforcement temperatures of less than 400^oC the theoretical result is only 80% of the numerical value. The error between the two sets of results increases with temperature such that at 700^oC the theoretical result is only 42% of the numerical. These errors are much larger than for the slab with an aspect ratio of one and there are three principle reasons for the difference:

1. internal energy in the concrete
2. compressive membrane action
3. geometric assumptions

At higher reinforcement temperatures some of the difference is due to the internal energy coming from the concrete as explained previously. This does not explain the error at temperatures of 400^oC or less, however, where the concrete contribution is small (see Table 6.3). Compressive membrane action will be contributing to the difference although it would appear from the analysis of the square slab that its contribution is small primarily due to the very large deflections involved. The principle source of error are the equations used to describe the deflected surface of the slab in Section 4.5.2. Although use of a double sine curve in Eq. 4.89 to represent the deflected shape is acceptable for a slab with an aspect ratio of one, as the aspect ratio increases this introduces errors as the actual deflected surface more closely resembles that of a 'bathtub' as described by Paik [110]. Use of a sine curve underpredicts the deflections in certain regions of the slab which in turn leads to the internal energy being underpredicted as the calculated mechanical strains which create the internal energy are smaller in both directions. The errors introduced by the geometrical assumption account for the majority of the 20% error between the results at temperatures of less than 400^oC.

It is noticeable that although the theoretical load capacity increases up to a reinforcement temperature of 300^oC, it then starts to fall. In contrast the load capacity of the square slab (see Fig. 6.17) increased up to 400^oC and only started to reduce as degradation of the steel began. This is again due to the assumed geometrical shape and the underprediction of the internal energy as described above. At higher temperatures more of the deflection is taken up by thermal strain. As the calculated

Temperature (°C)	Limiting deflection (mm)	Theoretical ultimate load (kN/m^2)	Numerical ultimate load (kN/m^2)	Theoretical ultimate load/ Numerical ultimate load	Steel energy (%)
100	614	9.77	12.02	0.81	98.5
200	621	9.81	12.29	0.80	98.5
300	634	9.85	12.49	0.79	98.5
400	641	9.72	12.53	0.78	98.5
500	649	8.17	11.63	0.70	81.0
600	658	4.93	8.01	0.62	72.3
700	670	2.02	4.85	0.42	52.1

Table 6.3: Summary of analyses of two-way spanning slab with aspect ratio of 1.5

deflections, and therefore strains, are already smaller than they actually would be this leads to greater errors in the internal energy. With increasing aspect ratio the effect of the geometric assumption would become more pronounced and the peak load capacity would be predicted at increasingly lower temperatures.

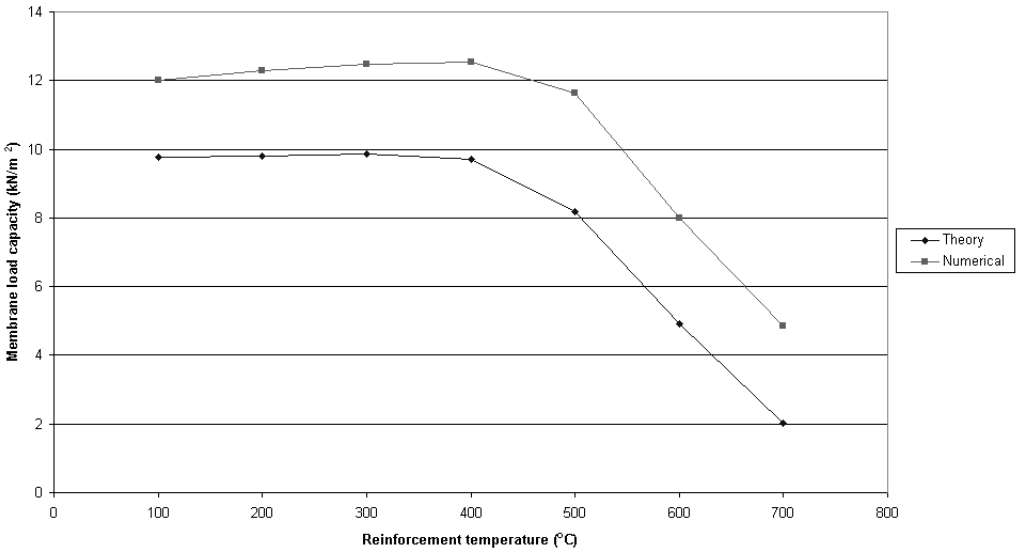

Figure 6.23: Failure envelope for a two-way spanning slab with an aspect ratio of 1.5

Reinforcement force response

The effect of the assumption regarding the deflected shape of the slab can clearly be seen when the forces in the reinforcement are examined. Initially the forces in the reinforcement spanning across the short span will be considered. Figures 6.24-6.28 show the forces at x=0.0625L, 0.125L, 0.1875L, 0.25L and 0.5L respectively. In the corner of the slab the response is similar to that seen in the square slab. The bending

stiffness in the corners causes tensile forces to develop in the reinforcement whereas the theoretical method calculates compressive forces (Figs. 6.24-6.25). At a position of 0.125L (Fig. 6.26) the calculated forces are virtually identical to those obtained from the numerical analyses, however, above 400^{o}C they are underpredicted. This is because the theoretical deflection at this point is less than that in the numerical model and, although this does not have such a significant effect on the forces at low temperatures, at higher temperatures it does as more of the total strain consists of thermal strain. From a position approximately one-quarter of the way along the length the theoretical forces and numerical forces are virtually identical as shown in Figs. 6.27-6.28.

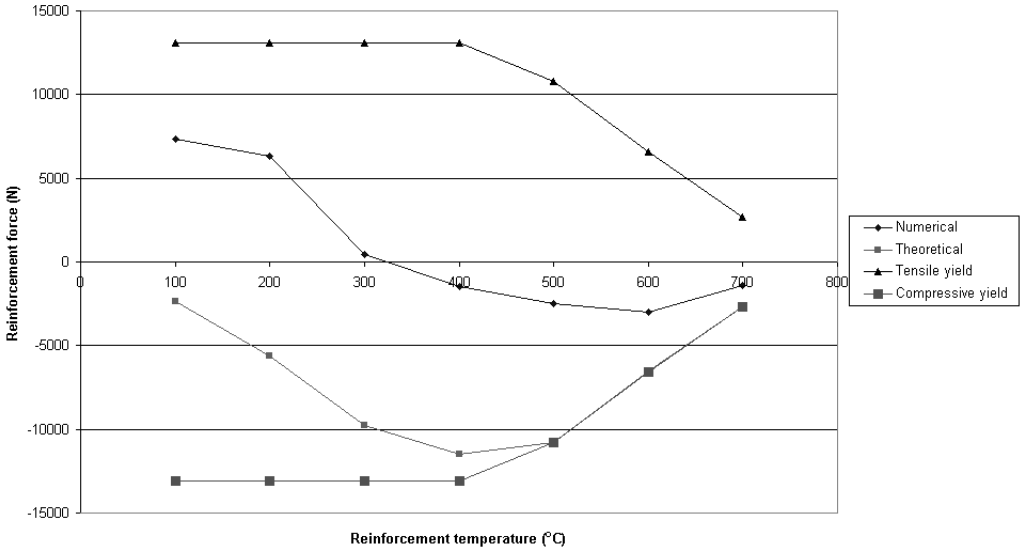

Figure 6.24: Forces in reinforcement across short span of rectangular slab at x=0.0625L

The errors in the calculated deflections also affects the forces in the reinforcement spanning across the long length of the slab. Figures 6.29-6.30 show the forces at y=0.083B and 0.167B respectively. It can be seen that compressive forces are being predicted whereas due to the bending stiffness of the slab in the corner the reinforcement is actually in tension. At a position of y=0.25B the forces are again underpredicted as shown in Fig. 6.31. In this instance the calculated strains in the long span are not as large as they should be because the deflected shape across the short span is not being described properly by the mathematics. If the theoretical equations were describing a 'bathtub' shape then the strains and stresses across the long span would be larger.

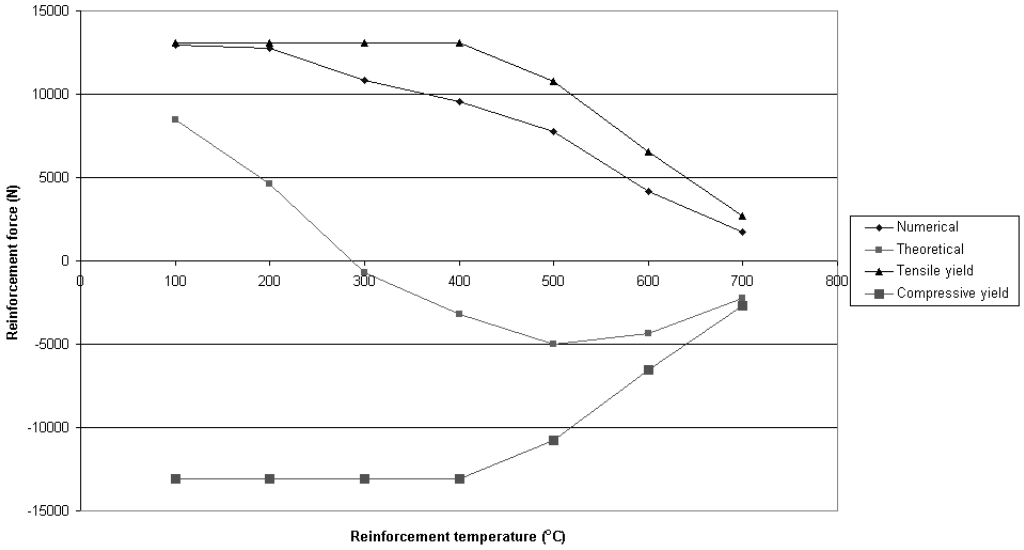

Figure 6.25: Forces in reinforcement across short span of rectangular slab at x=0.125L

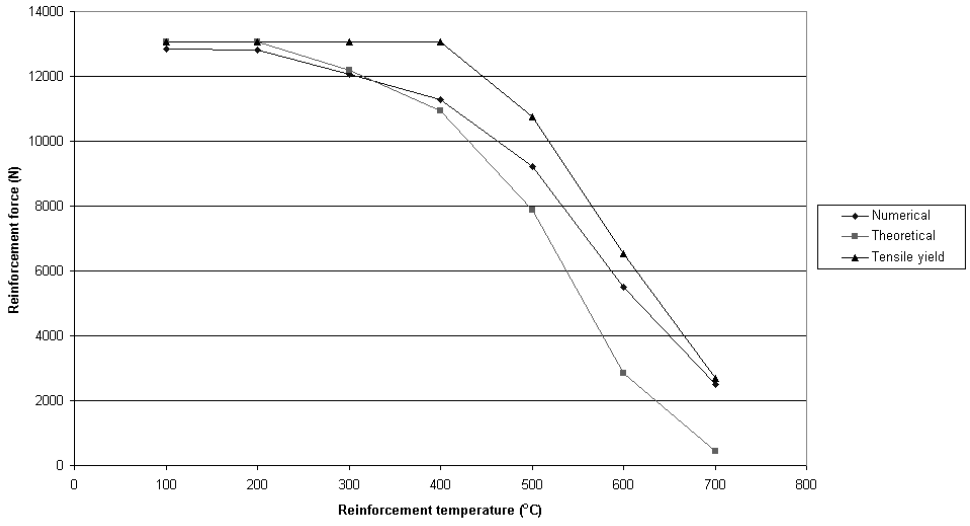

Figure 6.26: Forces in reinforcement across short span of rectangular slab at x=0.1875L

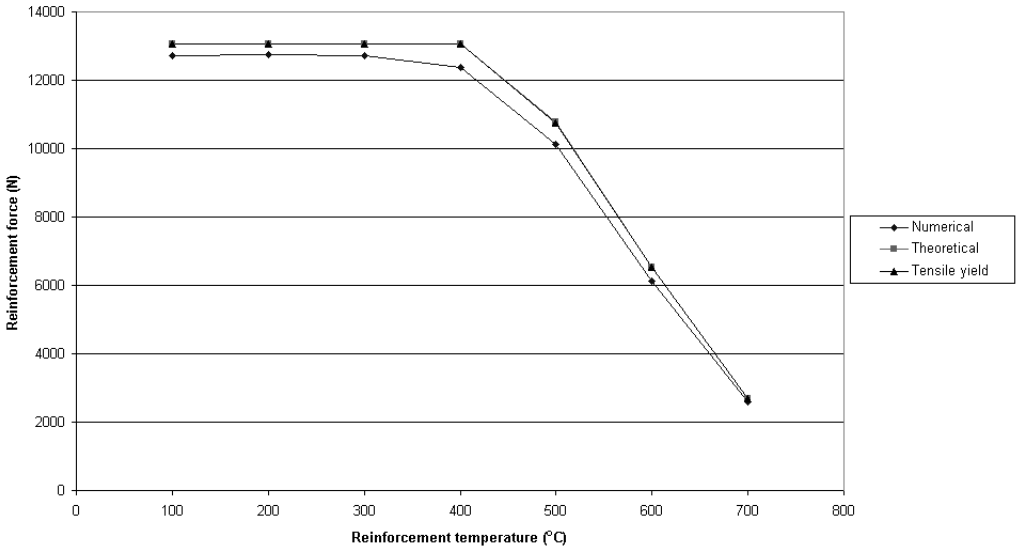

Figure 6.27: Forces in reinforcement across short span of rectangular slab at x=0.25L

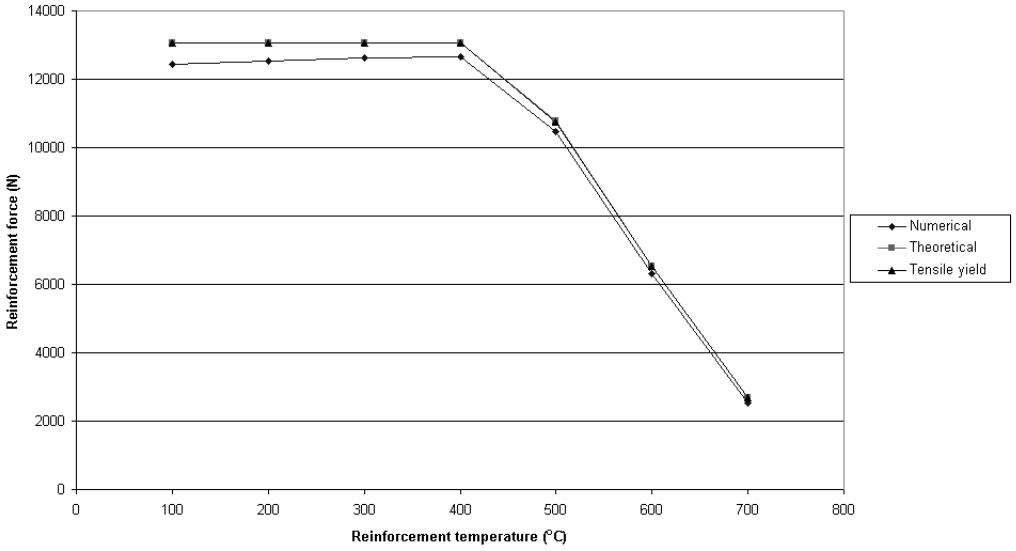

Figure 6.28: Forces in reinforcement across short span of rectangular slab at x=0.5L

Closer to the middle of the slab these effects are less noticeable because the deflections are so large that yield has been reached regardless of the temperature of the steel (see Figs. 6.32-6.33). However, although yield has been reached the calculated mechanical strain would be less than those from the numerical analyses resulting in not all of the internal energy being accounted for. This would lead to the calculated load capacity being conservative.

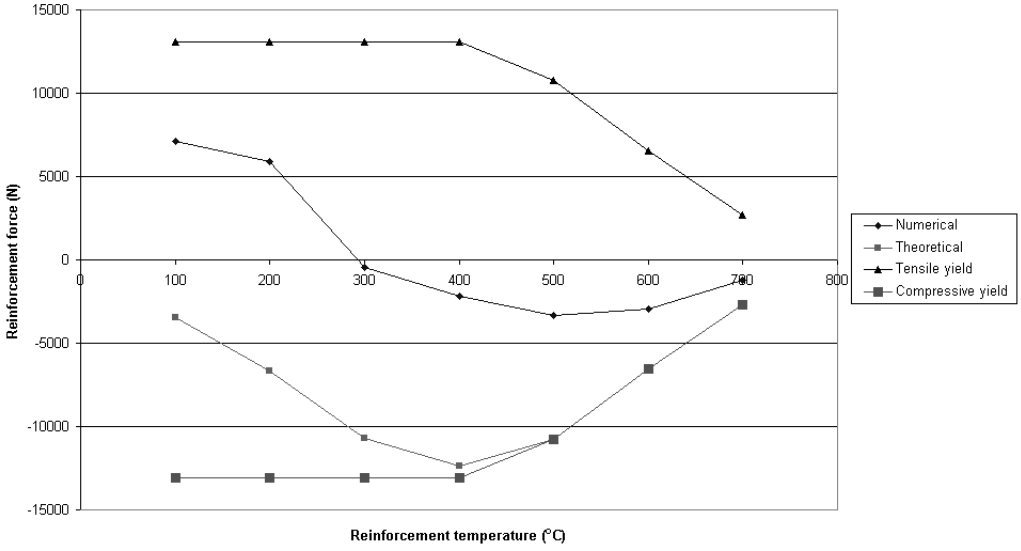

Figure 6.29: Forces in reinforcement across long span of rectangular slab at x=0.083B

6.6 Conclusions

The following conclusions can be drawn from this study:

- The design method can accurately predict the load-deflection response and ultimate load capacity of a one-way spanning slab.
- The theoretical results for a two-way spanning slab with an aspect ratio of one closely match those from the numerical model.
- With increasing aspect ratio the error between the theoretical and numerical results for a two-way spanning slab increase. This is due to assumptions made

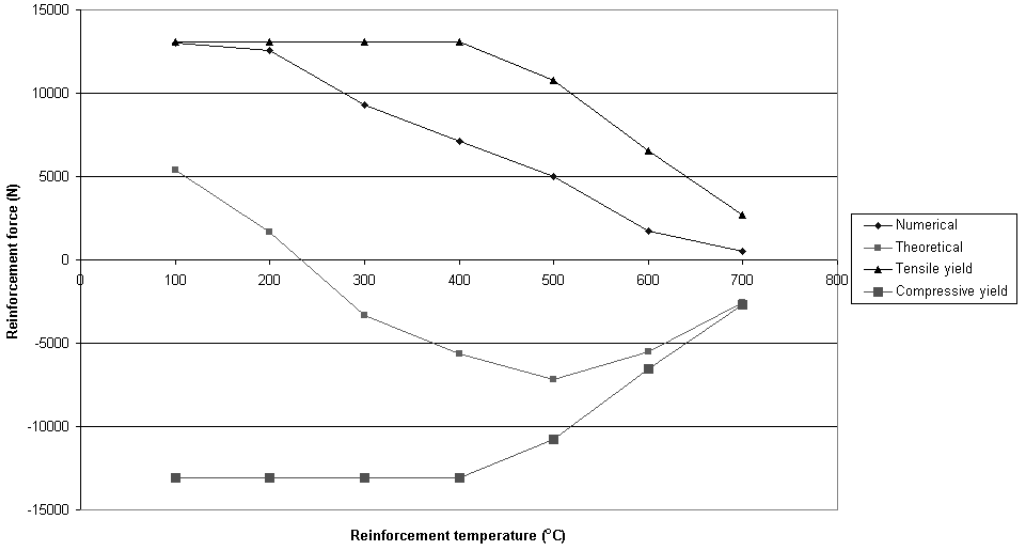

Figure 6.30: Forces in reinforcement across long span of rectangular slab at x=0.167B

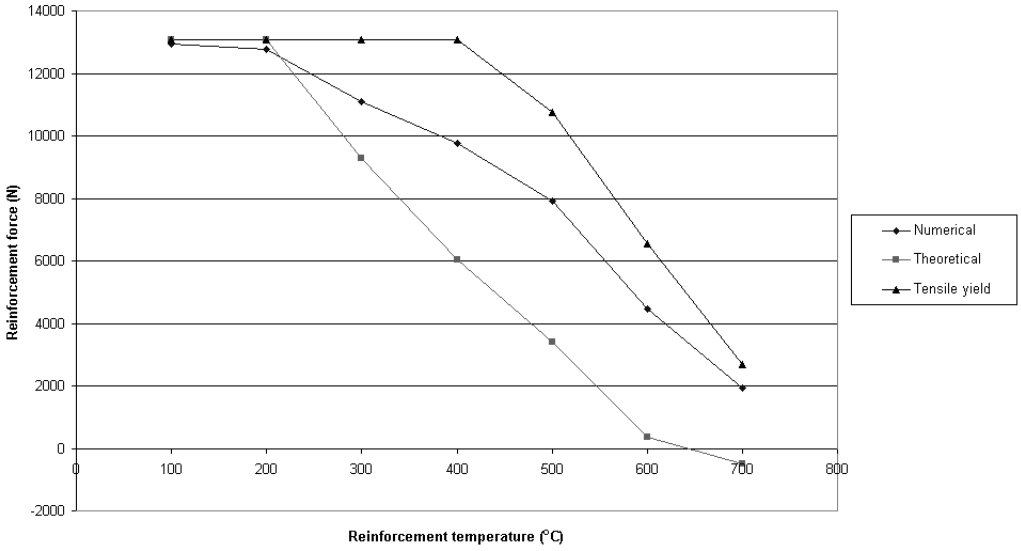

Figure 6.31: Forces in reinforcement across long span of rectangular slab at x=0.25B

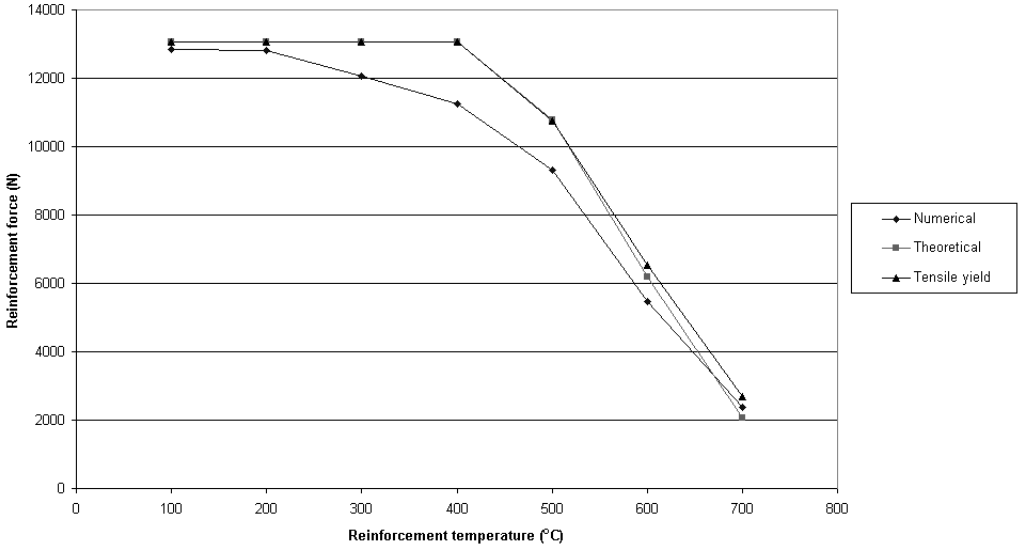

Figure 6.32: Forces in reinforcement across long span of rectangular slab at x=0.333B

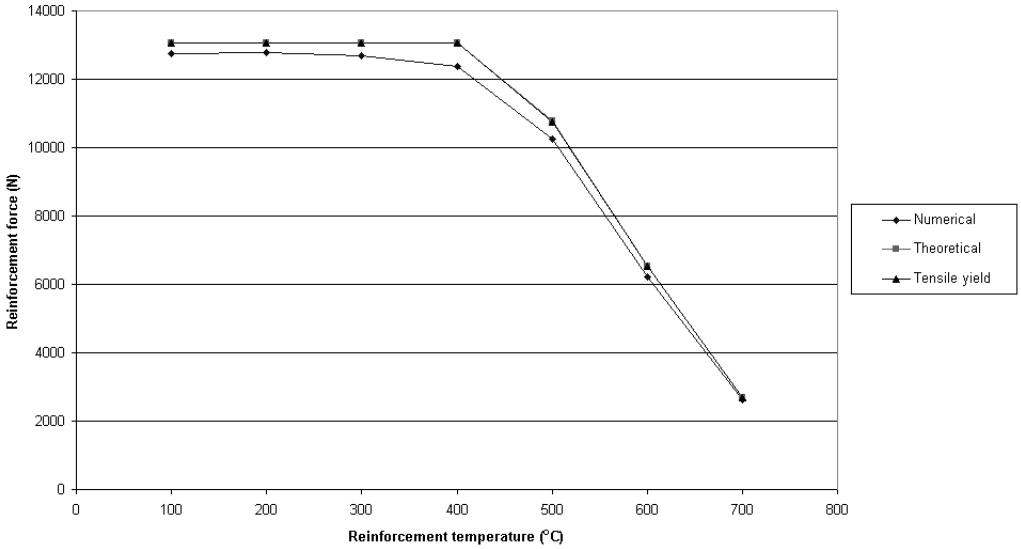

Figure 6.33: Forces in reinforcement across long span of rectangular slab at x=0.5B

with regard to the deflected surface shape of the slab and leads to the ultimate load being underpredicted.

- At low deflections the load is overpredicted due to assumptions regarding the sequence of load application, however, this does not seem to affect the calculated value for the ultimate load.

- The forces in the reinforcement can be accurately calculated for a slab with an aspect ratio close to one.

- Errors in the internal forces are introduced by the assumed deflected shape when the aspect ratio increases above one. This leads to the calculated ultimate load being less than that predicted by numerical modelling.

- Due to the high bending stiffness of the slab in the corners the stresses in the reinforcement are not accurately calculated using the membrane stress equations. This error does not significantly affect the result as this area contributes little internal energy.

- The structural behaviour is captured well over a large range of reinforcement temperatures.

- It becomes more difficult to draw comparisons at higher temperatures due to the need for higher concrete strengths to achieve convergence. This also has direct implications with regard to accurate numerical modelling of structural behaviour in fire as the tensile stress-strain behaviour may have a significant effect on the results obtained.

Chapter 7

Limit State Analysis of the Cardington Fire Tests

7.1 Introduction

The design method presented in Chapter 5 has been shown to produce results that compare well against those from numerical analyses of isolated slabs. In this chapter the method will be used to analyse four of the six fire tests that were carried out on the Cardington building; the British Steel corner test, the British Steel office demonstration test and both BRE tests. Neither the restrained beam or plane frame tests carried out by British Steel were appropriate to be analysed as they were primarily 2D tests rather than looking at the behaviour of a compartment.

In carrying out the analyses there were two aims. The first aim was to compare the deflections of the slab calculated using the design method against those that occurred during the fire tests. This would provide an indication of how accurately the method could analyse a real fire scenario as opposed to the computer models it had previously been compared against. Secondly, the ultimate capacity of each test was calculated based on the failure criterion specified in Section 5.3.3 i.e. a limiting mechanical strain of 2.5% is allowed to develop in the reinforcement. This was done for a range of reinforcement temperatures so that a failure envelope of load capacity against reinforcement temperature could be drawn. If the applied load on a slab and the

Member	Section size	Steel grade
9m secondary beam	305 x 165 x 40UB	S275
9m primary beam	610 x 229 x 101UB	S275
6m primary beam	356 x 171 x 51UB	S355
9m perimeter beam	356 x 171 x 51UB	S355
Upper internal columns	254 x 254 x 89UC	S355
Lower internal columns	305 x 305 x 137UC	S355

Table 7.1: Primary members in Cardington frame

temperature of the reinforcement are within this surface then a slab can be considered to be safe. Outwith the limits of the surface the slab will be deemed to have failed.

7.2 The Cardington Building

The Cardington test building was designed to represent an office building typical of those found in any city centre. It was an eight-storey structure with a steel frame and composite concrete floors. In plan it had three bays by five bays as shown in Figs. 7.1 and 7.2. The building was designed as non-sway with wind resistance coming from a central lift-shaft and two staircases at either end of the building. Stability was provided by bracing around these vertical concrete shafts.

The main steel frame was designed for a gravity load consisting of a dead load of 3.65kN/m^2 and an imposed load of 3.5kN/m^2. For design purposes the floor slab was assumed to be continuous or simply-supported over the secondary beams, these were at 3m centres and designed as simply-supported and acting compositely with the slab. Primary beams were designed in a similar manner. Shear studs ensured that composite action occurred between the beams and slab. Table 7.1 shows the section sizes and strengths of the primary steel members.

Connections consisted of flexible end plates for beam-column connections and fin plates for beam-beam connections. Design was based on the assumption that they were simply-supported and so transmitted shear but no moment. There was a large amount of rotational restraint, however, due to the composite action with the slab. At the connection this causes compressive forces in the beam and tensile forces in the slab

generating a large hogging moment. The connection is therefore semi-rigid rather than simply-supported [10].

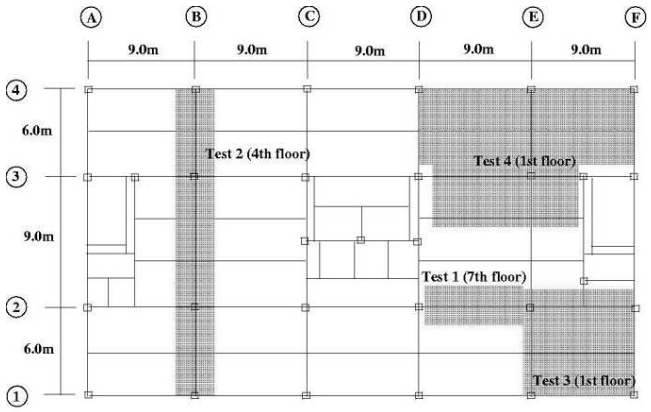

Figure 7.1: Plan of Cardington test building showing location of the British Steel fire tests [?]

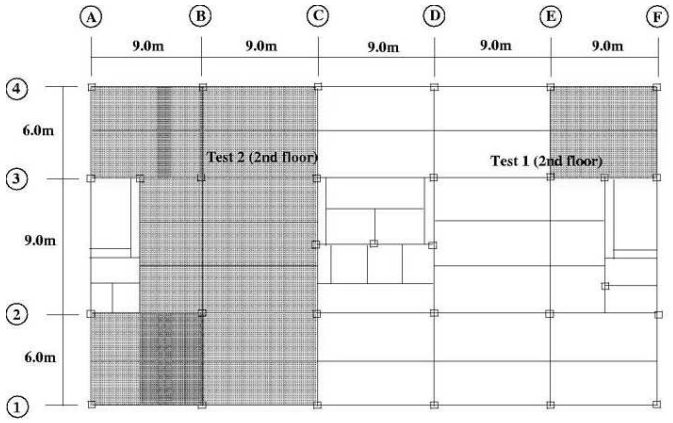

Figure 7.2: Plan of Cardington test building showing location of the BRE fire tests [?]

The floor system consisted of a steel deck acting compositely with lightweight concrete. It was anisotropic due to the ribs which ran along its length and was designed as one-way spanning perpendicular to the secondary beams. The overall depth was 130mm with a trough depth of 60mm. A standard A142 mesh was provided to ensure cracking did not occur. For design the depth of 130mm was used, however, the depth varied significantly over the building due to 'ponding'. Based on surveys of three sections of the building it was found that the maximum thickness was 173mm with the minimum thickness being 124mm [117]. Overall approximately 15% of the building had a floor area below the

design thickness.

Although designed as a series of independent and determinate members, when constructed the entire building was highly indeterminate [10]. This allowed the load carrying behaviour of the building to change when it is in a fire with the most significant change being in the slab. At ambient conditions the slab was designed for flexure and acting as one-way spanning with the ribs giving a much higher stiffness in one direction than the other. In a fire as the behaviour moves from small-deflection to large-deflection the slab isotropy of the slab needs to be defined in terms of the reinforcement rather than the deck geometry. In the Cardington frame a standard A142 anti-cracking mesh was used which would result in the slab membrane behaviour being isotropic as the mesh areas are equal both parallel and perpendicular to the ribs.

Tests of the steel used for the primary and secondary beams showed that the actual yield stresses were 308N/mm^2 for the Grade 43 (S275) and 390N/mm^2 for the Grade 50 (S355) steel. After 28-days the average crushing strength of the concrete was 47.1N/mm^2 [118]. It was assumed that the mesh reinforcement used had an ambient yield stress of 460N/mm^2 and a Young's modulus of 210kN/mm^2.

7.3 Analysis of Cardington Fire Tests

A summary of the theoretical results is contained in Table 7.2. The load capacity given in the table assumes that the reinforcement was at a peak temperature of 170^{o}C in all four tests. There is a lack of data regarding the temperature of the reinforcement, however, it is accepted that it did not go above 400^{o}C. The values in the table refer to the membrane load capacity of the slab only and do not consider any strength that would come from the secondary beams. Of the four tests analysed the only one that was near to failure was the BRE large compartment test. All of the other tests had a reserve capacity of at least 37%.

7.3.1 British Steel Corner Test

In this test a typical corner compartment measuring 10m x 7.6m was studied (see Fig. 7.1). Within the compartment there were two primary beams (one internal and one

	BS Corner	BS Demonstration	BRE Corner	BRE Large Compartment
Short span (m)	7.6	9	6	9
Long span (m)	10	9	9	21
Test load (kN/m^2)	5.48	5.48	5.48	5.48
Load capacity (kN/m^2)	8.70	9.35	9.84	5.75
Load/load capacity(%)	63.0	58.6	55.7	95.3
Test deflection (mm)	428	640	269	557
Theoretical deflection (mm)	547	566	382	860

Table 7.2: Summary of theoretical analysis of Cardington fire tests

external) and three secondary beams (one external and two internal). Fuel came from wooden cribs providing a load of 45kg/m^2. A maximum atmospheric temperature of 1,028^{o}C was measured and a maximum steel temperature of 1,020^{o}C.

The perimeter beams had ceramic fibre applied which limited their temperature rise. A maximum temperature of 250^oC was recorded on the lower flange whilst the web and upper flange were at temperatures of less than 200^{o}C. As most of their ambient strength was retained the external beams still provided a high degree of lateral and vertical restraint. All of the internal beams were left unprotected. Internal walls were built of lightweight concrete blockwork which would provide vertical restraint. For the analysis the dimensions of the slab were therefore taken as being 10m x 7.6m.

At a reinforcement temperature of 170^{o}C the membrane capacity of the slab was calculated to be 8.7kN/m^2, with a total load of 5.48kN/m^2 the slab was only at 63% of its limit capacity. During the test the maximum slab deflection was measured as 428mm. In comparison the theory predicted a deflection of 547mm would be needed to carry the applied load.

The difference between the experimental and theoretical results would be expected when the geometry of the test compartment is examined. There is a protected internal column at grid location E2 at a point 6m x 9m from the corner of the building. As this retained its strength it would provide a single point source of restraint to vertical deflections. If we consider the result from the BRE Corner Test the required theoretical deflection for a 6m x 9m compartment with good vertical restraint along all four boundaries was 382mm. The deflection for the British Steel test was higher than this because although the column provided restraint the primary and secondary beams that come off it are being heated and so cannot provide the same level of vertical restraint as the blockwork wall in the BRE test.

Figure 7.3 contains a plot showing the load capacity of the slab against the reinforcement temperature. Indicated on the chart is the actual load being carried and it shows that during the test the slab was well within the theoretical failure envelope. The membrane capacity increases from 8.62kN/m^2 at ambient to 8.80kN/m^2 at 400^{o}C. Above 400^{o}C the capacity decreases as the steel degrades and loses strength. Beyond a reinforcement temperature of approximately 550^{o}C the slab would not be able to carry the applied load within the 2.5% mechanical strain limit imposed.

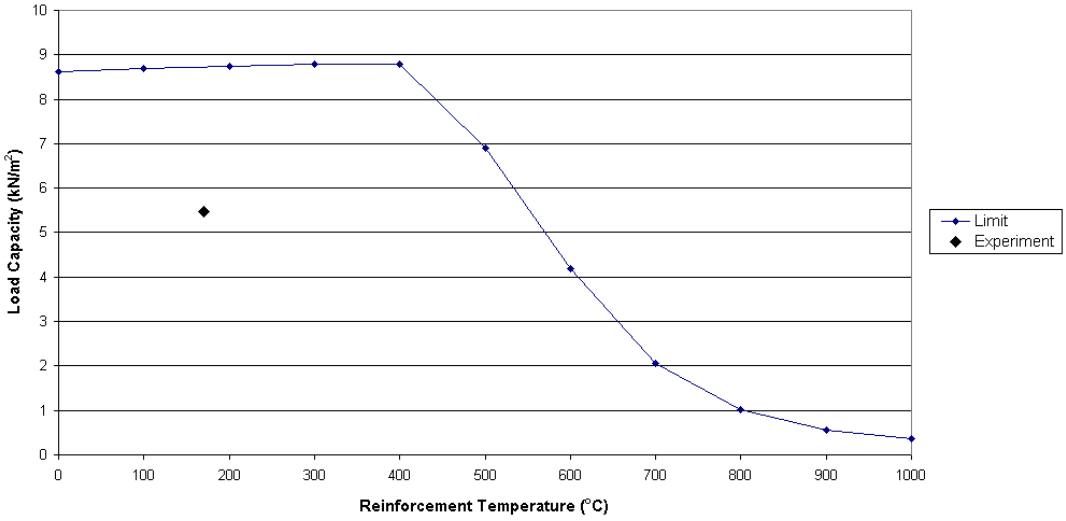

Figure 7.3: Failure envelope of British Steel Corner Test

The required deflection of the slab at various reinforcement temperatures to carry the test load of 5.48kN/m^2 is shown in Fig. 7.4. Up to 400^{o}C the response is linear and then as degradation occurs becomes increasingly non-linear.

Computer modelling has shown that in a rectangular compartment the tensile membrane action across the shorter span develops before, and carries more load, than that across the longer span [9, 13]. This trend is captured by the design theory. Figure 7.5 shows the mechanical strain in the centre of the slab in each span required to carry the test load of 5.48kN/m^2 for various temperatures. It can be seen that the mechanical strain in the short span is always the larger and is approximately double that in the long span. This would be expected due to the need for compatibility. In the long span the total strain is less than that in the short span leading to smaller

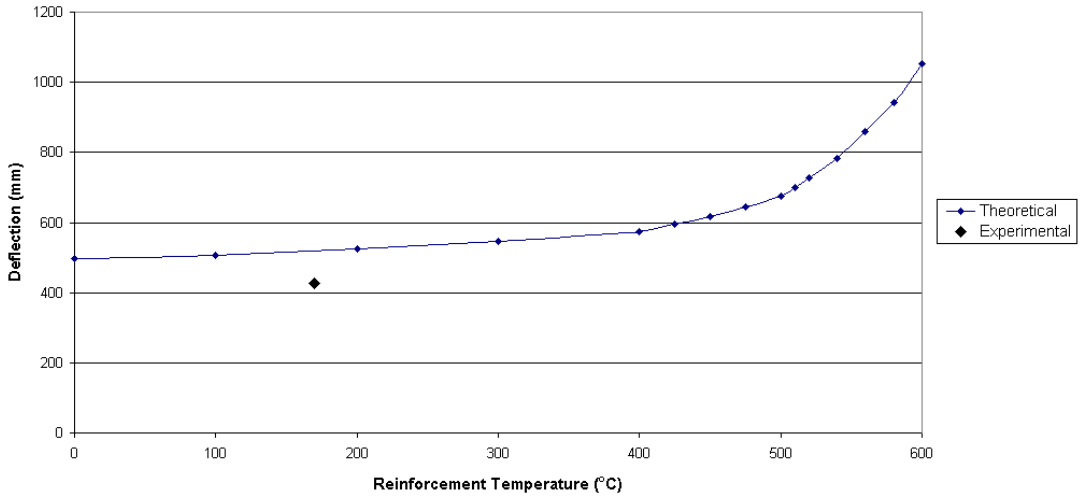

Figure 7.4: Temperature-deflection relationship of British Steel Corner Test for test load of 5.48kN/m^2

mechanical strains. As the internal work done is a function of the mechanical strain it can therefore be concluded that the most efficient method of increasing the load capacity of the slab would be to increase the amount of reinforcement across the short span.

As the temperature of the reinforcement increases from ambient the mechanical strain required at the centre of the slab to be able to support the test load reduces in both spans. In the short span the minimum mechanical strain occurs at a temperature of 200^{o}C, however, in the long span it occurs at 400^{o}C. This pattern is again due to the effects of compatibility. Figure 7.4 showed that as the reinforcement temperature increased from ambient to 400^{o}C the required deflection to carry the test load increased from 496mm to 574mm. The corresponding increase in total strain across the centre of the slab is less than the increase in thermal strain which results in smaller mechanical strains. Up to a temperature of 500^{o}C there is only a slight variation in the mechanical strains. Beyond this temperature they start to increase with the increase in the shorter span being larger than that in the long span by approximately 80%. This is again due to compatibility and shows that the reinforcement in the shorter span is contributing more internal energy than that in the long span.

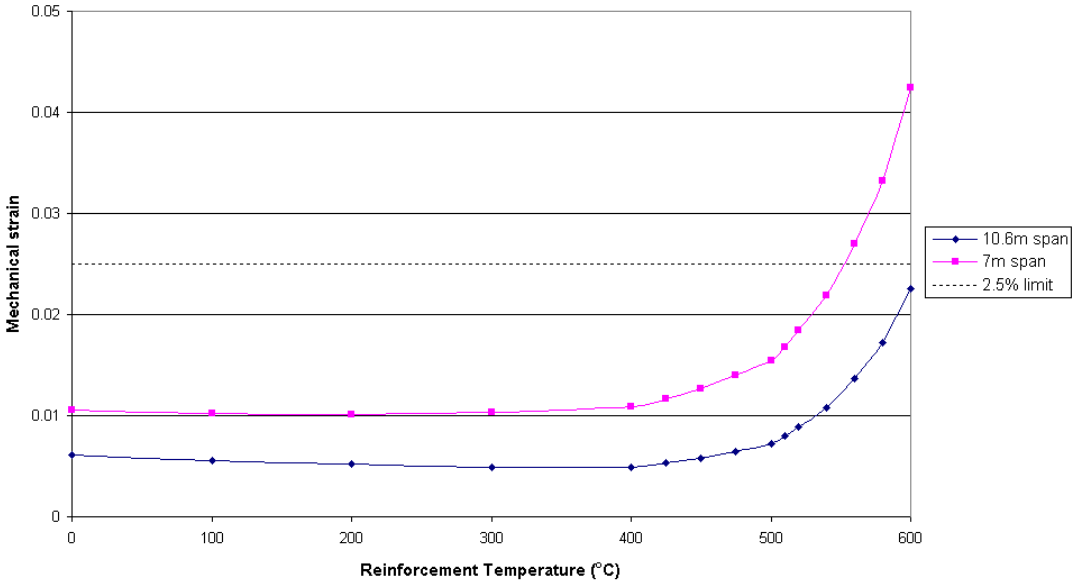

Figure 7.5: Temperature-mechanical strain relationship for British Steel Corner Test for test load of 5.48kN/m^2

7.3.2 British Steel Demonstration Test

Rather than using wooden cribs as a fuel, this test used real office furniture with an equivalent fire load to 45kg/m^2. This produced a maximum atmosphere temperature of 1,213^{o}C and a maximum unprotected steel temperature of 1,100^{o}C. The total enclosed area of the compartment was 180m^2 but the geometry was highly irregular (see Fig. 7.1). Protection was applied to all columns and beam-column connections.

For the analysis the section of the compartment between gridlines D and E was chosen. It was treated as being 9m square. In comparison with the other tests studied this one did not have such a clearly defined panel to analyse. Although the primary beam along gridline E had a low load ratio it was at an extremely high temperature (approximately 1,000^{o}C) due to the severity of the fire and deflected by 600mm during the test. Similarly the external edge beam deflected, though only by 100mm. Internally vertical support came from the blockwork wall used to create the compartment.

A maximum theoretical load capacity of 9.35kN/m^2 was calculated which means that the slab was only using 59% of its capacity. During the test the maximum recorded

deflection in the section being analysed was 640mm. Using the analytical method the deflection required to carry the applied load was 566mm. When analysing the other Cardington tests the analytical method has generally over-predicted the deflection required to carry the applied load when being applied to two-way spanning slabs. In this instance the deflection was under-predicted. Given the actual support conditions in the test, however, this is not surprising as the deflection of the internal primary beam was such that vertical restraint was only available on three of the slab boundaries. If the internal beam had been providing stronger vertical support then the test deflections would have been smaller and closer to the theoretical value.

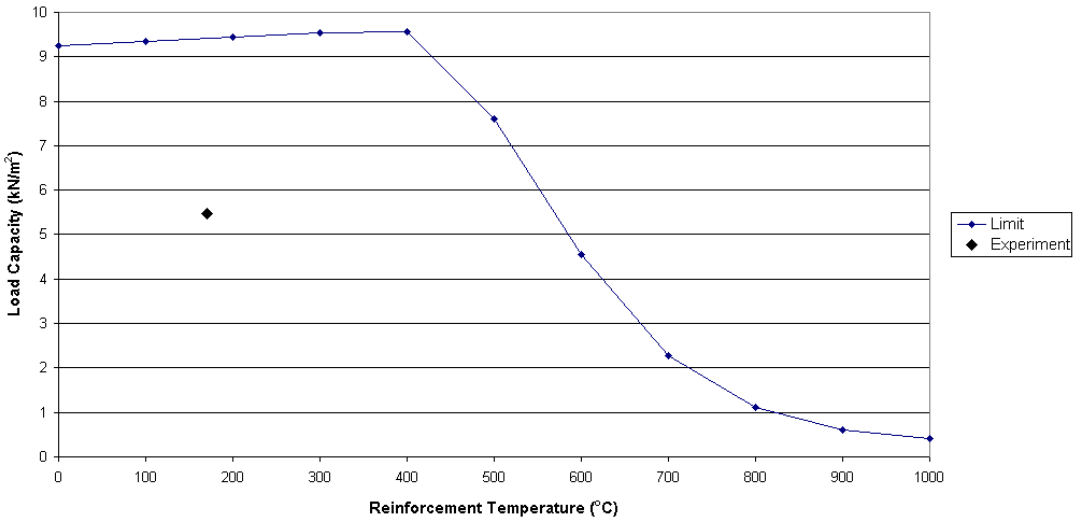

Figure 7.6: Load capacity of British Steel Demonstration Test

Figure 7.6 showing the ultimate load capacity of the slab against reinforcement temperature follows a similar pattern to that of the British Steel Corner Test. Up to a temperature of 400^oC the load capacity increases but above that temperature material degradation reduces the capacity. The maximum reinforcement temperature capable of supporting the test load is approximately 570^oC.

If the reinforcement temperature is increased from ambient to 400^oC the deflection required to carry the test load increases from 546mm to 613mm as shown in Fig. 7.7. This is an increase of 12.3%. In comparison the required increase for the British Steel Corner Test was 15.7%. This shows the benefit of having a smaller aspect ratio, much

more efficient use can be made of the reinforcement as both spans contribute equally to carrying load.

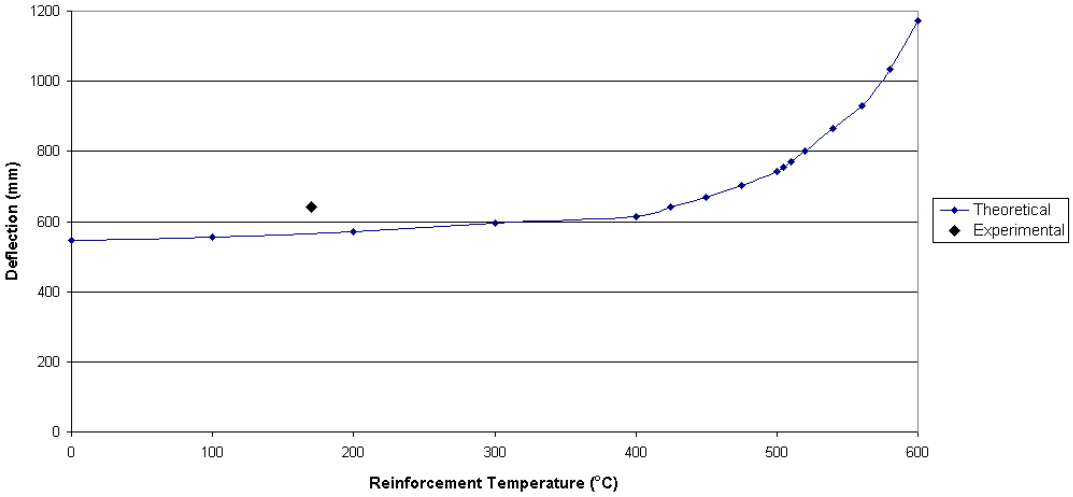

Figure 7.7: Temperature-deflection relationship of British Steel Demonstration Test for test load of 5.48kN/m^2

Figure 7.8 shows the mechanical strain against temperature for the Demonstration Test. The required mechanical strain is at a minimum at a temperature of 200^{o}C. At 500^{o}C there is a sharp increase in the rate of change of mechanical strain due to material degradation and the 2.5% limiting mechanical strain is reached at a temperature of 570^{o}C.

7.3.3 BRE Corner Test

The first BRE test consisted of a 6m x 9m compartment in the corner of the building between the second and third floors (see Fig. 7.2). Wooden cribs on the floor provided a fire load of 40kg/m^2. For a modern office building this is an extremely high fire load as it is within the 90% fractile [119]. A maximum recorded atmosphere temperature of 1051^{o}C was reached after 102 minutes. The fully exposed secondary beam in the centre of the compartment reached a maximum temperature of 903^{o}C. The walls used to construct the compartment provided vertical restraint along three of the four boundaries. These also served to shield the beams above them which were all left

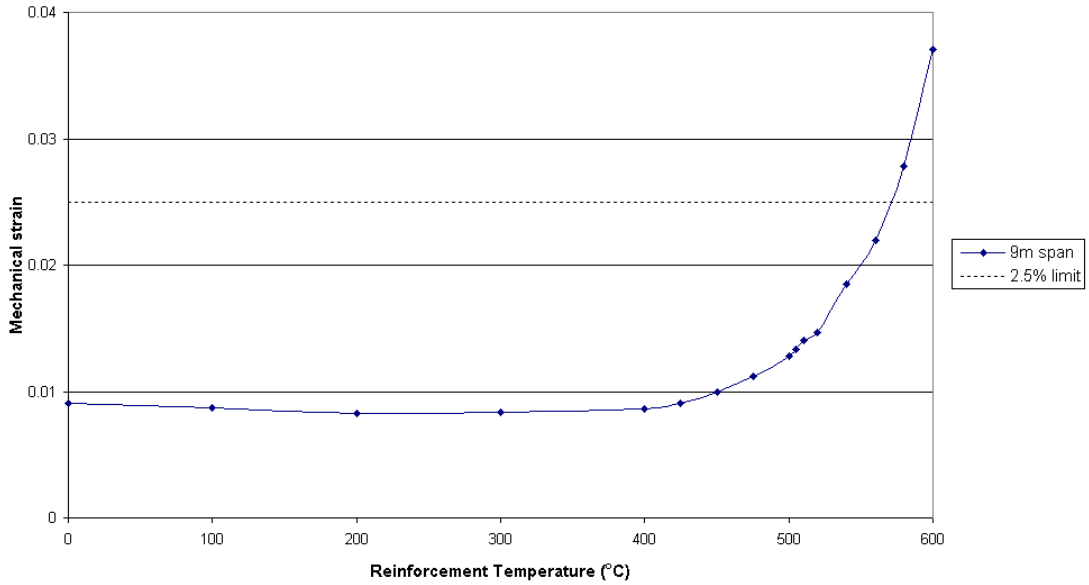

Figure 7.8: Temperature-mechanical strain relationship for British Steel Demonstration Test for test load of 5.48kN/m^2

unprotected from the fire. The external beam on gridline F was built into the brickwork wall and so was unaffected by the fire as it only reached very low temperatures. Non-uniform temperature distributions in the internal beams on gridlines 3 and E due to the steel-stud partitions resulted in lateral deflections due to thermal bowing. On the fourth wall on gridline 4 two windposts provided vertical restraint to the edge beam. The vertical restraint provided by the compartment boundaries and the low temperatures of the beams mean that the test boundary conditions will closely resemble those that are assumed for the design method i.e. vertical and translational restraint.

Figure 7.9 shows the membrane load capacity of the slab for various reinforcement temperatures, it can be seen that the slab had a significant reserve load capacity before failure would occur. Below a steel reinforcement temperature of 400^{o}C the membrane load capacity of the compartment was found to be approximately 9.84kN/m^2. This is only 56% of the load that it was carrying and is the lowest utilisation factor of the four tests analysed. At the applied load level the maximum reinforcement temperature that could be allowed would be approximately 570^{o}C.

It is interesting to note that the load capacity peaks at 300^{o}C and then starts to fall.

This is unlike the behaviour of all the other tests where the theoretical capacity peaked at 400^{o}C and is probably due to the aspect ratio of the slab. As explained in Section 4.5.4 the theoretical equations used to describe the deflected shape, stress and strain distributions lose accuracy with increasing aspect ratio. In this test this causes the load capacity to be under-predicted as the internal energy is not fully accounted for. This has more effect at higher temperatures where larger thermal strains cause the mechanical tensile strains and hence internal energy in the slab to be under-calculated away from the centre of the slab hence why the load capacity at 400^{o}C is less than at 300^{o}C.

Based on an assumed reinforcement temperature of 170^{o}C the required theoretical deflection to carry the actual slab load of 5.48kN/m^2 was 382mm, the maximum deflection reached in the test was 269mm. There will be two principal reasons for the difference; firstly, the underprediction of the internal work done due to the limitations described in the theoretical equations and secondly, the theory does not properly account for the arching action that will occur due to compressive membrane forces in areas of the slab that have small deflections. To compensate a larger deflection will be required to be able to carry a given load. The secondary beam spanning along the length of the compartment would have a small amount of load capacity but at a temperature of over 900^{o}C its strength has been reduced to only 6% of that at ambient.

Figure 7.10 shows that if the reinforcement temperature is increased from 0 to 400^{o}C the deflection required to carry the test load increased from 352mm to 456mm, a change of 29.5%. This is much larger than that seen in any of the other tests and is due to the aspect ratio of the slab. The British Steel Corner Test had an aspect ratio of 1.3 whereas this test has an aspect ratio of 1.5. This is having a significant effect on the structural behaviour and load carrying mechanism.

Mechanical strains in Fig. 7.11 follow a similar pattern to those of the British Steel Corner Test with the strains acros the short span being much larger than those across the long span. Examining the rate of change of mechanical strains (see Fig. 7.12) clearly illustrates the effect of the aspect ratio on the structural response. If the steel is at a high enough temperature that it starts to degrade the rate of change of mechanical strain increases and there is a marked difference between the two directions with the rate of change of mechanical strain in the long span being only 32.2% that found in

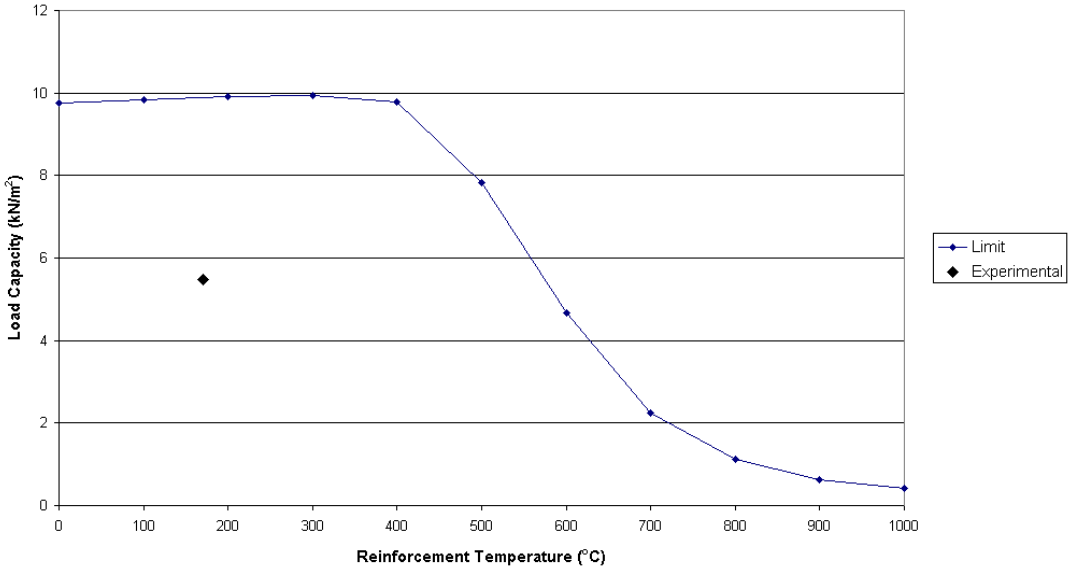

Figure 7.9: Load capacity of BRE Corner Test

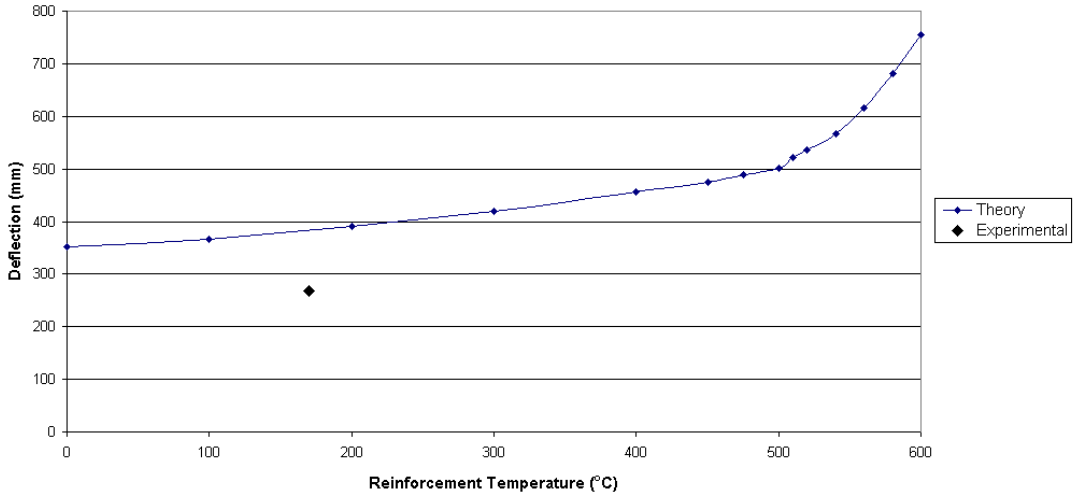

Figure 7.10: Temperature-deflection relationship of BRE Corner Test for test load of 5.48kN/m^2

the short span. The difference here is much more pronounced than for the British Steel Corner Test where the corresponding value was 57.0%. This is again due to the larger aspect ratio of the BRE test.

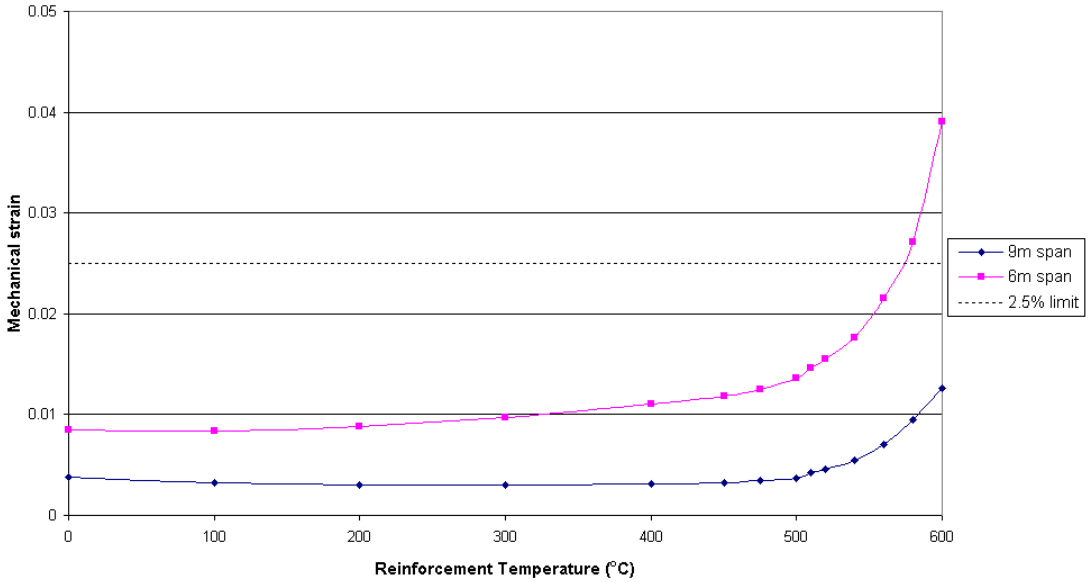

Figure 7.11: Temperature-mechanical strain relationship for BRE Corner Test for test load of 5.48kN/m^2

7.3.4 BRE Large Compartment Test

This test was conducted across the entire width of the building (21m) and over two bays (18m) giving a total area of 340m^2. Internally the compartment was created by constructing a stud-partition with 15mm deflection allowance as had been used in the BRE corner test. The wall was built 0.5m before gridline C which meant that the primary beams along this gridline were outwith the fire compartment. Wooden crates with an equivalent fire load of 40kg/m^2 were used as a fuel source, however, they were situated far apart which meant they burned individually rather than as one after flashover had occurred. The result of this was that the fire was less severe than that of the BRE corner test with a maximum recorded atmosphere temperature of 763^{o}C. A maximum steel temperature of 691^{o}C was measured.

For the purpose of the analysis the 9m x 21m section between gridlines B and C was

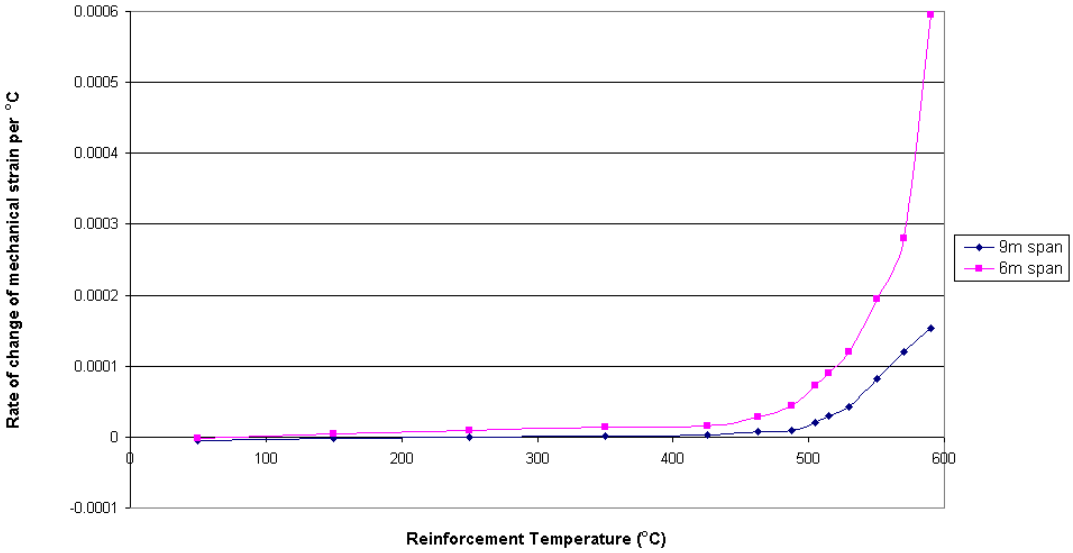

Figure 7.12: Rate of change of mechanical strain with temperature for BRE Corner Test for test load of 5.48kN/m^2

chosen (see Fig. 7.2). The section was treated as one-way spanning due to the large aspect ratio of 2.33. At this ratio the load carrying capacity in the long span across the width of the building will be small in comparison to that of the small span. Although the wind posts attached to the edge beams will limit deflections at either end of the compartment resulting in load being carried through arching of the slab, over the majority of the slab the load carrying mechanism will be tensile catenary action across the short span.

The primary beams along gridlines B and C were designed with a low load ratio [**?**]. As the compartment stopped short of gridline C those beams were not heated and thus retained their full strength and could provide vertical support. Although the beams on gridline B were heated their low load ratio, and in comparison with the other tests relatively low temperature, meant that deflections were small. In the 9m central span a deflection of 60mm was recorded whilst in the 6m outer spans it was only 45mm.

Of the four tests analysed this was the one closest to failure. The calculated load capacity of the slab at a reinforcement temperature of 170^{o}C was only 5.75kN/m^2 which meant that the slab was using 95% of its available strength. Figure 7.13 illustrates

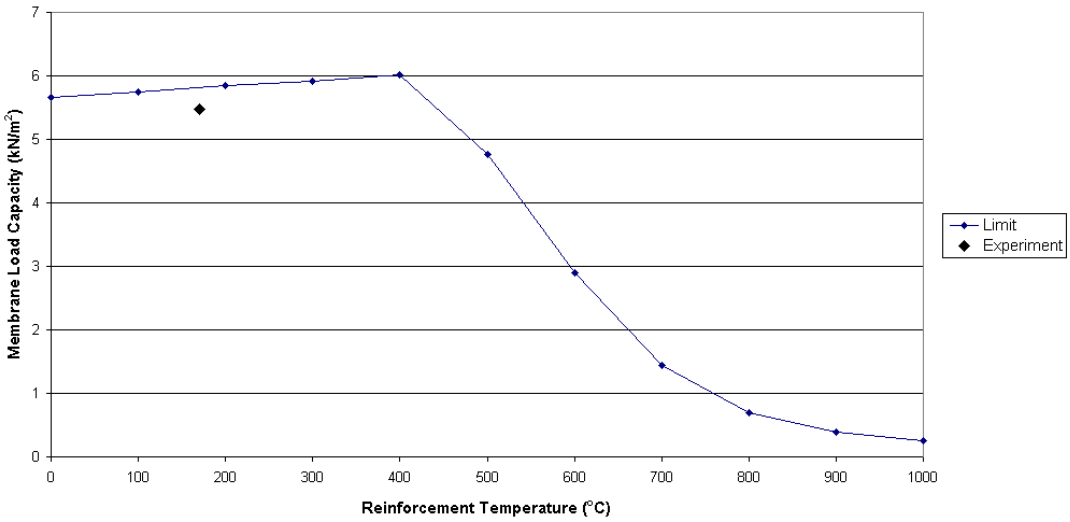

Figure 7.13: Load capacity of BRE Large Compartment Test

how close the slab was to failure. In comparison with the other tests a much lower reinforcement temperature of 440^{o}C would have resulted in failure. During the test a maximum vertical deflection of 557mm was measured. This is smaller than the calculated deflection of 860mm required to hold the applied load. The difference is due to the additional capacity of the secondary beams. In the other three tests analysed the unprotected steel beams reached temperatures which would reduce their yield stress to less than 6% of their ambient strength, with this level of degradation any contribution from the beams would be small. At the maximum temperature of 691^{o}C recorded in this test, however, they would have a reduced, but nonetheless important, contribution to make to carrying load. This will be considered later.

Figure 7.14 shows that no increase in deflection is needed to carry the test load if the reinforcement temperature is increased from 0^{o}C up to 400^{o}C. This is because in a 1-way spanning slab, once the thermal strain has been overcome and yield has been reached the rate of change of internal work done, and hence the load carrying capacity, increases at the same rate for a given deflection assuming the yield stress has not reduced. Above 400^{o}C the gradient of the line is much higher (by approximately three times) than in the other tests. This is because the slab is at such a high percentage of its load capacity.

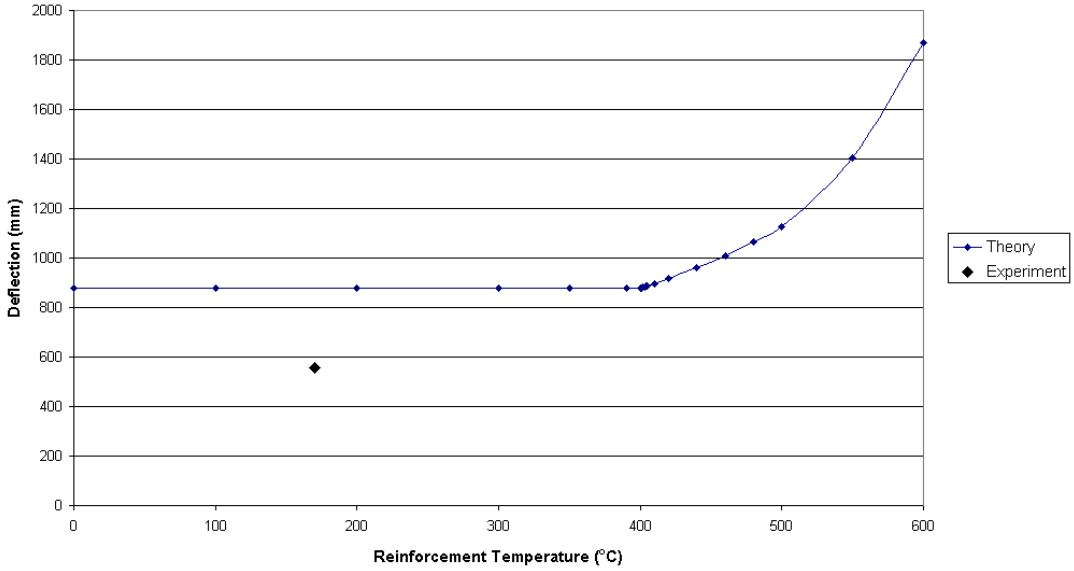

Figure 7.14: Temperature-deflection relationship of BRE Large Compartment Test for test load of 5.48kN/m^2

As the required deflection to carry the test load does not change up to a temperature of 400^{o}C the mechanical strain reduces as can be seen in Fig. 7.15. It is however always close to the 2.5% limiting mechanical strain used to define failure. The limiting strain is reached at a temperature of only 440^{O}C which is much lower than any of the other tests.

Contribution of unprotected secondary beams

If the beams are considered to be pin-ended, thus ignoring any rotational restraint given by the slab, then their capacity at any deflection is easily calculated. This can then be added to the capacity of the slab. It was assumed that the secondary beams were at a temperature of 693^{o}C and that there was no variation in the temperature over the beam section. For this test the deflection required for the slab-beam system to be able to carry the applied load was calculated as 576mm. This result is much closer to the maximum test deflection of 557mm.

Figure 7.16 contains a revised load capacity envelope for the test including the capacity of the beams. It shows that even though the beam is at a temperature of just below 700^{o}C it can carry approximately twice the load of the slab at the maximum allowable

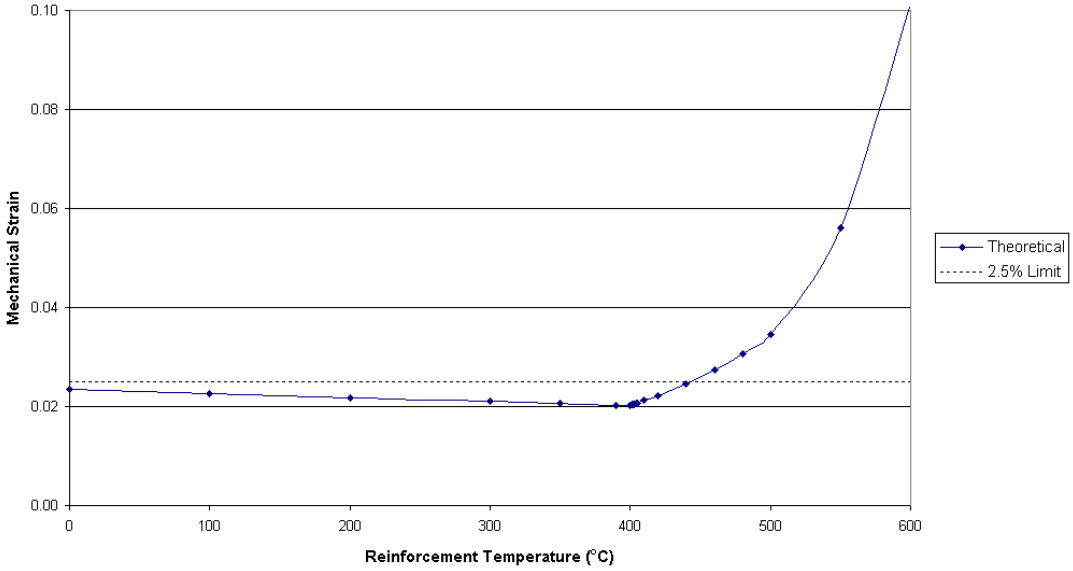

Figure 7.15: Temperature-mechanical strain relationship for BRE Large Compartment Test for test load of 5.48kN/m^2

deflection. Adding the contribution of the beams to that of the slab calculated previously increases the ultimate capacity of the floor system to 15.7kN/m^2 at a reinforcement temperature of 170^{o}C. This would mean that the whole system was using only 35.4% of its available capacity.

Although it is straightforward to calculate the contribution of the beam it is not without error. In this instance the maximum temperature of the beam was 691^{o}C. At such a high temperature the majority of the beams deflection will be caused by thermal strains and any mechanical strains will be relatively small. However, due to the highly non-linear stress-strain curve at this temperature a small error in the mechanical strain can give a large variation in the mechanical stress that should be used for any calculation. This is not so critical for the steel reinforcement in the slab, being at a much lower temperature the stress-strain curve is less non-linear and the ratio of thermal strain to mechanical strain is smaller so any errors arising from this will not be so significant.

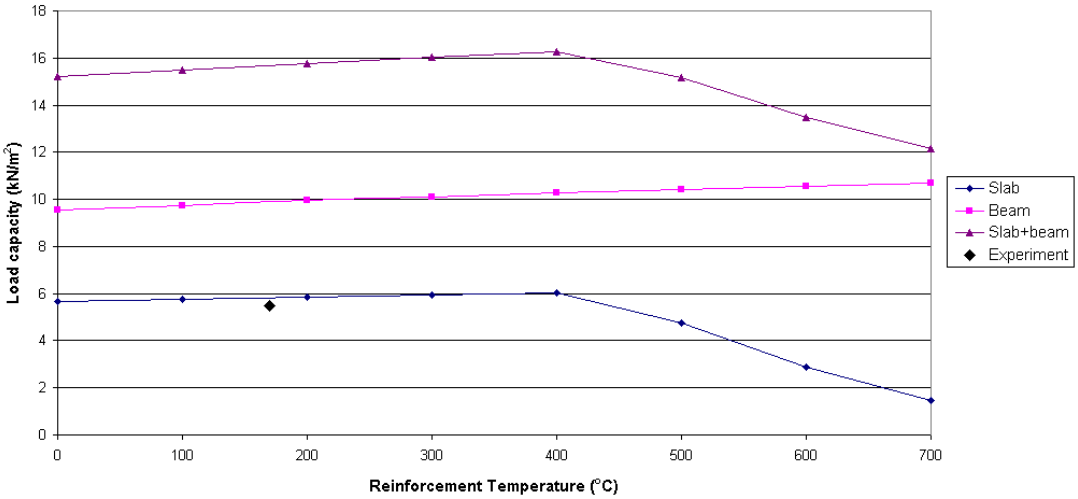

Figure 7.16: Load capacity of BRE Large Compartment Test including secondary beams

7.4 Conclusions

Four of the six Cardington tests have been analysed and it has been shown that they all had a significant reserve of strength available. The three two-way spanning analyses (both British Steel tests and the BRE corner test) were using between 56 and 63% of their available capacity. No account was taken of the capacity of any secondary beams in these tests as they were at such high temperatures that their strength was negligible.

The only test that was close to failure was the BRE large compartment test where the slab was at 95% of its theoretical ultimate capacity. This was because the load was being carried through one-way catenary action due to the geometry of the test layout. Lower temperatures meant that the secondary beams did not degrade as much as in the other tests and so contributed significant strength to the floor system. Had the temperatures in the test been nearer to those of the other tests then the slab might have failed.

It was found that the reinforcement in the short span was contributing more to the load carrying capacity than that in the long span. This is because at any deflection the strain in the short span will be larger than in the long span resulting in more internal

energy. The most efficient method therefore of increasing the membrane load capacity of a laterally restrained slab would be to increase the area of reinforcement across the short span.

Chapter 8

Conclusions and Future Work

8.1 Introduction

The research described in the preceding chapters investigated the membrane behaviour of composite floor slabs in fire, in particular theoretical methods of describing their structural response. This chapter summarises the work and provides guidelines for possible further research.

8.2 Conclusions

- The SCI design guidance for composite buildings in fire has not altered the ambient failure mechanism and does not consider restraint to thermal expansion. It does, however, provide a quick method for an engineer to use in a design office.
- The HERA design guide considers the contribution of unprotected secondary beams to the plastic moment capacity of the slab, however, in doing so they ignore the effects of restrained thermal expansion.
- Analytical methods describing the structural behaviour of beams and plates under thermal loading were developed. These produced accurate results for the deflections and membrane stresses when compared against those from numerical models. Thermal expansions forces were dealt with better than thermal bending moments.

- The stress-strain distribution in a plate can vary significantly depending on the aspect ratio of the plate and the temperature distribution through its depth. This agrees with earlier computational work at the University of Edinburgh studying the effect of temperature distribution on the structural behaviour of composite slabs. The theoretical solution for the thermal behaviour of plates captured this well.

- The most accurate results were obtained for plates with an aspect ratio of one. As the aspect ratio was increased errors were introduced due to the equation describing the deflected shape.

- A design method was developed to calculate the membrane load capacity of composite floor slabs in fire. It considered the temperature distribution through the depth of the slab and the stress and strain distribution due to the thermal loading. An energy method was used to determine the load capacity.

- It was assumed that all of the load was carried through the steel reinforcing bars. Any contribution from compressive membrane action or bending capacity of the concrete was ignored. Ignoring these additional load carrying mechanisms will lead to a conservative result.

- Failure of the slab was defined as being when a limiting mechanical strain was reached in any of the reinforcing bars. These were based on values given in the Eurocodes that specify a limit of 2.5% for normal ductility steel and 5% for high ductility steel.

- Secondary beams along an internal edge of a slab panel may require the shear capacity of the beam-column connections to be increased. This is due to the change in the load transfer mechanism from one-way bending to two-way membrane leading to a redistribution of the loads.

- The beam-column connections of an external beam will have a horizontal shear force due to the membrane forces as well as the usual vertical shear force. This double shear action should be considered in the design.

- When compared against results from numerical analyses the design method can predict the load-deflection response of one-way slabs and two-way spanning slabs

with an aspect ratio close to one. The ultimate load capacity was accurately predicted based on the assumed failure criterion of a limiting mechanical strain.

- With an aspect ratio greater than one the ultimate load capacity was underpredicted in comparison with the numerical results. This is due to the error in the description of the deflected shape leading to the internal energy being underpredicted.

- Four of the six Cardington tests were analysed using the proposed design method. All were found to have a significant reserve capacity. The theoretical deflections calculated to be necessary to carry the test loads agreed well with those recorded during the tests.

- The British Steel Corner Test was found to have an ultimate load capacity of 8.70kN/m^2. During the test the panel was at 63.0% of capacity.

- The British Steel Demonstration Test was found to have an ultimate load capacity of 9.35kN/m^2. During the test the panel was at 58.6% of capacity.

- The BRE Corner Test was found to have an ultimate load capacity of 9.84kN/m^2. During the test the panel was at 55.7% of capacity.

- The BRE Large Compartment Test was found to have an ultimate load capacity of 15.7kN/m^2. During the test the panel was only at 35.4% of capacity.

- In both British Steel tests and the BRE Corner Test the beams were at very high temperatures and did not contribute to the load capacity. For the BRE Large Compartment Test the beams were extremely significant. Ignoring the beam contribution gave a load capacity of only 5.75kN/m^2. Had the beams achieved the same high temperatures as in the other tests then this test would have been using 95.3% of capacity and would have been very close to failure.

8.3 Recommendations for further work

There are many areas which need to be further researched with regards to the design method presented in this thesis. It was found that with an aspect ratio greater than one errors were introduced due to the equation used to describe the deflected shape

of the slab. This was necessary to achieve a close form solution which can be easily solved without the need for an iterative technique. It would be possible to use empirical factors to improve the stress-strain distribution as has been done previously for buckling of plates by Paik [110]. The results at the moment are conservative in comparison with the numerical models, however, the degree of conservatism could be reduced. In doing so it would need to be verified that this was not leading to results which overestimated the slabs capacity.

As it stands it can be a time consuming procedure to obtain a result using the design method. Particularly for two-way spanning slabs where every reinforcing bar requires an individual calculation. There is a computer programme in development which would allow a result to be obtained quickly and efficiently. At the moment it is capable of carrying out the calculations involved in stage 1 of the method to determine the design fire and the resulting temperature distribution through the slab. This needs to be extended to include stages 2 and 3 for the structural part of the analysis.

For typical slab sizes it would be straightforward to produce a series of design charts. These would detail the ultimate load capacity against reinforcement temperature for a range of slabs sizes and reinforcement arrangements and would allow an engineer to quickly determine the ultimate load capacity in a fire of a slab.

The numerical modelling undertaken in this research was limited. A more extensive series of analyses needs to be undertaken which would look at a wider range of variables such as the temperature distribution through the slab, a more extensive range of geometries, the effect of profiled decks and the level of restraint required to achieve the assumed boundary conditions. However, the real test of the method would be in comparison with experimental results. These would need to be carried out on slabs with boundary conditions representative of those found in a real building and carried through to collapse. Until this happens it will be very difficult to determine the degree of safety in the method and to properly answer the question of when failure has been reached.

Bibliography

[1] *Steel and Composite Structures Behaviour and Design for Fire Safety.* Spon Press, 2002.

[2] T.Z. Harmathy. *Fire Safety Design and Concrete.* Longman Scientific and Technical, 1st edition, 1993.

[3] ENV. *Eurocode 3, Design of composite steel and concrete structures*, 1994.

[4] *Fire and Buildings.* Applied Science Publishers Ltd, 1972.

[5] ENV. *Eurocode 2, Design of concrete structures*, 1992.

[6] *BS8110 Part 2: Structural use of concrete: Code of Practice for special circumstances.*

[7] U. Schneider. Concrete at high temperatures - a general review. *Fire Safety Journal*, Vol.13(1):55–68, 1988.

[8] S.Lamont. *Behaviour of of Steel Framed Structures in Fire.* PhD thesis, University of Edinburgh, 1997. http://www.civ.ed.ac.uk/researc/fire/project/thesis.html.

[9] A.M. Sanad, S. Lamont, A.S. Usmani, and J.M. Rotter. Structural behaviour in fire compartment under different heating regimes - part 1 (slab thermal gradients). *Fire Safety Journal*, 2000.

[10] Behaviour of steel framed structures under fire conditions. Technical Report Main Report, DETR-PIT Project, School of Civil and Environmental Engineering, University of Edinburgh, 2000. available at www.civ.ed.ac.uk/research/fire/project/technicalreports.html.

[11] A.Y. Elghazouli, B.A. Izzuddin, and A.J. Richardso. Numerical modelling of the structural fire response of a steel-framed building. Technical report, Imperial College, 2000.

[12] A.M. Sanad. PIT Project Research Report SM1: Studies using numerical models: effect of steel section in British Steel Test 1. Technical report, University of Edinburgh, 2000.

[13] A.M. Sanad, S. Lamont, A.S. Usmani, and J.M. Rotter. Structural behaviour in fire compartment under differemt heating regimes - part 2 (slab mean temperatures). *Fire Safety Journal*, 2000.

[14] M. Gillie. PIT Project Research Report SS2: FEAST modelling of tensile membrane action in Cardington test 1. Technical report, University of Edinburgh, 2000.

[15] A.S. Usmani, J.M Rotter, S. Lamont, A.M. Sanad, and M. Gillie. Fundamental principles of structural behaviour under thermal effects. *Fire Safety Journal*, 2001.

[16] *Beams, Plates, and Shells.* McGraw-Hill Book Company, 1976.

[17] *Thermal Stresses I.* North-Holland, 1986.

[18] *Structural Design for Fire Safety.* Wiley, 2001.

[19] V. Babrauskus and R.B. Williamson. The historical basis of fire resistance testing - part 1. *Fire Technology*, 1978.

[20] V. Babrauskus and R.B. Williamson. The historical basis of fire resistance testing - part 2. *Fire Technology*, 1978.

[21] British Standard Insitution. *BS476 Parts 20-23: Fire tests on building materials and structures*, 1987.

[22] D. Drysdale. *An Introduction to Fire Dynamics.* John Wiley and Sons, 1985.

[23] S.H. Ingberg. Fire loads. *Quarterly Journal of the National Fire Protection Association*, Vol. 22:43–61, 1928.

[24] S. Lamont, B. Lane, A.S. Usmani, and D.D. Drysdale. Assessment of the fire resistance test with respect to beams in real structures.

[25] British Standard Insitution. *BS5950 Part 8: Code of Practice for Fire Resistant Design*, 1990.

[26] *BS5950 Part 4: Code of practice for design of composite slabs with profiled steel sheeting.*

[27] British Standard Institution. *BS8110 Part 1: Structural use of concrete: Code of practice for design and construction*, 1997.

[28] ENV. *Eurocode 2: Design of concrete structures-Part 1.2 General rules - Structural fire design*, 1996.

[29] ENV. *Eurocode 3: Design of steel structures - Part 1.2: General rules - Structural fire design*, 2001.

[30] *Fire resistance of steel frame buildings.*

[31] J. Dowling. Fire protection using off-site applied intumescent coatings. *Proc. Instn Civ. Engrs Structs and Bldgs*, 1997.

[32] A.H. Buchanan. Fire engineering for a performance based code. *Fire Safety Journal*, 23(1):1–16, 1994.

[33] I. Barry. Passive resistance. *Fire Prevention*, 2002.

[34] Y. Sakumoto. Research on new fire-protection materials and fire-safe design. *Journal of Structural Engineering*, 1999.

[35] U. Wickstrom and E Hadziselimovic. Equivalent concrete layer thickness of a fire protection insulation layer. *Fire Safety Journal*, 1996.

[36] K.W. Johansen. Yield line. *Journal of Construct. Steel Research*, Vol. 33(1):71–85, 1995.

[37] R. Park. Tensile membrane behaviour of uniformly loaded rectangular reinforced concrete slabs with fully restrained edges. *Magazine of Concrete Research*, Vol. 16(46):39–44, 1964.

[38] J.R. Eyre. Direct assessment of safe strengths of rc slabs under membrane action. *Journal of Structural Engineering*, 1997.

[39] Y.C. Wang. Tensile Membrane Action in Slabs and its Application to the Cardington Fire Tests. Technical report, Building Research Establishment, 1996. Paper presented to the second Cardington Conference 12-14 March 1996.

[40] C.G. Bailey and D.B. Moore. The structural behaviour of steel frames with composite floor slabs subject to fire: Part 1: Theory. *The Structural Engineer*, 2000.

[41] A.H. Buchanan. Fire engineering for a performance based code. *Fire Safety Journal*, 1994.

[42] G.V. Hadjisophocleous, N. Benichou, and A.S. Tamin. Literature review of performance-based fire codes and design environment. *Journal of Fire Protection Engineering*, 9(1):12–40, 1998.

[43] B.J. Meacham and R.L.P Custer. Performance-based fire safety engineering: an introduction of basic concepts. *Journal of Fire Protection Engineering*, 1995.

[44] J.M. Watts. Performance based codes. *Fire Technology*, 1994.

[45] G.M.Newman, J.T.Robinson, and C.G.Bailey. Fire Safe Design: A new approach to multi-storey steel framed buildings. Technical report, Steel Construction Institute, Ascot, UK, 2000.

[46] British Standard Institution. *BS7974: Application of fire safety engineering principles to the design of buildings*, 2001.

[47] D. Charters. Engineering a solution. *Fire Engineers Journal: Fire Prevention*, 2000.

[48] British Standard Institution. *PD7974: Application of fire safety engineering principles to the design of buildings-Part 3:Structural response and fire spread beyond the enclosure of origin(Sub-system 3)*, 2001.

[49] O. Pettersson. Practical need of scientific material models for structural fire design - general review. *Fire Safety Journal*, 1988.

[50] G.M.E. Cooke. An Introduction to the Mechanical Properties of Structural Steel at Elevated Temperatures. *Fire Safety Journal*, Vol.13(1):45–54, 1988.

[51] B.R. Kirby and R.R. Preston. High Temperature Properties of Hot-rolled, Structural Steels for Use in Fire Design Studies. *Fire Safety Journal*, Vol.13(1):27–37, 1988.

[52] Y. Anderberg. Modelling Steel Behaviour. *Fire Safety Journal*, Vol. 13(1):17–26, 1988.

[53] C.L. Clark. *High Temperature Alloys*. Pitman, 1953.

[54] U. Schneider. Behaviour of concrete under thermal steady state and non-steady state conditions. *Fire and Materials*, 1976.

[55] G.A. Khoury, B.N. Grainger, and P.J.E. Sullivan. Strain of concrete during first heating to 600C under load. *Magazine of Concrete Research*, Vol.37:195–215, 1985.

[56] C.Ehm. *Experimental Investigations of the Bi-axial strength and deformations of concrete at high temperatures*. PhD thesis, Technical University of Braunschweig, 1985. In German.

[57] F. Lea and R. Stradling. The resistance to fire of concrete and reinforced concrete. *Engineering*, 1922.

[58] F. Ulm, O. Coussy, and Z.P. Bazant. The "chunnell" fire. i: Chemoplastic softening in rapidly heated concrete. *ASCE Journal of Engineering Mechanics*, 1999.

[59] British Steel plc. The behaviour of multi-storey steel framed buildings in fire. Technical report, Swinden Technology Centre, 1999.

[60] G.C. Clifton et. al. Design of multi-storey steel framed buildings with unprotected secondary beams or joists for dependable inelastic response in severe fires. *HERA Steel Design and Construction Bulletin*, 2001.

[61] Structural fire engineering investigation of broadgate phase 8 fire. Technical report, Steel Construction Institute, Ascot, UK, 1991.

[62] C.I. Smith. The broadgate phase eight fire on twenty-third june, 1990. In *Proceedings of the Institution of Mechanical Engineers, Materials and Design Against Fire*, pages 143–150, 1992.

[63] B.A. Izzuddin and A.S. Elnashai. *ADAPTIC: A program for Adaptive Dynamic Analysis of Space Frames, User Manual.* Imperial College, London, 1989.

[64] A.M. Sanad. BS/Test1 reference ABAQUS model using beam general section. Technical report, University of Edinburgh, 2000.

[65] M. Gillie. PIT Project Research Report MD3: BS/TEST1 model using FEAST with shell elements. Technical report, University of Edinburgh, 2000.

[66] A.M. Sanad. PIT Project Research Report MD10: BS/Test3 reference ABAQUS model using beam general section. Technical report, University of Edinburgh, 2000.

[67] M.G. Gillie. PIT Project Research Report MD11: BS/Test3 reference ABAQUS model using FEAST with shell elements. Technical report, University of Edinburgh, 2000.

[68] M. Gillie, A.S. Usmani, and J.M. Rotter. Modelling of Heated Composite Floor Slabs with Reference to the Cardington Experiments. *Fire Safety Journal*, 2000. submitted.

[69] A.M. Sanad, J.M. Rotter, A.S. Usmani, and M.A. O'Connor. Composite beams in large buildings under fire - numerical modelling and structural behaviour. *Fire Safety Journal*, 2000.

[70] A.S Usmani. Application of fundamental structural mechanics principles in assessing the cardington restrained beam test. In *Structures in Fire Proceedings of the First International Workshop.*

[71] M. O'Connor. PIT Project Research Report MD4: BS/Test1 ABAQUS model using shell elements for the beam and beam general section for the slab. Technical report, British Steel, 2000.

[72] M. O'Connor. PIT Project Research Report MD5: BS/Test1 ABAQUS half-floor model using elastic shell for slab. Technical report, British Steel, 2000.

[73] M. O'Connor. PIT Project Research Report MD6: BS/Test1 ABAQUS half-floor model using beam general section for the slab. Technical report, British Steel, 2000.

[74] M. O'Connor. PIT Project Research Report MD7: BS/Test2 ABAQUS model using shell elements for the beam and beam general section for the slab. Technical report, British Steel, 2000.

[75] M. O'Connor. PIT Project Research Report MD8: BS/Test2 ABAQUS half-floor model using elastic shell for the slab. Technical report, British Steel, 2000.

[76] M. O'Connor. PIT Project Research Report MD9: BS/Test2 ABAQUS model using beam general section for the slab. Technical report, British Steel, 2000.

[77] M. O'Connor. PIT Project Research Report MD12: BS/Test3 ABAQUS half-floor model using elastic shell for the slab. Technical report, British Steel, 2000.

[78] M. O'Connor. PIT Project Research Report MD13: BS/Test3 ABAQUS half-floor model using elastic shell with rotational discontinuities. Technical report, British Steel, 2000.

[79] M. O'Connor. PIT Project Research Report MD14: BS/Test4 ABAQUS half-floor model using elastic shell with rotational discontinuities. Technical report, British Steel, 2000.

[80] A. Y. Elgazhouli. PIT Project Research Report MD15: Models of all the Cardington tests using ADAPTIC. Technical report, British Steel, 2000.

[81] J.M. Rotter, A.M. Sanad, A.S. Usmani, and M. Gillie. Structural performance of redundant structures under local fires. In *Proceedings of Interflam '99*, volume Vol. 2, Scotland, 1999.

[82] A.S.Usmani and S.Lamont. Key events in the structural response of a composite steel frame structure in fire. In *Proceedings of the SiF'02, The Second International Workshop for Structures in Fire*, pages 351–368, Christchurch, New Zealand, March 2002.

[83] A.M. Sanad. PIT Project Research Report SM1: Studies using numerical models: effect of increasing live loads in British Steel Test 1. Technical report, University of Edinburgh, 2000.

[84] A.M. Sanad. PIT Project Research Report SM4: Studies using numerical models: effect of slab temperature variation in British Steel Test 1. Technical report, University of Edinburgh, 2000.

[85] J.M. Rotter and A.S. Usmani. PIT Project Research Report TM1: Behaviour of highly indeterminate composite frame structures in fire. Technical report, University of Edinburgh, 2000.

[86] A.S. Usmani and J.M. Rotter. PIT Project Research Report TM2: Fundamental principles of structural behaviour under thermal effects. Technical report, University of Edinburgh, 2000.

[87] S. Lamont. PIT Project Research Report TM3: Study of thermal expansion and bowing in a restrained beam. Technical report, University of Edinburgh, 2000.

[88] C.G.Bailey. Membrane action of unrestrained lightly reinforced concrete floor slabs at large displacements. *Engineering Structures*, 2001.

[89] C.G.Bailey, D.S.White, and D.B.Moore. The tensile membrane action of unrestrained composite slabs simulated under fire conditions. *Engineering Structures*, 2000.

[90] A.Y. Elghazouli, B.A. Izzuddin, and A.J. Richardson. Numerical modelling of the structural fire behaviour of composite buildings. *Fire Safety Journal*, 2000.

[91] M. Gillie, A.S. Usmani, and J.M. Rotter. A structural analysis of the first cardington test. *Journal of Constructional Steel Research*, 2001.

[92] Z. Huang, I. Burgess, R. Plank, and C. Bailey. Comparison of bre simple design method for composite floor slabs in fire with non-linear fe modelling. In *Proceedings of the Second International Structures in Fire Workshop.*

[93] Z. Huang, I.W. Burgess, and R.J. Plank. Non-linear analysis of reinforced concrete slabs subjected to fire. *ACI Structural Journal*, 1999.

[94] C.G. Bailey. Efficient arrangement of reinforcement for membrane behaviour of composite floor slabs in fire conditions. *Journal of Constructional Steel Research*, 2003.

[95] C. Clifton. Design of multi-storey steel framed buildings with unprotected secondary beams or joists for dependable inelastuc response in severe fires. In *Proceedings of the Second International Structures in Fire Workshop.*

[96] *Concrete Structures.*

[97] M.N. Bapu Rao. Thermal bending of thick rectangular plates. *Nuclear Engineering and Design*, 54:115–118, 1979.

[98] Y.C. Das and B.K. Rath. Thermal bending of moderately thick rectangular plate. *AIAA Journal*, 10(10):1349–1351, 1972.

[99] B.E. Gatewood. *Thermal Stresses.* McGraw-Hill Scientific Publications, 1st edition, 1957.

[100] S.P. Timoshenko and S. Woinowsky-Krieger. *Theory of Plates and Shells.* McGraw-Hill, 1959.

[101] P. Biswas. Large deflection of heated elastic plates under uniform load. *Mechanique Appliquee*, 20(4):585–592, 1975.

[102] B. Banerjee and S. Datta. Large deflections of elastic plates under nonstationary temperatures. *Proceedings of the ASCE, Journal of the Engineering Mechanics Division*, 105(EM4):705–711, August 1979.

[103] M.L. Williams. Large deflection analysis for a plate strip subjected to normal pressure and heating. *Journal of Applied Mechanics*, 77:458–464, 1955.

[104] M.W. Wilcox and L.E. Clemmer. Large deflection analysis of heated plates. *Journal of the Engineering Mechanics Division, ASCE*, 90(EM6):165–189, 1964.

[105] P. Biswas. Nonlinear analysis of heated orthotropic plates. *Indian Journal of Pure and Applied Mathematics*, 12(11):1380–1389, 1981.

[106] B.A. Boley and J.H. Weiner. *Theory of Thermal Stresses.* Dover Publications, 1997.

[107] V. Birman. Buckling and bending of beams subject to a nonuniform thermal field. *Mechanics Research Communications*, 1990.

[108] *Foundations of Solid Mechanics.* Prentice-Hall, 1965.

[109] M.Foray and M.Newman. The postbuckling analysis of heated rectangular plates. *Journal of Aerospace Sciences*, 29:1262, 1962. Technical note.

[110] J.K. Paik, A.K. Thayamballi, and B.J. Kim. Large deflection orthotropic plate approach to develop ultimate strength formulations for stiffened panels under combined biaxial compression/tension and lateral pressure. *Thin-Walled Structures*, 2001.

[111] C. G. Bailey, I.W. Burgess, and R.J. Plank. Computer simulation of a full-scale structural fire test. *The Structural Engineer*, 74(6):93–100, 1996.

[112] Eurocode 1: Basis of design and actions on structures. Technical Report ENV 1991-2-2, Brussels, European Committee for Standardisation, 1996.

[113] R.P.Johnson and R.J.Buckby. *Composite structures of steel and concrete - Volume 2: Bridges.* Collins, London, U.K., 1986.

[114] Eurocode 2: Design of concrete structures. Technical Report ENV 1992-1-1, Brussels, European Committee for Standardisation, 1992.

[115] Hibbet, Karlson and Sorenson, Providence, Rhode Island, USA. *ABAQUS/Standard Users' Manual,Vols II, Ver 6.3*, 2002.

[116] Hibbet, Karlson and Sorenson, Providence, Rhode Island, USA. *Getting Started with ABAQUS/Standard, Ver 6.3*, 2002.

[117] P.S. Rose, C.G. Bailey, I.W. Burgess, and R.J. Plank. The influence of floor slabs on the structural performance of the cardington frame in fire. *Journal of Constructional Steel Research*, 1998.

[118] P.N.R. Bravery. Cardington Large Building Test Facility. Technical report, iki, c1993.

[119] C.G.Bailey, T.Lennon, and D.B.Moore. Behaviour of full-scale steel-framed buildings subjected to compartment fires. *The Structural Engineer*, 1999.